2013

Cyclic Voltammetric and Square Wave Anodic Stripping Voltammetric Analysis of Lead and Cadmium Utilizing the Novel Titanium Dioxide/ Zirconium Dioxide/ Tween 80 Carbon Paste Composite Electrode

Phuong Khanh Quoc Nguyen
Wright State University

CYCLIC VOLTAMMETRIC AND SQUARE WAVE ANODIC STRIPPING VOLTAMMETRC ANALYSIS OF LEAD AND CADMIUM UTILIZING THE NOVEL TITANIUM DIOXIDE/ ZIRCONIUM DIOXIDE/ TWEEN 80 CARBON PASTE COMPOSITE ELECTRODE

A dissertation submitted in partial fulfillment of the requirements for the degree of Doctor of Philosophy

By

PHUONG KHANH QUOC NGUYEN

B.S., Wright State University, 2010

2013

Wright State University

WRIGHT STATE UNIVERSITY

GRADUATE SCHOOL

November 15, 2013

I HEREBY RECOMMEND THAT THE DISSERTATION PREPARED UNDER MY SUPERVISION BY Phuong Khanh Quoc Nguyen ENTITLED Cyclic Voltammetric and Square Wave Anodic Stripping Voltammetric Analysis of Lead and Cadmium Utilizing the Novel Titanium Dioxide/ Zirconium Dioxide/ Tween 80 Carbon Paste Composite Electrode BE ACCEPTED IN PARTIAL FULFILLMENT OF THE REQUIREMENTS FOR THE DEGREE OF Doctor of Philosophy.

_____
Suzanne Lunsford, Ph. D.
Dissertation Director

_____
Don Cipollini, Ph. D.
Director, Environmental Sciences Ph. D. Program

_____
R. William Ayres, Ph.D.
Interim Dean, Graduate School

Committee on
Final Examination

_____
Suzanne Lunsford, Ph. D.

_____
Doyle Watts, Ph. D.

_____
Joseph Caruso, Ph. D.

_____
Rachel Aga, Ph. D.

_____
Songlin Cheng, Ph. D.

ABSTRACT

Nguyen, Phuong Khanh Quoc, Ph.D., Environmental Sciences Ph.D. Program, Wright State University, 2013. Cyclic Voltammetric and Square Wave Anodic Stripping Voltammetric Analysis of Lead and Cadmium Utilizing the Novel Titanium Dioxide/ Zirconium Dioxide/ Tween 80 Carbon Paste Composite Electrode.

Heavy metals, particularly Lead (Pb) and Cadmium (Cd), had been long identified as hazardous pollutants in the environment. Joining the continuous effort to alleviate this dilemma, a new electro-chemical sensor has been developed to assess the level of Pb and Cd in aqueous environment. The current work describes the utilization of two different electro-analytical techniques, cyclic voltammetry (CV) and square wave anodic stripping voltammetry (SWASV), in conjunction with the novel Titanium Dioxide/ Zirconium Dioxide/ Tween 80 (TiO_2/ ZrO_2/ Tween 80) carbon paste composite electrode to qualitatively and quantitatively analyze Pb and Cd. In this dissertation, along with a comprehensive literature review of recent electro-chemical sensors developed to quantify heavy metals, theoretical background overview of the different analytical and spectroscopic techniques employed in this study is also provided. With respect to cyclic voltammetric analysis, CV is used to optimization of electrode synthesis conditions, estimate the TiO_2/ ZrO_2/ Tween 80 carbon paste composite electrode active surface area, optimize the working pH, and calculate two kinetic parameters, electron transfer coefficient (α) and heterogeneous electron transfer rate constant (k_0), for the oxidation-

reduction process of Pb and Cd at the electrode surface. Furthermore, quantitative analysis of Pb and Cd via cyclic voltammetry is also carried out. In addition, square wave anodic stripping voltammetric analysis of Pb and Cd was conducted at part per billion concentration range for both metals. For this analysis, Pb and Cd are quantitatively measured, both individually and simultaneously. Moreover, the effects of environmental interferences on the performance of the electrode is also investigated via SWASV using two modeling surface active substances and six common di-valence metals. Asides from quantitative analysis in modeling solution, SWASV analysis of Pb and Cd is also carried out in two different river waters and one well water sample, with inductively coupled plasma optical emission spectroscopy (ICP-OES) being employed as verification method. Successful detection of Pb and Cd in real water samples illustrates the potential of the newly developed electrode for real world applications. And lastly, scanning electron microscopy and X-ray photoelectron spectroscopy are utilized to investigate the morphology and chemical characteristics of the electrode surface to better understand the logic behind the electro-chemical reaction between the analytes and electrode surface. The ultimate goal of the project is to create a novel sensor that not only possesses favorable electrochemical characteristics (electro-chemical stability, selectivity, and enhanced electro-catalytic activity)to quantify Pb and Cd at trace levels, but also suitable for mass commercial production (easy to produce at marginal unit cost).

Table of Contents

List of Figures

List of Tables

ACKNOWLEDGEMENTS

I wish to express my most sincere gratitude and appreciation to my mentor and dissertation advisor, Dr. Suzanne Kay Lunsford, for her assistance and continuous support. She has always believed in me since the first day I started research in the field of electrochemistry. Although many times I have failed, my mentor never doubted me and has always been there to cheer me on. Without her guidance and continuous motivation, completion of this dissertation would not be possible.

I would like to thank my committee members, Dr. Doyle Watts, Dr. Joe Caruso, Dr. Rachel Aga, and Dr. Songlin Cheng for your encouraging words and thoughtful criticisms during my research and writing process. Your contribution to my development is deeply appreciated.

I also would like to thank Dr. Don Cipollini, Dr. Steve Higgins, the Environmental Sciences Ph.D. program, and the Chemistry department for your financial and structural supports over the years.

And finally, to my parents, Khanh Quoc Nguyen and Kim Hue Thi Nguyen, I would like to express my uttermost appreciation, not only for their love and caring during my whole life, but also for the never-ending encouragement and emotional support they have given me during this whole process. Thank you for always being there for me when I needed most, you are the most important people in my life, always have been and always will be.

I. Introduction

1) Research Perspective/ Rationale

In the past, the use of electrochemical sensors in quantifying metallic pollutants in aqueous environment have been limited to academic settings due the traditional use of mercury-based sensors. However, as the field of electrochemistry has gradually moved away from mercury-based electrodes and novel mercury-free sensors are being developed continuously, practical applications of electrochemical sensors in the field of environmental science have gained more and more attention. Following the current trend in electrochemical sensor development, my research goal is to develop a TiO_2/ZrO_2 carbon paste composite electrode to detect trace levels of lead and cadmium in aqueous environment. The proposed sensor is expected to not only possess the favorable electro-catalytic properties for detecting Pb and Cd, but also has the characteristics suitable for mass product and commercial usage (eco-friendliness, affordability, selectivity, mechanical stability, and physical rigidity). This electrode is prepared using sol-gel metal oxides (TiO_2 and ZrO_2), but rather than dipping the electrode surface in TiO_2/ZrO_2 sol-gel mixture before heating, the sol-gel metal oxides are directly incorporated into the carbon paste during the homogenization process, hence the term "carbon paste composite".

Although using sol-gel materials as modifying reagents for electrochemical sensors is still relatively new, sol-gel modified electrodes have been found to be useful in a variety of electrochemical applications as sol-gel materials have highly porous surfaces which offer more electro-active area thus enhancing sensitivity [1, 2]. "Sol" is a dispersion of colloidal particles in a liquid, and a "gel," which is formed after pore-liquid is removed from the sol, is an inter-connected, rigid network of sub-micrometer sized pores and polymeric chains [3, 4]. Due to the solid/dry nature of the proposed composite electrode, it does not need special storage

accommodation as it is not susceptible to shrinking, swelling, and leaching like polymer and metal films modified electrodes [5, 6]. Furthermore, chemically incorporated functional groups in the sol-gel have been shown to increase mechanical stability and chemical selectivity of the modified electrodes, thus leading to more stable and reproducible analytical measurements [7]. Of the many sol-gel integrated functional groups, ZrO_2 and TiO_2, which exhibit low toxicity, good thermal stability, and good wear resistance, have been shown to possess good catalytic properties, which are beneficial in enhancing electrode sensitivity [8, 9]. Even though sol-gel materials offer several advantages, unfortunately, electrodes modified with sol-gel reagents also possess a number of shortcomings. For example, physical polishing/ cleaning of sol-gel modified electrode surfaces can cause damage to solid functionalized structure, gel cracking can result from excessive heating/drying, and small defects on sol-gel surface can lead to significant variation in analytical measurements [3, 5].

Even though carbon paste electrode exhibits weaknesses such as: unsuitable for applications that require regular surface renewal (unless a mechanism for refilling the paste is available) [10], and inconsistency in mixing and packing of the carbon paste can lead to errors in analytical measurements. However, carbon paste electrode (CPE) as modifying template it offers several distinct advantages such as low background current, large potential window, high conductivity, and long lifetime [11, 12]. Furthermore, besides the exceptional mechanical stability, CPE is one of the simplest templates to construct [10]. The bare CPE is made by packing carbon paste (mixture of graphite powder and binding liquid) into a holder, such as a glass tube, which has a metal wire for electrical contact. It is worth mentioning that, unlike other solid electrode templates whose compositions are fixed, CPE can be custom-made by varying the ratio of the paste components for specific packing design [11]. Besides the ease of construction,

which is a valuable characteristic in term of mass production suitability, CPEs are also relatively cheap to produce and virtually non-toxic [12, 13], which are attractive features for commercial utilization. Moreover, CPE represents one of the most flexible substrates for preparing modified electrode. The modifying reagents can be mixed directly into the carbon paste (most often used technique due to simplicity), mechanically coated onto CPE, or electrochemically deposited onto CPE [10, 11]. These advantages of CPE make it one of the most popular working electrode templates today [14].

2) Lead and Cadmium Profile

a) Lead (Pb)

Lead is a natural occurring element that has four isotopic forms: ^{208}Pb, ^{207}Pb, ^{206}Pb, and ^{204}Pb. Of the four isotopes, ^{208}Pb is the most abundant as it makes up more than 50% of total Pb. Lead isotopes are stable products resulted from radioactive decay of 3 elements: uranium, actinium, and thorium. Even though Pb is not a very abundant element, its ore deposits are widely distributed throughout the world. Lead can be neutral or has 2+ or 4+ charge. In ordinary environment, Pb(II) is the primary form, while Pb(IV), being much less common, is typically found in lead containing compounds or forms under extremely oxidizing conditions. Metallic lead is also very rare in nature. When lead metal is exposed to air or water, formation of lead oxides, lead sulfate, and lead carbonates films is spontaneous, and these films acts as protective covers that slow down the corrosion process of the underlying metal [15-17].

The most important lead ores are galena (PbS), anglesite ($PbSO_4$), and cerussite ($PbCO_3$). In 2003, lead mining from Alaska and Missouri accounted for 96% of total domestic lead production. The United States is third in the world, after Australia and China, in lead production.

Primary lead is obtained from mined ore, while secondary lead is obtained from scrap metal, which comes mostly from recycled lead batteries. Lead is used in the form of pure or alloy metal or as chemical compounds. Besides its low melting point (~ 600K) and being resistive to corrosion, lead also exhibits other economically profitable features such as ease of casting/fabrication, high density, and electrochemical reactive with acid. These features are the reasons why Pb has been extensively utilized in many industrial applications [15]. Historically speaking, prior to 1970s, tetraethyl lead was used in the United States as "anti-knock" additive in gasoline. Also, lead arsenates were used as herbicides, insecticides, and rodenticides until 1960s. Furthermore, before the late 1970s, lead-based paint was still legal in the US although lead concentration in chips of lead-based paint was found to range from 1 to 5mg/cm^2 [18, 19]. However, as public awareness of lead toxicity increased in recent decades, such usages of lead have been either severely restricted or no longer legal in the US. Nowadays, lead is used in manufacturing storage batteries, sheets and pipes for nuclear and X-ray shielding, cable covering, noise control materials, chemical resistant linings, ammunitions, pigments (used in glass making), ceramic glazes, caulk, and many other applications. Even though its usages are quite diverse, the biggest use of lead today is in making batteries for cars and other transportation devices; in the US, more than 80% of lead is used in manufacturing batteries [15].

Lead is dispersed in the environment primarily through anthropogenic activities. Anthropogenic sources of lead include mining and smelter, manufacturing of lead-containing products, coal and oil burning, and waste incineration. Lead compounds can undergo transformation in the environment, but lead (as an element) cannot be destroyed. Natural processes such as weathering, runoff, precipitation, and stream/river flow transfer lead continuously between air, water, and soil. Historically speaking, the primary source of lead in the

environment has been anthropogenic emission to the atmosphere. Atmospheric deposition is the largest source of lead found in soil and water. Compare to air emission, aquatic releases of lead from industrial facilities are much less. Also, the solubility of lead compounds in aqueous environment is dependent upon the pH, hardness, and salinity of the water. In some regions, typically older residence, significant amount of lead, however, can still be present in drinking water due to the use of lead pipes for interior plumbing. According to the EPA, the concentration of lead in drinking water should not exceed 15ppb [20]. Even though a significant amount of lead is released to land, this constitutes a much lower exposure hazard than air and water releases as most of the lead released to land becomes tightly bound and immobilized [15, 16].

General population exposure to lead is most likely through ingestion of contaminated food and water, or by inhalation of lead particulates in the air. Exposure may also result from engaging in hobbies that use lead such as making fishing weights, stained glass, and pottery glazes. Occupational exposure is very high for workers in lead smelting/refining facilities, battery manufacturing plants, construction, firing ranges, and radiator repair shop. The most common source of lead exposure to children is lead-based paint [21-23]. The symptoms of acute exposure to high concentration of lead include: abdominal pain, constipation, cramps, nausea, vomiting, anorexia, and weight loss [24]. Short and long term exposure to lead has been linked to hypertension, changes in cardiac conduction and rhythm [25], anemia [26], muscle weakness, joint pain, lower bone density, periodontal bone loss, delayed mineralization in teeth [27-30], decreasing activity of hepatitis lipase and mixed-function oxygenases [31, 32], proximal tubular nephropathy, glomerular sclerosis, interstitial fibrosis, changes in thyroid, pituitary, and testicular hormones [33-37], alteration in scotopic retinal function [38], impaired response to T-cell mitogens, impairment in peripheral nerve conduction, lead encephalopathy (irritability, poor

attention span, headache, muscle tremor, delirium, convulsion, paralysis, and coma) [39-41], impairment in reaction time, visual contrast sensitivity, and postural balance, intellectual deficiency, poor hand-eye coordination, decreasing hearing acuity, learning impairment, increasing absenteeism and anti-social behavior [42-47], reduction in fertility, low sperm quality [48, 49], decreasing height and delayed sexual development, chromosomal aberrations and DNA damage, and increasing risk of brain, stomach, lung, rectal, and bladder cancer [50-54].

b) Cadmium (Cd)

Cadmium is a soft, silver-white metal that is found in the earth and associates with zinc, lead, and copper ores. As the result, cadmium is extracted as a by-product during production of the listed metals. Furthermore, the metal can also be recovered from used batteries. Approximately 3kg of cadmium is produced for each ton of zinc. About 80% of cadmium production is associated with zinc production and the other 20% is associated with copper and lead production. The recycling rate of cadmium from spent nickel-cadmium batteries is still low as it is estimated that, in 2005, the recovery rate of cadmium from batteries is only about 12%. Common commercial cadmium compounds include cadmium oxide, cadmium chloride, cadmium sulfide, cadmium sulfate, and cadmium carbonate. Metallic cadmium, its alloys, and its compounds are used in manufacturing a variety of consumer and industrial products. Some examples of these products are cadmium-based batteries, plastic pigments, ceramics, glass, heat stabilizer, coating on steel, photocopying/photography, dyes, vacuum tubes, lubricants, ice-nucleation agents, semi conductors, fertilizer, and fungicide. From the listed applications, nickel-cadmium battery manufacturing is the biggest source of cadmium consumption (approximately 83% of all cadmium use). Even though cadmium is still being used widely throughout the world,

as environmental impacts result from cadmium toxicity become more apparent, the use of cadmium has been declining steadily in the recent years [55-58].

Besides natural emission of cadmium from volcanic eruption, forest fires, and other natural phenomena, cadmium can also be released into the atmosphere through metal production activities, fossil fuel combustion, and waste incineration. The main cadmium compounds in the air are cadmium oxide, cadmium chloride, and cadmium sulfate. In the atmosphere, cadmium can travel a long distance then deposits on surface soil and water [59]. The main sources of cadmium in soil are atmospheric deposition, direct application of phosphate fertilizers, and sewage sludge disposal. Cadmium mobility in soil depends on several factors, but the most important factors are pH and availability of organic matters. Cadmium contaminated waste discharge from industrial facilities is the biggest source of cadmium release in water. In surface and ground water, cadmium can exist as hydrated ions or complexes with inorganic/organic compounds. Migration of cadmium in water depends mostly on the solubility of the cadmium complexes [60-64].

The general population is exposed to cadmium through ingestion of food and water, or inhalation of particulates in the air or tobacco smoke. According to the EPA, the concentration of cadmium in drinking water should not exceed 5ppb [20]. For non-smokers, food is the major source of exposure, while cigarette smoke is the major exposure source for smokers. As the result of phosphate fertilizer usage and disposing of municipal waste, cadmium is introduced into the food chain [56, 60]. Cadmium level is relatively high in leafy vegetables such as lettuce and spinach as well as in shellfish and organ meats. Occupational exposure to cadmium is highest for workers in cadmium smelting, welding, and soldering facilities, electroplating industries, and operations associate with manufacturing cadmium compounds. Children are exposed to cadmium

primarily through food ingestion [55]. The symptoms associate with acute inhalation exposure to cadmium are severe dyspnea and wheezing, chest pain, persistent cough, weakness and malaise, nausea and abdominal pain [63]; acute exposure to cadmium by inhalation can be fatal, those who survive may have permanently impaired lung function. Nausea, vomiting, salivation, abdominal pain, cramp and diarrhea are the symptoms typically associate with acutely oral exposure to cadmium [64]. Short and long term exposure to cadmium via inhalation has been linked to emphysema, lung inflammation, chronic rhinitis, loss or impairment of the sense of smell [65, 66], calcium deficiency, osteoporosis, decreasing glomerular filtration rate, tubular dysfunction [67, 68], lung and prostate cancer [69, 70]. Also, short and long term oral exposure to cadmium has been linked to low blood pressure, cardiac rhythmic disturbances, histo-pathologic lesions of heart tissues [71-73], severe irritation to gastrointestinal epithelium, anemia (due to reduced gastrointestinal absorption of iron), osteomalacia, osteoporosis, bone fracture, low bone density [64, 74- 77], renal failure, hyperthermia and metabolic acidosis, chromosomal aberrations and DNA damage [78-81].

Children are more susceptible than adults to health risk due to lead and cadmium exposure because their gastrointestinal absorption of these metals is greater, and their blood-brain barrier, blood-testis barrier are immature. Children also have different damage repair capacity than adults, and for the same level of exposure, children experience higher internal toxicity dosage per unit body mass compare to adults [15, 55].

3) Theoretical Background

a) Introduction to Electrochemistry

For many years, electrochemists have studied the relationship between chemical parameters and measurements of electrical quantities. Two major electroanalytical techniques that have been extensively utilized in this field of study are potentiometric and potentiostatic methods. Both of these techniques require at least two electrodes and a contacting solution, as these are the basic components of an electrochemical cell. Such electrochemical cell can either be galvanic (producing electricity) or electrolytic (consuming electricity from an external source). Potentiometric (zero current) technique concerns with measurement of potential between two electrodes to obtain information on sample composition. Two major applications of potentiometry are direct potentiometric measurement (based on ion selective electrodes) and potentiometric titration. Potentiostatic (non-zero current) technique (voltammetry), on the other hand, employs potential as a controllable parameter to drive redox reaction at electrode/solution interface. Quantification of resulting current with respect to target analyte's concentration reveals information about electroactive species being studied. Some examples of potential controlled methods are: normal pulse (NP) polarography, square wave (SW) polarography, cyclic voltammetry, stripping voltammetry (anodic/cathodic), and adsorptive-catalytic stripping voltammetry [82].

When an electron transferring process is taking place, a net charge separation is developed between the working electrode and the solution. This creates a potential difference at the electrode/solution interface. This potential difference, $\Delta\phi_{m/s}$, is defined as:

$$\Delta\phi_{m/s} = \phi_m - \phi_s \qquad (1)$$

Where ϕ_m is the potential of the electrode material and ϕ_s is the potential of the solution.

Since direct measurement of $\Delta\phi_{m/s}$ is not experimentally feasible with a single interface, a reference electrode, which has constant potential drop across its solution interface, is introduced into the electrochemical cell. The potential difference (E) being measure is as followed:

$$E = (\phi_m - \phi_s) + \text{constant} \qquad (2)$$

Where $(\phi_m - \phi_s)$ reflects the working electrode potential and the constant reflects reference electrode's potential. This system represents a simple two-electrode cell.

In a reduction with electrons being transferred, the equilibrium potential, E_{eq}, is established by the Nernst equation as followed:

$$E_{eq} = E^0 + (RT/nF)\ln([O]/[R]) \qquad (3)$$

Where E^0 is the standard electrode potential with respect to standard hydrogen reference electrode, F is the Faraday constant, R is the universal gas constant, [O] and [R] are concentrations of oxidized and reduced species at electrode surface, respectively. Equilibrium electrochemical potential measurements allow electrochemists to obtain various equilibrium constants (formation, solubility product, etc.) [83].

If negligible current is passed through solution, equation (2) is approximately correct; however, if a finite current is present, the equation (2) becomes:

$$E = (\phi_m - \phi_s) + \phi_{ref} + iR \qquad (4)$$

The first and second term in equation (4) represent the potential at the working electrode and reference electrode, respectively. The third term, iR, accounts for the potential drop due to passage of current between two electrodes in solution. R is the internal resistant of solution, such internal resistant can be suppressed via addition of inert supporting electrolytes. Due to the passage of finite amount of current, chemical composition of the reference electrode may be altered, which makes ϕ_{ref} no longer constant. To resolve this problem, a third electrode, auxiliary

electrode, is introduced into the electrochemical cell. Via electronic setup, current is only allowed to flow between working and auxiliary electrode, thus ϕ_{ref} will remain constant as no current flows through the reference electrode. An electrochemical cell that contains all three electrodes, working, reference, and auxiliary, is known as a three-electrode system [83, 84].

Current (i) can be defined as the product of the number of electrons transferred (n), electrode surface area (A), Faraday constant (F), and the flux (J).

$$i = -nFAJ \qquad (5)$$

The flux can be thought of as the quantity of material reacting at the electrode surface area per second, or simply the rate of mass transport. Mathematically, the flux is defined by the Nernst-Plank equation as followed:

$$J(x,t) = -D[\partial C(x,t)/\partial x] - (zFDC/RT)[\partial \phi(x,t)/\partial x] + C(x,t)V(x,t) \qquad (6)$$

In order to make sense of the terms in equation (6), modes of mass transport must be defined. These are: diffusion (movement due to concentration gradient), migration (movement due to charge gradient), and convection (movement due to fluid flow or due to density gradient). In equation (6), the first term accounts for diffusion mass transport where D is the diffusion coefficient and $\partial C(x,t)/\partial x$ is concentration gradient. The second term reflects migration mass transport as $\partial \phi(x,t)/\partial x$ is the charge gradient, z and C are charge and concentration, respectively. The third term in the equation represents convection mass transport where V(x,t) is the hydrodynamic velocity and C(x,t) is the concentration. The x and t parameters indicate position and time, respectively.

It would be extremely complicated to quantify current if all three terms in equation (6) are significant. So to simplify the situation, migration mass transport can be suppressed by adding excess inert salts, and convection mass transport can be significantly reduced by using

quiescent solution [82, 83]. Once the second and third terms in equation (6) become negligible, current can be defined by diffusion parameter as followed:

$$i = nFA\ D[\partial C(x,t)/\partial x] \qquad (7)$$

Consider a simple redox reaction: $O_{(aq)} + ne^- \Leftrightarrow R_{(aq)}$, with k_{red} and k_{ox} being the forward and reverse heterogeneous rate constants, respectively. The flux for both anodic and cathodic processes can also be written as:

$$J_a = k_{ox}[R] \qquad (8)$$

$$J_c = -k_{red}[O] \qquad (9)$$

By substituting the flux expression from equation (8) and (9) into equation (5), the anodic and cathodic current can be written as:

$$i_a = -nFAk_{ox}[R] \qquad (10)$$

$$i_c = nFAk_{red}[O] \qquad (11)$$

Since the net current (i_{net}) is the sum of cathodic and anodic current, by combining equation (10) and (11), the net current can be expressed as followed:

$$i_{net} = nFA(k_{red}[O] - k_{ox}[R]) \qquad (12)$$

Via substitution using Arrhenius equation and activation free energy expressions (derivation can be found in reference 83and 84), k_{red} and k_{ox} can be written as a function of the difference between applied potential and formal potential of redox couple ($E-E_0$):

$$k_{red} = k^0 e^{[-\alpha nF(E-E0)/RT]} \qquad (13)$$

$$k_{ox} = k^0 e^{[(1-\alpha)nF(E-E0)/RT]} \qquad (14)$$

Where k^0 is the standard heterogeneous rate constant and α is the transfer coefficient, which takes on values between 0 and 1. By substituting the rate constant expressions in equation (13) and (14) into equation (12), the net current can be written as:

$$i_{net} = nFAk^0 ([O]e^{[-\alpha nF(E-E0)/RT]} - [R]e^{[(1-\alpha)nF(E-E0)/RT]}) \quad (15)$$

Equation (15) is known as Eyring equation, which shows that net current depends on both the potential and surface concentration of both redox forms.

The net current can also be expressed in term of exchange current (i_0), where $i_0 = nFAk^0[R]^{\alpha}[O]^{1-\alpha}$and equilibrium potential as defined in Nernst equation above. The resulted expression is as followed:

$$i_{net} = i_0 (e^{[-\alpha nF(E-Eeq)/RT]} - e^{[(1-\alpha)nF(E-Eeq)/RT]}) \quad (16)$$

The expression above is known as Butler-Volmer equation. The quantity $E-E_{eq}$ is known as overpotential. Butler-Volmer equation can be used to extract information on i_0 and α, which are important kinetic parameters. For sufficient large overvoltage (either positive or negative), one of the exponential term in equation (16) will become negligible compare with the other one. For instant, at large negative overpotential, equation 16 can be simplified to:

$$i_{net} = i_0 e^{[-\alpha nF(E-Eeq)/RT]} \quad (17)$$

The logarithmic form of equation (17) is:

$$\ln(i_{net}) = \ln(i_0) - \alpha nF(E-Eeq)/RT \quad (18)$$

Equation (18) is known as Tafel equation, which is linear at large overpotential. By plotting $\ln(i_{net})$ versus overpotential, α can be determined from the slope and i_0 can be calculated from the y-intercept [82, 84, 85].

Assuming no Faradaic process (electron transfer) is taking place at the electrode surface, there is an electrical double layer at the electrode surface. Such double layer reflects the ionic zones formed in solution due to excess charge at electrode surface. The inner layer, closest to electrode surface, contains solvent molecules and specifically adsorbed ions. The imaginary plane that goes through the center of the specifically adsorbed ions is called the inner Helmholtz

plane (IHP). Solvated ions, limited by salvation shell, cannot come as close to electrode surface; however, these solvated ions do interact with the electrode surface via long-range electrostatic forces (nonspecifically adsorbed). The imaginary plane that crosses the center of the nonspecifically absorbed ionic layer is called the outer Helmholtz plane (OHP). The two layers described previously are compositely known as the Helmholtz layer. Another layer, which is called diffuse or Gouy layer, whose thickness depends on the ionic concentration of solution, is a three-dimensional region of scattered ions, which extended from OHP to bulk solution. The potential-distance profile of the Helmholtz layer, spanning from electrode surface to OHP, is linear; while the potential-distance profile of the diffuse layer is exponential. Double layer structure has not only been found to affect electron transfer rate, its formation also leads to charging current (the current resulted from charging the double layer at electrode-solution interface upon a change in potential), which is problematic in electrochemical experiments that involve very low concentration of electroactive species [82, 85].

b) Cyclic Voltammetry

Cyclic voltammetry (CV) offers a qualitative approach to study behavior of an electrochemical system. CV is often the first experiment performed in an electroanalytical study as it provides information on the kinetics of electron transfer and redox potential locations. The method involves linearly scanning a potential range, both forward and backward, on a working electrode. The resulting current is plotted against applied potential to make a cyclic voltammogram [82, 83]. When the applied potential is sufficient to induce electron transfer, a peak is recorded on the voltammogram. There are several important parameters on a cyclic voltammogram; these include the peak potentials and peak currents. Locations as well as appearance of these features provide information on system reversibility and electron transfer

kinetic. In a reversible system, as soon as reduction or oxidation become thermodynamically favorable, electron transferring takes place as the result of rapid electrode kinetic. The current increases rapidly and drops down as quickly right after reaching a maximum, a peak. On the reverse scan, the same behavior is observed. The applied potentials where the peak currents occur is termed peak potentials. The average of these potentials is the redox couple's formal potential. Separation between anodic and cathodic peak potentials, ΔE_p (in V), for a reversible couple is independent of the scan rate but depends upon the number of electrons (n) involve in the transferring process:

$$\Delta E_p = E_{p,a} - E_{p,c} = (0.059/n) \qquad (19)$$

The peak current (i_p) for a reversible redox couple is defined by Randles-Sevcik equation as follow:

$$i_p = (2.69x10^5)n^{3/2}ACD^{1/2}\nu^{1/2} \qquad (20)$$

Where A is the electrode surface, C is the concentration, D is the diffusion coefficient, and ν is the potential scan rate. According to equation (20), the peak current magnitude is directly proportional to the analyte's concentration and square root of the potential scan rate.

For slow kinetic process, irreversible system, the peak currents are reduced in size and the peak potentials are dependent of the potential scan rate as they shift further away from the formal potential as scan rate increases. The peak current of an irreversible couple is defined as follow:

$$i_p = (2.69x10^5)\alpha^{1/2}n^{3/2}ACD^{1/2}\nu^{1/2} \qquad (21)$$

As indicated in equation (21), the peak current of an irreversible couple is still proportional to the concentration and the square root of the scan rate. However, because of the

transfer coefficient, α, under identical conditions, peak current of an irreversible couple would be smaller than that of a reversible system [83, 84].

An electrochemical system can also be a quasi-reversible; this type of behavior is an intermediate of the two extreme cases discussed above. A redox couple is identified as quasi-reversible when its heterogeneous electron transfer rate constant value, k^0, is between $2x10^{-2}$ and $3x10^{-5}$ cm/s. The voltammogram of a quasi-reversible system, controlled by both kinetic and mass transport parameters, is a function of $k^0/\sqrt{(\pi aD)}$, where $a = nFv/RT$. Therefore, at a very large scan rate, $k^0/\sqrt{(\pi aD)}$ is very small, a quasi-reversible system will appear irreversible and vice versa for very small potential scan rate [82].

Besides electron transfer kinetic and locations of redox peak potentials/currents, CV can also be used to study coupled electrochemical reaction mechanism, interfacial adsorption-desorption behavior of electroactive species, and effect of media on redox process. However, cyclic voltammetry remains mostly a qualitative technique as charging current limits CV sensitivity to approximately 10^{-5} M [82, 86].

c) Stripping Voltammetry

Voltammetric stripping analysis is a powerful technique in quantifying trace levels of organic and inorganic species, especially metals. Its high sensitivity is attributed to a combination of effective pre-concentration methods and high signal-to-noise ratio measurement techniques. The first step of stripping analysis is pre-concentration of analytes onto working electrode surface. Two or three orders of magnitude in sensitivity enhancement is achieve in stripping analysis compare to conventional solution phase measurement because analytes can be pre-concentrated onto electrode surface by a factor of 100 to 1000. Pre-concentration of metals, in the case of anodic stripping voltammetry (ASV), is typically done via application of controlled

cathodic potential for a specific amount of time. The deposition potential is usually 0.3 to 0.5V more negative than the standard reduction potential of the least easily reduced metal ion. Deposition efficiency depends upon the surface area of the working electrode and the deposition time (up to the point of saturation). Pre-concentration is most effective if the electrode is rotated or the solution is stirred as such convection will continuously transport analytes to the electrode surface [85].

Before any further discussion of stripping analysis process, two important pulse voltammetric techniques utilized stripping voltammetry must be addressed, these are differential pulse and square wave voltammetry. The goal of pulse voltammetry is to lower detection limits of voltammetric measurements by selective sampling of current locations where the ratio of Faradaic current (analytical signal current) to charging (background) current is maximized, thus eliminating the effect of charging current. The difference between various pulse voltammetic techniques is the excitation waveform and current sampling methodology [82].

One popular pulse voltammetric method often used in stripping analysis is differential pulse voltammetry (DPV). In DPV, fixed magnitude pulses, superimposed on a linear potential ramp, are applied to working electrode. The current is sample twice, just before the pulse application and at the end of the pulse. The current measured at the first sampling point is subtracted from that of the second sampling point and the current difference is plotted against applied base potential. Besides being discriminative against charging current, another feature of DPV that contributes to increasing sensitivity is its ability to "recycle" metal ions. That is: metal ions can make multiple contributions to analytical signal as only a portion of oxidized ions can diffuse away before the potential is returned to a value at which metal is re-deposited. Due to these features, measurements as low as 10^{-9} M have been reported for DPV. However, favorable

selection of pulse magnitude and scan rate often requires a trade-off among sensitivity, resolution, and speed. Square wave voltammetry (SWV) is another pulse method that is often used in stripping analysis. This is a large-amplitude differential pulse technique in which a symmetrical square wave is superimposed on a staircase potential. The current is sampled twice during each square wave cycle, once at the end of forward and once at the end of reverse pulse. The difference in current between the two points is plotted versus the applied base potential. Not only that SWV possesses the charging current discriminative nature and analyte "recycling" property of DPV, SWV's sensitivity is further enhanced (3-4 time better) compare to DPV as the analytical net current, which is the difference between the forward and reverse currents, is larger than both the forward and reverse components. Another advantage of SWV over DPV is its speed as a complete voltammogram can be recorded in a few seconds using SWV compare to 2-3 minutes using DPV [82, 84].

In anodic stripping voltametry (ASV), following pre-concentration, the potential is scan anodically typically with DPV or SWV. Two parameters are of interest in an anodic stripping voltammogram: the peak potentials (used to identify the metals) and the peak currents' height, which is proportional to metal concentrations. Cathodic stripping voltammetry (CSV) is the counter part of ASV. It involves anodic deposition of analytes, such as cyanide, sulfide, various thiols and halide ions, follows by stripping in the negative potential direction. Another stripping voltammetric technique is adsorptive stripping voltammetry (AdSV). In AdSV, pre-concentration is based on the adsorptivity (adherent tendency) of the analytes to electrode surface. However, this pre-concentration technique does have potential dependency. Besides cation analysis (via insoluble complexes formation), AdSV has been promoted extensively for organic molecules, especially in pharmaceutical industry [87].

d) Atomic Emission Spectroscopy

Atomic emission spectroscopy (AES) is a powerful method, capable of simultaneous multi-element analysis, to quantify trace levels of metals. Operation of AES is based on the principle that electrons in an atom can be promoted (excited) to higher energy levels by absorbing radiation in the form of heat (from flame or plasma). As these excited electrons relax back to the ground state, they emit radiation equal to absorbed energy in the form of light at characteristic wavelengths. By careful selection of wavelengths to monitor, using a wavelength selection device such as a monochromator or a polychromator, identification of elements present in sample is possible as each element has its own set of emission spectrum. Furthermore, the concentrations of different metals in the sample can be obtained by measuring their photon emission intensity profile. Such photon radiation information can be converted into electrical signal by transducers (photomultiplier tubes or photodiodes) for readout/recording convenience.

In atomic emission spectroscopy, the analytes must be converted into free atoms in order to emit or absorb radiation. This conversion step is known as atomization. In atomic emission spectroscopy, continuous atomization of the analytes is accomplished in several processes. In continuous atomization, the heating stages/processes occur sequentially under the influence of heat from the atomizer. Firstly, the sample must be introduced into the flame or plasma (excitation sources) in the form of aerosol (aspiration) by a device called a nebulizer. The most common type of nebulizer is the pneumatic nebulizer; concentric tube, cross-flow, and fritted-disk nebulizer are some example of pneumatic nebulizers. Once entering the excitation source, the heat evaporates the solvent, leaving solid particles in dry aerosol; this process is termed desolvation. After desolvation, the heat from flame or plasma subsequently vaporizes the solid

particles to produce free atoms (volatilization). In vapor phase, analyte can exist as free atoms, ions, or molecules [88, 89].

Atomic emission spectroscopy using flame as excitation source is useful in determining alkali metals and other easy-to-excite elements. However, common flames are not hot (energetic) enough for flame atomic emission spectroscopy (FAES) to detect elements with high excitation energies. Plasma sources, on the other hand, are several thousand degrees hotter than flame sources, which leads to a wider range of detectable elements, higher atomization efficiency, and lower detection limits. The flames used in FAES are chemical flames in which a chemical reaction takes place in gas phase between a fuel and an oxidant (air or oxygen). Some common flames are: C_3H_8/air, C_3H_8/O_2, H_2/air, H_2/O_2, C_2H_2/air, C_2H_2/O_2, and C_2H_2/N_2O. The choice of flame in a given application depends on several factors. For FAES, it is desirable to choose a flame that can provide high atomization efficiency and sufficient excitation energy. However, hotter flames generally produce more ionized species and more susceptible to spectral overlap problems [88, 90].

As mentioned, plasma could be used as another excitation source in AES. The most common type of plasma used in AES is inductively coupled plasmas (ICP). The main body of an ICP torch consists of a quartz tube surrounded by an induction coil connected to a high-frequency generator. Argon, acts as supporting gas for the plasma, can be heated up to 10,000 K by the induced current. Some advantages of ICP compare to flame sources are: high temperature and long sample residence time (lead to higher atomization efficiency), high electron density in argon and low level of molecular species (less ionization and molecular interferences), and no explosive gases involves. Besides ICP, there are two other less common sources of plasma that are used in AES: microwave plasmas and direct current (DC) plasmas. Microwave plasmas

usually do not attain thermodynamic equilibrium, which results in lower gas temperature and lower atomization efficiency compare to ICP. In DC plasmas (plasma jets), sample volatilization is typically not complete due to short residence time [88-90].

Detection limits in FAES: <0.1 ng/ml (Ca, Li, Na), 0.1-10 ng/ml (Al, Ba, Cu, Cr, Cs, Ga, K, Mg, Rb, Sr), 10-100 ng/ml (Ag, Co, Fe, Mo, Tl), 100 ng/ml – 5 µg/ml (Au, Bi, Cd, In, Ni, Pb, Sn, Ti, V), >5 µg/ml (Zn) [88].

Detection limits in ICP-AES: 0.005 -0.05 ng/ml (Ba, Be, Ca, Cu, Mg. Mn, Sr, Ti), 0.05-0.5 ng/ml (Ag, Al, B, Cd, Co, Cr, Eu, Fe, Ge, In, La, Mo, Na, Ni, Sc, V, Zn, Zr), 0.5-15 ng/ml (As, Au, Bi, Er, Ga, P, Pb, Pt, Sb, Si, Te, Th, W) [88].

Interferences in AES can be classified into three categories: spectral interferences, chemical interferences, and physical interferences. Physical interferences are independent of analyte type, in which sample constituents can affect solution viscosity, density, shape of flame and plasma, thus altering nebulization and desolvation efficiency [88].

Overlapping lines spectral interference is very problematic in atomic emission spectroscopy. This is due to interfering species emit radiation within the bandpass of the wavelength selection device. Such interference can be atomic line emission (narrow line) or molecular band emission (broad emission bands superimpose on narrow atomic analyte lines). Such interference can be minimized by using wavelength selection device with higher resolution, by proper choice of analyzing wavelength, or by changes in atomization conditions. As the richness in spectral lines in inductively coupled plasma is much greater than flame due to higher excitation temperature, spectral interference in ICP is potentially more troublesome. Even though background emission in FAES is typically not considered a source of spectral interference, background emission due to recombination of argon ions with electrons in ICP does require

careful consideration. Correction for such background emission can be accomplished by taking background readings on either side of the line of interest; modern instruments also have soft-wares that have routines for de-convolution of overlapping spectral lines [88, 89, 91, 92].

The common chemical interferences in atomic spectroscopy are: solute volatilization interference, dissociation interference, and ionization interference. Solute volatilization interferences are anions and cations that can form low volatile compounds with analyte , such interference can be alleviated by adding releasing agents (cations that react with interfering anions) or protective agents (chemicals that form stable but volatile species with the analyte). Dissociation interferences are concomitants in the sample that influence the degree of dissociation of analyte compounds in vapor phase by altering flame temperature or catalyzing side reactions; analytes that form oxides or hydroxides in flame are most susceptible to dissociation interferences. Dissociation interference could be minimized by using very hot flame. Ionization interference occurs when the population of ionized analyte is significant enough to alter the accuracy of the measurement; this type of interference is more problematic in flame sources as electron density is low, ionization suppressors (chemicals that provide high electron concentration) can be used to resolve ionization interference. Another chemical interference that pertains to AES is excitation interference, where a chemical species can alter the atomizer temperature and thus the fraction of excited analyte atoms. In general, ICP-AES suffers less chemical interferences and matrix effects compare to FAES [88, 89, 91, 92].

e) Scanning Electron Microscopy

Scanning electron microscopy (SEM) is one of the most popular and powerful techniques for examination and characterization of microstructure morphology and composition. In electron microscopy, electron beam is used instead of light source as in optical light microscopy. As

resolution limit is defined as the minimum distance in which the two structures can still be clearly distinguished, in light microscopy, limiting resolution is a function of the illuminating source wavelength according to Abbe equation:

$$R = 0.612\ \lambda\ (N.A.)^{-1}$$

Where R is the resolution, λ is the illuminating source wavelength, and N.A. is the numerical aperture. At a certain source wavelength, if the image is view at a higher resolution than the limiting resolving power, the image would appear blurry. Optical light microcopy has limiting resolution of approximately 200nm [93, 94].

The scanning electron microscope employs a focused electron beam to scan across the surface of sample systematically. The electron beam interacts with the specimen surface to produce signals in form of emitting or deflected electrons that can be converted into visual signal for image display. Unlike light microscopy, in which resolving power depends upon the light source wavelength, for SEM, diameter of the electron beam is the ultimate limiting factor that affects resolution [94]. As mentioned, signals produced from electron beam/sample interactions are used to form the SEM image. When incident electron beam strikes the surface of the sample, most of the electrons in the beam penetrate into the sample some distance before they encounter specimen atomic particles. This creates a region of interaction called primary excitation zone, from which a variety of signals are produced. The depth and volume of this primary excitation zone depend upon the electron beam energy, or accelerating voltage, and the specimen composition. The depth and volume of the excitation region generally increase with higher beam energy and decrease with higher specimen atomic number. Electron beam/sample interactions that produce image forming signals are of two primary groups: elastic interaction and inelastic interaction. In elastic interaction, the electrons from the incident beam collide with the specimen

atomic nucleus or outer electron shells, which results in the electrons from the beam being deflected. There is little energy loss in an elastic interaction, thus these backscattered electrons (BSEs) are highly energetic. Inelastic interaction results in the incident electrons transferring substantial amount of energy to the sample atoms, causing ionization of these atoms and releasing secondary electrons (SEs). These SEs are characterized by low energy (typically about 3-5eV), and due to their low energy, most of these SEs are reabsorbed by the specimen. Only a small number of secondary electrons that are close to the sample surface can escape from the sample though they can only travel a few nanometers. Even though, backscattering electron signal and secondary electron signal are used in image formation of SEM, it must be noted that these are not the only signals produced when an electron beam and specimen surface interacts, other useful analytical signals include: characteristic X-ray, Auger electrons, cathode-luminescence, and others [93, 95].

Backscattered electron signal can provide both composition and topographical information of the sample. A BSE is an electron that experiences a single or multiple scattering events and escapes the sample surface with energy greater than 50eV. Approximately 10-50% of incident electrons are backscattered upon impact with the specimen and roughly 80% of these electrons retain their initial energy. Since BSE signal is almost proportion to atomic number, this signal provides great atomic contrast in SEM image. It must be noted that only those BSEs that travel in a straight path from the specimen to the detector can be used to form BSE image. Also, due to the fact that BSEs are highly energetic, they are not easily absorbed by the specimen, thus the region of sample from which BSEs are produced is much bigger compare to that SEs. For this reason, the resolution of a SEM image produced by BSE signal is much lower compare to SE image. However, since BSEs can come from a wide range of penetration depth, BSE image

carries information about features deep below the sample surface. As useful as BSE signal is in forming SEM image, it limited resolution makes it less desirable compare to SE signal. Most SEM images are formed using SE signal as this analytical signal can produce image with resolved surface structure down to a few nanometers. As mentioned previously, since secondary electrons can only escape the sample surface for a marginal distance, they can be used to accurately mark the electron beam position, thus gives very high topographic resolution. And since most of the secondary electrons actually escaped come from or near the sample surface, surface texture and morphology are most accurately represented by SE signal. The quality of a topographical image produced by SE signal is dependent upon the number of secondary electrons that can actually reach the detector. In an SE image, regions that have structures that prevent the SEs from reaching the detector will appear darker in contrast to those with unobstructed electron path to the detector. Even though SE signal can produce higher resolution SEM images than BSE signal, BSE signal can provide better contrast difference than SE signal. It is worth mentioning that SEs can be produced by three different means: true SEs resulted from electrons from incident beam causing ionization of sample atoms (SE1), SEs resulted from BSEs colliding with sample atoms during deflection events (SE2), and SEs produced when BSEs hit the microscope chamber wall (SE3). Of the three types of secondary electron, only SE1 component provides high resolution signal about the sample [93-96, 99].

As mentioned, volume and depth of the primary interaction zone depend on the power or accelerating voltage of the electron beam. High accelerating voltage allows the electrons to travel further into the sample thus more information on deeper features can be gained. However, the bigger/deeper an interaction zone is, the less detailed topographical information is present in an SEM image. Typically, the accelerating voltage used in forming SEM image is about 5kV. The

electron beam accelerating voltage in low-voltage SEM is 1-2kV. The use of low accelerating voltage not only results in a higher emission efficiency of "close to the surface" SEs, which provides more topographic structure details in the SEM image, it also help reduce charging influence of the electron beam. Charging of the sample can be either positive or negative. When the sample is positively charge (electron input into sample is less than electron output from the sample), the image will appear bright, and when the sample is negatively charged, the image will appear dark. Frequently, as the charges in the sample changes, the image will appear to drift across the screen. In more severe cases where the charge on the sample is sufficiently large, the sample can reflect the incident electron beam causing a scan of the SEM chamber to display. Furthermore, for low atomic number materials, high accelerating voltage can often result in a semi-transparent looking image [93, 95, 98].

A conventional SEM column consists of several main components: an electron gun, condenser and objective lenses, apertures, and signal detectors. The column must be operated in a high-vacuum environment to ensure electron beam can travel without being scattered by air or contamination.

The electron gun in modern SEM must be able to produce a high current, stable electron beam with small spot size and have different adjustable energy levels. Traditionally, SEM systems use tungsten filament and lanthanum hexaboride filament electron guns. However, the current trend in modern SEM is to use field emission electron guns as these provide better brightness, smaller electron beam diameter, lower energy dispersion, and longer lifetime than tungsten and lanthanum hexaboride electron guns. Tungsten guns have been used for a long time, especially for low magnification imaging, due to their reliability and low cost [94, 100]. The most common tungsten electron gun consists of three parts: a V-shaped tungsten filament (the

cathode), a Wehmelt cap, and an anode. The tungsten filament is heated to more than 2800K via application of negative potential to cause the electrons to be emitted from filament tip. The anode is grounded so that the electric field between the filament and anode plate forces the electrons to accelerate toward the anode. The Wehnelt cap, with negative bias to repulse the electrons, provides a crude focusing of the electron beam. The electron emission efficiency increases with increasing filament current upto the point of saturation. Over heating the filament, i.e. applying current pass saturating current, only slightly increases the electron emission efficiency but will reduce the filament lifetime significantly. Lanthanum hexaboride guns are alternatives for tungsten guns. Lanthanum hexaboride has lower work function than tungsten, thus at the same heating temperature, lanthanum hexaboride guns provide better electron emission than tungsten guns. Furthermore, the lanthanum hexaboride guns have smaller electron beam spot size (higher resolution) and smaller chromatic aberration than tungsten guns. However, lanthanum hexaboride guns have limited lifetime as lanthanum hexaboride is readily oxidized at elevated temperature and more susceptible to contamination. Tungsten filament and lanthanum hexaboride filament electron guns are examples of thermionic sources, which require elevated temperature to release electrons from metal surface. Although they are inexpensive, disadvantages such as short lifetime, low brightness, and large energy spread make them less desirable. Field emission electron guns (FEGs) are great alternative for thermionic electron guns. In FEGs, a sharp tip tungsten wire is used as the electron source; the electrons are drawn toward the anode by a strong electric field forms on the wire tip rather than by filament heating. There are three types of FEGs being used in SEM system [95]. The first is cold field emission source, in which the electron gun is operated at room temperature. The second type is thermal field emission source, which requires elevated operating temperature. And last is the Schottky emitter

source; this type of FEG is more preferable to the other two as it can deliver substantially higher emission efficiency at similar energy spread. Even though FEGs offer several advantages over thermionic source, their use is still limited because they require ultrahigh vacuum environment to stabilize the electron beam and prevent contamination [93].

Electron lenses are used to de-magnify the electron beam diameter so narrow electron spot can be formed on sample surface (enhancing the resolution). The two electron lenses used in SEM systems are condenser and objective lenses. As the electron beam passes through the anode plate, the condenser lenses are used to converge and align the beam into a relatively parallel stream. The position of the focal point can be controlled by adjusting the current applied to the condenser lenses. A condenser aperture is used along with the condenser lenses to exclude scattered electrons after the beam passed through the lenses. As the electron beam below the condenser aperture diverges, the objective lens is used to focus the electron beam onto the sample surface and to supply further magnification. There are three designs of objective lens: asymmetric pinhole lens, symmetric immersion lens, and snorkel lens (most preferred). The apertures are not only used to exclude scattered electrons, it can also be used to control spherical aberration of the objective lens. There are two types of apertures: real (which is at the base of the objective lens), and virtual (which is placed above the objective lens). The electron beam shape and sharpness are controlled by these apertures. Decreasing the aperture size will reduce the beam convergence angle thus enhance the depth of field (the portion of the image that appears acceptably in focus) for the same work distance (which is the height of the electron beam cone between the real aperture and the specimen surface). Longer work distance will result in larger depth of field, which is desirable for observation of sample with large topographic variation.

However, if the specimen surface is relatively flat, in which depth of field is not as important, a shorter work distance is typically desired so higher resolution can be achieved [93, 99].

Lens defect can cause cross section of the electron beam to vary in shape, i.e. forming an elliptical cross section instead of a circular one. This results in stretching of image along different direction, a condition known as astigmatism. A "stigmator", which is a series of coils surrounding the electron beam, can be used to correct astigmatism. Besides astigmatism, lens defect can also cause spherical aberration. This is when the peripheral electrons are deflected more than the electrons closer to the beam center, which leads to poor resolution. Reduction of focal length, aperture diameter, and accelerating voltage are useful in reducing spherical aberration. Chromatic aberration is another effect of lens defect. Chromatic aberration is the result of electrons in the beam having different velocities and thus different wavelengths. The differing wavelengths cause the electrons to be brought to focus at different points which results in a blurry image. Chromatic aberration can be corrected by using electron guns with low energy spread and reducing accelerating voltage [98].

As the electron beam is focused into one spot on the sample surface, image forming signals are produced. These signals are recorded to quantify specimen topography and composition via suitable detectors. However, this information only comes from one single spot. In order to form an image, the electron beam must be moved from place to place by a scanning system. This task can be accomplished by scanning coils as these can modulate electron beam trajectory. Primary image forming signal detectors used in SEM systems are solid state BSE detector for backscattered electrons, and Everhart-Thornley (ET) detector for both secondary and backscattered electrons. The ET detector is a key component in the SEM. The front of the detector has a Faraday cage (collector screen), which is positively charged to attract low energy

secondary electrons. If the cage is negatively biased, then BSEs are detected. Once inside the cage, the SEs are accelerated to a scintillator, which is a metal coated disk; as the electrons hit the scintillator, their energy is converted into photon of light. The photon is subsequently transferred to a photomultiplier tube (PMT) via a polished quartz light pipe. In the PMT, photon energy is reconverted into electrons; the PMT voltage, after pre-amplification, is used to modulate the brightness display of the SEM image using cathode ray tube (CRT). Most SEM systems use two types of CRTs, one for viewing (long persistence phosphor, low resolution) and one for photography (short persistence phosphor, high resolution). The scanning process of the CRT is synchronized with the electron beam by a scanning signal generator so a point to point image of the scanned area can be produced. A camera can also be used along with the CRT to record the image on film [94- 96, 98].

Conductive and semi-conductive materials can be readily observed by SEM with minimal sample preparation as long as sample is properly mounted on observing stage/template. Non-conductive samples, such as biological materials, require treatment of coating with conductive film, most often gold coating in a sputtered coater, before SEM can be used. Besides metal coating, most biological samples also require extensive sample treatment to remove water, solvent, and other materials that could vaporize into the SEM column [94, 97].

b) X-ray Photoelectron Spectroscopy

X-ray photoelectron spectroscopy (XPS), which is also known as electron spectroscopy of chemical analysis, is one of the most powerful techniques in studying chemical and structural composition of a sample surface. In XPS, X-ray radiation is used to impact the sample surface so that photoelectrons are emitted from sample atoms. The kinetic energies (KE) of these photoelectrons are measured by a spectrometer whose work function is ϕ. The binding energies

(BE) of the photoelectrons are the interested parameters, which are used in elemental and chemical identification and analysis. Binding energy of a photo electron is a function of its measured kinetic energy according to the following relationship:

$$BE = h\nu - KE - \phi$$

Where hν is the X-ray source energy, the work function, ϕ, of the spectrometer, which is an instrument specific quantity, is included in the equation above to account for the loss of kinetic energy of the photoelectron as it travels through the spectrometer (Steve Higgins, personal communication). The binding energy of a photoelectron is characteristic of the orbital where it originated and the final state of photoemission [101, 102].

The technique of XPS is known as a surface sensitive technique as only electrons from the top few atomic layers (approximately 10nm) can escape without loss of kinetic energy and contribute to the analytical signal, the deeper electrons will also escaped but with some loss of energy due to inelastic collisions and will contribute to background signal [103]. X-ray photoelectron spectroscopy enables qualitative identification of almost all elements in the periodic table, except hydrogen and helium. Simple identification can be accomplished by taking low resolution spectra (survey scans) over a broad binding energy range. If chemical state and quantitative atomic concentration of sample atoms are of interest, then high resolution spectra can be recorded in specific region of binding energy. Furthermore, angle-resolved XPS and XPS imaging can provide information on spatial distribution and chemical composition of atoms in the sample. If the sample is a thin film, XPS can be used to determine the film thickness and morphology [101, 104].

X-ray photoelectron spectroscopy utilizes soft X-ray (200-1500eV) to examine core-level electrons. As mentioned previously, photoelectrons are emitted as X-ray radiation is impinged on

the sample surface. These photoelectrons are collected by electron optics and directed into an electron analyzer where they are sorted by energy. The number of photoelectrons at each energy mark is then transduced into electrical signal via an electron detector. The photocurrent is then converted and processed into a spectrum. In XPS, ultrahigh vacuum environment is required to maintain sample surface cleanliness/integrity, and minimize scattering of the photoelectrons by other gas molecules. At the sample surface, the monochromatic X-ray beam can have a diameter ranging from 5mm to 1μm. And also as mentioned, even though photoelectrons are produced in the specimen through the entire X-ray penetration volume, due to short inelastic mean free path (the distance the electrons can travel without losing energy due to interaction), only photoelectrons produced at the top several atomic layers can retain their characteristic energies and contribute to the analytical signal while deeper photoelectrons will only contribute to background noise [101, 103].

One of the main components in an XPS instrument is the X-ray source. In XPS, the X-ray sources must be able to produce beams with sufficient energy to overcome binding energies of core electrons. Also, the X-ray emission must have high intensity and narrow linewidth. Common X-ray sources in XPS are: NaKα, MgKα, AlKα, ZrLα, TiKα, and CuKα. Of these, MgKα (1253.6eV) and AlKα (1486.6eV) are most commonly used in commercial XPS systems. In an XPS X-ray source, a large electrical potential is applied between the cathode, usually a heated tungsten filament, and the anode, this result in a high flow of electrons being accelerated toward the anode surface. As the electrons from the cathode strike the anode, X-ray radiation is generated in two processes: bremstrahlung radiation and X-ray fluorescence. In the bremstrahlung process, electrons from the cathode experience continuous deceleration as they approach the anode nucleus. The loss of kinetic energy from these electrons decelerating results

as a continuous spectrum of X-ray emission. In X-ray fluorescence, the core electrons of the anode atoms are ejected by the energetic cathode electrons. As higher level electrons relax down to the vacant "holes", they emit characteristic X-ray radiation. As the result of the two processes, the X-ray emission spectrum of the X-ray source is a continuous spectrum with superimposed characteristic peaks. Such X-ray radiation can be used directly without any further modification on the sample. Even though direct X-ray sources can result in high photoelectron throughput to the detector, the major disadvantage associates with direct X-ray sources is sample damaging due to bremstrahlung radiation. To circumvent this problem, a monochromator can be used to select desired emission lines and remove bremstrahlung continuum. The crystal used in such monochromator must be able to withstand X-ray energy yet still produce high intensity output of desired wavelengths. The most common X-ray source/monochromator configuration is the AlKα X-ray source/quartz crystal monochromator. Besides the X-ray sources discussed above, X-ray radiation from synchrotron source (continuous energy radiation resulted from electrons moving at very high speed in circular orbit) is also used in XPS; however, due to high monetary cost and limited accessibility, the use of synchrotron radiation in X-ray photoelectron spectroscopy is still very limited [101, 105, 106].

As mentioned, the sample-emitted photoelectrons are directed into an electron energy analyzer by collecting lens to be sorted by energy. Although the linewidths of the measured photoelectron peaks mostly depend on the X-ray source's linewidth, the sensitivity and resolution of a XPS spectrometer depend upon its electron energy analyzer. Concentric hemispherical analyzer (CHA), which is also called hemispherical sector analyzer, is the most common energy analyzer in XPS due to its superior resolution. The CHA consists of two stainless steel hemispheres with negative potentials, at different magnitudes, applied to both

hemispheres. The photoelectrons ejected by the sample are focused into the analyzer entrance slit; the photoelectrons traveling through the space between the hemispheres are separated by kinetic energy via varying the applied voltage of the hemispheres. As the electrons exit the analyzer, they enter an electron detector, such as an electron multiplier tube or a microchannel plate, where electronic signal is converted into electrical signal for spectral processing and production [101].

As the photoelectrons being emitted from the specimen, the sample becomes positively charged. The charged surface can affect the kinetic of the photoelectrons which lead to error in measuring energy of the electrons. With conductive samples, such sample charging can be alleviated by electrically connecting the sample to the spectrometer. This electrical contact allows accurate measurement of the photoelectrons energies as the spectrometer is set to measure the electrons kinetic energies with respect to its own Fermi level [105]. Electrical connection, however, is not beneficial in reducing charge of non-conductive samples. Therefore, different techniques of charge neutralization must be used. Some of these techniques are: using flood guns to pump low energy electrons into sample to replace emitted photoelectrons, using non-monochromatic X-ray source, placement of low energy electron sources, i.e. metallic walls, close to sample, and application of external bias [107, 108].

Sample damaging by the X-ray is a big concern in XPS experiments. Damage from X-ray radiation is more severe in soft biological samples, polymers, and thin film specimens [109]. Physical damages include creation of point defects, changes in surface crystal structures, and changes in surface topography. Chemical damages not only result from X-ray radiation but also from secondary electrons generated as by-products. Such chemical damages include changes in oxidation state of sample atoms, and chemical bond cleavage. Furthermore, chemical

composition of the specimen surface can also be altered by the X-ray radiation. X-ray radiation can lead to increase adsorption of background gas molecules, desorption of chemisorbed species, migration of surface species, and enhanced surface reactivity. In general, the use of monochromatic X-ray sources is recommended to reduce sample damage as the radiation energy is substantially lower [101].

An X-ray photoelectron spectrum is a plot of photoelectron count versus binding energy. The peaks in the range of 0-15eV typically associate with valence electron emission. Since valence electron orbitals are often delocalized or hybridized, peaks representing ejection of valence electrons are closely spaced thus give rise to valence bands appearance. These valence band spectra, when used in conjunction with core level spectra which include characteristic core level peaks appearing at higher binding energy, can be very useful in identifying similar compounds. In low binding energy region of the spectrum, spectral background noise can be attributed to secondary electron emission, while at higher binding energy portion of the spectrum, inelastic electron scattering is the main contributor to the background noise. Typically, prior to analysis, background noise is removed using various schemes such as linear or Shirley removal scheme, principle component analysis, and polynomial approximation [103, 109, 110].

Typically, data on binding energies of the photoelectrons is sufficient for elemental identification as one can compare experimentally determined binding energies to tabulated values. In many cases, a low resolution survey spectrum is sufficient for such purpose. However, if chemical state analysis is desired, then a high resolution spectrum must be obtained. Chemical shift information can be very useful in determining the sample atoms chemical state as shift in binding energy reflects change in specimen oxidation state as well as presence of other chemically active components around the interested species. Besides its qualitative aspect, XPS

also offer quantitative capability, although the sensitivity level is not very great. By integrating the spectral peak areas, the concentrations of different elements in the sample can be determined [101, 111].

X-ray photoelectron spectroscopy can also be used to produce spatially resolved images, which is known as mapping of sample surface. XPS imaging provides information of surface species composition and morphology. The first method of XPS imaging involves focusing the X-ray beam diameter to a smallest possible spot. The image can be collected by either scanning the X-ray beam across the sample surface or by moving the sample under a fixed X-ray beam. The disadvantages associated with this XPS imaging technique are low spatial resolution (resolution is limited by X-ray beam diameter), and time consuming (each XPS image must be built pixel-by-pixel). Another method of surface mapping using XPS is parallel XPS imaging. This technique utilizes position-sensitive 2D electron detector to acquire sample surface data. Although the image is still built pixel-by pixel, the second method of imaging provides much better spatially resolved images (around 3μm) compare to the first imaging method as the resolution in the second imaging technique is only limited by the lens system. Angle-resolved XPS allows the sample to be analyzed at various depths by tuning the takeoff angle of the photoelectrons via tilting the sample. By reducing the takeoff angle, the escape depth of the photoelectrons is reduced, which leads to more surface-sensitive information present in the spectrum. By recording and analyzing XPS spectra as a function of depth into the sample, depth-profiling of sample is possible. Angle-resolved XPS, therefore, can be used to estimate the thickness of a film layer. Furthermore, angle-resolved XPS can be combined with XPS imaging to produce 3D information on the sample [101, 112].

4) Stripping Voltammetric Analysis of Heavy Metals: Literature Review of Different Macro Electrodes

In the past few decades, tremendous progress has been made in developing electrochemical sensors to detect and quantify trace levels of polluting metals in aqueous environment. The development of these sensors not only utilizes the chemical properties of various modifying reagents to promote interaction with metal ions, but also looks into techniques to modify the morphology of the sensors' surface to enhance sensitivity. A comprehensive, although not exhaustive, literature review of various types of macro electrodes that have been developed and studied to quantify trace levels of heavy metals (including, but not limited to, Pb and Cd) via stripping voltammetric analysis in the past two decades is presented in subsequent sections of this document.

a) Mercury-based Electrodes

Mercury-based electrochemical sensors have been extensively employed in stripping voltammetric analysis of metals at trace levels. Mercury-based electrodes are known for their high sensitivity, large potential windows, and wide range of detectable metals [113, 127]. Besides the famous hanging mercury drop electrode (HDME), mercury film modified electrodes are also quite popular. The following section provides a review of recent developments in mercury film modified carbon electrodes.

The use of ultrasound during deposition of mercury film on glassy carbon electrode (GCE) and during deposition of lead and cadmium ions onto electrode surface was proven to be beneficial as sensitivity of stripping analysis improves by one order of magnitude [114]. The application of ultrasound is postulated to improve mass transport efficiency thus enhancing deposition efficiency. Mercury (optimal concentration of 0.2mM) is deposited on GCE surface at

optimal condition of -1V for 30 seconds at pH =4.6 under optimal untrasound intensity of $30Wcm^{-2}$. Nafion coating is applied to GCE surface (mixture of 10µl Nafion and 5µl N,N-Dimethylformamide is spin coated on GCE) prior to Hg film deposition to maintain the film integrity during insonication. Lead and cadmium are co-deposited onto Nafion coated Hg-CPE at -1.25V for 30 seconds (also in presence of untrasound). The detection limit for both metals is estimated to be 0.3nM, with linear stripping peak response range from 5 to 50nM. Reproducibility of the electrode response (for Cd only) is expressed as relative standard deviation (RSD), at Cd concentration of 10nM, as 1.2% for 10 measurements. Batch injection analysis (BIA) has also been shown to be useful in stripping analysis of Pb and Cd using Nafion coated Hg-GCE [115]. Unlike conventional pre-concentration method, in BIA, small volume of the to-be-deposited analytes is injected from a micropipette tip toward the electrode surface [104]. Using BIA, Hg is coated on Nafion modified GCE surface by injecting 10µl of 0.1M Hg solution toward the electrode surface at potential of -1V, this potential is held for an additional 60 seconds after injection. Also using BIA, Pb and Cd are co-deposited on Nafion coated Hg-GCE via 4 successive injections of 25µl at 10 seconds increment under constant potential of -1V. Detection limits are estimated to be 2.0nM for Cd and 4.0nM for Pb. BIA offers two distinct advantages over conventional pre-concentration technique- it requires very small amount of sample and uses much less Hg [116].

Besides improving pre-concentration technique, adding modifying reagents to Hg films can also enhance the electrodes' sensitivity and selectivity to metals. Incorporation of silver on Nafion coated Hg-GCE has been investigated in quantification of Pb and Cd [117]. In order to deposit the Ag/Hg amalgam film on the electrode surface, the Nafion coated GCE (made by spin-coating 5µl Nafion solution on GCE and cured in IR light for 10 minutes) is submerged in

Ag/Hg solution (1:1 molar ratio) for 3 hours. The electrode is subsequently doped with 0.5M H_3BO_3 for 300 seconds at constant potential of -0.6V. At optimal potential of -1V, Pb and Cd are co-deposited for 120 seconds at pH=4.5. The stripping peak current linear response range is 1 to 48ppb for both metals with estimated detection limits of 0.34ppb and 0.55ppb for Pb and Cd, respectively. Reproducibility of electrode response is reported in term of relative standard deviation as 3.13% for Cd and 3.61% for Pb at 30ppb (n=8). Anodic stripping analysis of Pb and Cd using poly(ester sulfonic acid) modified mercury-glassy carbon electrode (PESA-Hg-GCE) is also studied [118]. Ten microliters of 25% PESA solution (made by dissolving PESA in water/acetone solvent) is spin-coated on GCE, the electrode is cured in warm (70 ^{0}C) air stream for 1 minute. Mercury is co-deposited with Pb and Cd for 64 seconds at potential of -1V. Peak current response linearity range is 10 to 100ppb for both metals as the detection limits are estimated to be 5.9ppb for Pb and 3.4ppb for Cd. Comparing with Nafion coated Hg-GCE, the PESA-Hg-GCE performs better in the presence of non-ionic surface active surfactant (SAS) Triton X. Polypyrole (PP) and its derivatives, poly(acenaphtho[1,2-c]pyrrole) (PANP), and poly(4,9-dihydro-o-benzenonaphtho[2,3-c]pyrrole) (PDBNP), are investigated as modifying reagents for Hg-GCE in detection of Pb and Cd [119]. The polymers are individually electro-deposited on GCE surface at 1.1V (PP), 0.85V (PANP), and 1.15V (PDBNP). The polymers are subsequently reduced by applying -0.5V until the current levels off. Lead and cadmium are co-deposited with mercury under optimal potential of -1.25V for 120 seconds at pH=4.6 in the presence of ultrasound (intensity of 20Wcm^{-2}). Stripping peak current magnitudes for both metals are highest for PDBNP and worst for PP. This is explained by the difference in polymers' backbone structure: the more closely packed the backbone, the less activity with metal ions. Thiocyanate modified Hg-GCE is another electrode system that has been investigated to quantify

Pb and Cd at trace level [120]. Thiocyanate (optimal concentration = 5mM) and mercury are co-deposited with target metals at optimal potential of -1.5V for 300 seconds at pH=5.6. Thiocyanate is postulated to facilitate Hg plating and prevents formation of mercuric oxide at the electrode surface, thus improving pre-concentration efficiency. Reproducibility assessment reveals RSDs of six measurements at concentration of 90ppb are 1.7% for Cd and 2% for Pb. Dimethylglyoxime (DMG), for Cd detection, and 2,2'-bipyryridyl (Bpy), for Pb detection, have been proven to be useful chelating agents for Hg-CPE modification [121]. The chelating agents are individually co-deposited with mercury for 6 minutes at optimal potential of -0.8V. Voltammetric stripping signal of Cd at DMG-Hg-GCE is linear in the range range of 1 to 80ppb, with estimated detection limit as 0.1ppb. Cadmium is pre-concentrated under optimal potential of -1V for 5 minutes at pH=9. Similarly, stripping response of Pb at Bpy-Hg-GCE is linear in the range of 1 to 100ppb, with estimated detection limit as 0.1ppb. Lead is pre-concentrated under optimal potential of -0.6V for 5 minutes at pH=4. The use of catechol and its derivatives, 4-methyl catechol, 4-t-butyl catechol, and resorcinol, as complexing reagents has been shown to be beneficial in quantifying Pb and Cd using Hg-GCE [122]. It is proposed that the ring substituents can function as complexing ligands. The metal ions are allowed to react with the complexing reagents before being deposited onto Hg-GCE surface. Different metal complexes are pre-concentrated onto Hg-GCE at different potentials. Lead complexes are deposited at 0.14V for 180 seconds, while cadmium complexes are deposited at 0.4V for 180 seconds. The metal ions are subsequently stripped cathodically. For both metals, cathodic stripping peak current magnitudes are highest when resorcinol is used as complexing reagent. The worst responses are obtained when catechol is used.

The discussion so far pertains to only glassy carbon electrode template; however, Hg film can also be deposited on other carbon electrodes, for example, the impregnated carbon paste electrode [123]. Carbon powder (after heated to 500 ^{0}C) is wax impregnated by mixing with ceresin wax and n-hexane. The mixture is then heated until n-hexane evaporated. The working electrode paste is made by mixing wax impregnated carbon powder with silicon oil at 5:3 (w/w) ratio. Mercury film is deposited onto electrode surface by applying potential of -0.9V for 5 minutes at pH=4.5 to 0.1mM Hg(II) solution. The optimal pre-concentration potential and time interval for Cd and Pb are -0.75V and 120 seconds. The detection limit (for Pb only) is estimated to be 1.1ppb. Besides film modification, mercury can also be deposited on electrode surface as nano-droplets. The use of nano-droplets Hg-chitosan-multiwalled carbon nanotubes modified screen printed carbon electrode (NanoHg-CTS-MWCNTs-SPE) to detect trace level Cd and Pb has been shown to be promising [124]. Five millimeters of chitosan stock solution is refluxed with 5ml of multiwalled carbon nanotubes for 10 hours. The previous mixture is printed onto SPE to form CTS-MWCNTs-SPE. Mercury nano-droplets are deposited on CTS-MWCNTs-SPE under potential of -1.3V for 1 hour at pH=5. Lead and cadmium are co-deposited onto electrode surface for 300 seconds at pH=4.8 under optimal potential of -1.2V. The detection limits for Pb and Cd are estimated to be 12nM and 23nM, respectively. Relative standard deviations are calculated for 10 measurements at concentration of 600nM as 3% for Cd and 4.5% for Pb. Stripping peak current interference from K, Na, Ca, Mg, Fe(II), Zn, F, Cl, and Br is not significant for this electrode system.

Besides mercury film sensors, modification reagents can also be applied on hanging drop mercury electrode (HDME). Oxine (8 -hydroxyquinoline) modified HDME has been shown to be able to quantify Pb and Cd at part per billion level [125]. Oxine (at optimal concentration of

20μM) is co-deposited with Pb and Cd onto HDME at -1.1V for 60 seconds at pH=7.7. Anodic stripping current responses are linear in the range of 1.9 to 10ppb for Cd and 3.5 to 10ppb for Pb; detection limits are calculated to be 0.59 and 0.93ppb for Cd and Pb, respectively. Relative standard deviation measurements for 5 experiments are 5.5% for Cd at concentration of 1.9ppb and 4.1% for Pb at concentration of 3.5ppb. Xylenol orange has also been shown to be a useful complexing reagent when used in conjunction with HDME [126]. Lead and cadmium are co-deposited with xylenol orange (at 4.0μM) on HDME surface at -1.5V for 60 seconds (pH=5.5). Stripping current response is found to be linear in the range of 5 to 200ppb for Pb and 10 to 200ppb for Cd. The detection limits are estimated to be 0.98 and 1.18ppb for Pb and Cd, respectively. Relative standard deviations are 2.1% for Cd and 2% for Pb (obtained from 10 measurements at metal concentration of 100ppb). One hundred folds excess of Mn, Mo(VI), Fe(II), and 20 folds excess of Ni, Cr(III), Co do not appear to interfere with Pb and Cd stripping peak signals.

b) Sensors Modified With Bismuth and Other Metals

As popular as mercury-bases sensors are, they are not ideal for commercialization due to the toxic nature of mercury. Significant progress has been made in the effort to move away from mercury-based electrodes. Several other less toxic metals have been proposed as replacements for mercury in modifying electrochemical sensors for quantification of heavy metals. In particular, bismuth-based electrodes have gained a lot of attention in this field as the sensitivity of these electrodes has been shown to be comparable to that of mercury-based electrodes. The following section provides a review of recent developments in bismuth-based electrodes as well as other metal-based sensors in quantification of trace levels heavy metals in aqueous environment.

Nano-molar level detection of Zn, Cd, Pb, and Cu has been reported by using bismuth film modified graphite-polyurethane composite electrode [128]. Working graphite-polyurethane composite paste, which is known to be eco-friendly, is made by mixing graphite powder and polyurethane (from vegetable oil) in 3:2 (w/w) ratio. Bismuth(III) (at optimal concentration of 48μM) is co-deposited with the metals of interest onto graphite-polyurethane composite electrode at optimized potential of -1.4V for 120 seconds. Bismuth film is postulated to form low-temperature melting alloys with target metals thus facilitating deposition of these metals on the film. Stripping peak current response linearity ranges for Zn, Cd, Pb, and Cu are 4-15nM, 4-100nM, 4-40nM, and 4-150nM, respectively. The detection limits are estimated for the four metals as 0.6nM for Zn, 2.2nM for Cd, 1.1nM for Pb, and 2.7nM for Cu. Interference study reveals that stripping signals appear to be slightly enhanced at low concentration (1-5ppm) of surface active surfactants (SAS) (Triton X and albumin), but at SAS concentration higher than 10ppm, the stripping peak current is suppressed. Bismuth film is also used to modify edge plane pyrolytic graphite electrode [129]. The process of making the EPPGE electrode will be described later. Bismuth film is co-deposited with Pb and Cd on to EPPGE at optimal potential of -1.2V for 120 seconds at pH=4.5. The optimal concentration of Bi solution used is 1ppm. Compared to stripping peak current responses of Bi-EPPGE, the responses at bare EPPGE are much lower (at concentration of 25ppb, Cd stripping peak magnitude is 10 times smaller and Pb stripping peak is 3 times smaller). The linear response ranges of current signal are 0.1 to 100ppb for Cd and 0.1 to 300ppb for Pb; the detection limits are estimated to be 0.06 and 0.08ppb for Cd and Pb, respectively. Besides EPPGE, Bi film is also applied on graphite-epoxy composite electrode to detect lead and cadmium [130]. The process of making graphite-epoxy composite electrode will also be discussed later. Bismuth, at optimal concentration of 0.4mg/l, is co-deposited with Pb and

Cd under optimized potential of -1.3V for 120 seconds at pH=4.5. The ranges of linear response are 50 to 150 ppb for Pb, with corresponding detection limit of 23.1ppb, and 10 to 100ppb for Cd, with an estimated detection limit of 2.2ppb. Glassy carbon electrode is also used as deposition template for Bi film [131]. Bismuth is co-deposited with Pb and Cd under optimized potential of -1.2V for 120 seconds at pH=4.5, the optimal concentration of Bi is 0.4mg/l. Compare to Hg-GCE, at 50ppb, Bi-GCE is two times more sensitive in Pb detection and three times more sensitive in Cd detection. Both metal stripping current responses are linear in the range of 5 to 200ppb, with estimated detections limit (for Pb only) as 1.1ppb. Relative standard deviation measurements are 2.4% for Cd and 4.4% for Pb (at concentration of 80ppb and n=22). The Bi-GCE is further modified by Nafion-graphene film in a separate study [132]. Graphene, which is made up of planar sheets of sp^2-bonded carbon atoms packed into a honeycomb-like lattice, is dispersed into Nafion solution via ultrasonic agitation for 30 minutes. Five microliters of the previous suspension is spin-coated onto GCE surface. The combination of Nafion and graphene is postulated to not only discriminate against SAS interference but also enhance electrode sensitivity due to nano-structural organization of the graphene sheets. Bismuth is co-deposited with Pb and Cd at optimal potential of -1.2V for 120 seconds. The detection limit for both metals is estimated to be 0.02ppb, with linear response range of 0.5 to 50ppb for Pb and 1.5 to 30ppb for Cd. Besides Nafion-graphene Bi-GCE, polyaniline coated bismuth film modified glassy carbon electrode (PANI-Bi-GCE) is another electrode system that has been shown to be useful [133]. Aniline monomers (at optimal concentration of 5mM) is deposited onto GCE via multiple pulse potentiostatic electro-polymerization (pulse voltammetry in short) to make PANI-GCE. Lead and cadmium are co-deposited with Bi (at concentration of 1.25μM) at optimized potential of -1.3V for 120 seconds. At lead and cadmium concentration of 25nM, the stripping

peak current responses of PANI-Bi-GCE are twice as large compared to those of PANI-GCE. Linearity response range is 25 to 150nm for both metals, while the detection limits are estimated to be 11.1 and 16.5nm for Cd and Pb, respectively. Reproducibility of electrode stripping signal is expressed in terms of relative standard deviation at concentration of 25nM (n=10) as 5.95% for Cd and 3.31% for Pb. Interference study reveals that the Cd peak is more sensitive to SAS interference than Pb stripping peak. Modification of carbon paste electrode (CPE) with fibrinogen (an abundant protein in blood) and Bi film to quantify Pb and Cd has also been reported [134]. The working paste is made by mixing 1g of carbon powder with 300µl of paraffin oil. Fibrinogen is deposited on CPE is by submerging the electrode in fibrinogen solution (5g/l) at pH=7 for 10 minutes. Bismuth (optimal concentration of 0.5mg/l) is deposited onto fibrinogen modified CPE by applying constant potential of -1.2V for 120 seconds to form Fbg-Bi-CPE. Lead and cadmium are pre-concentrated onto Fbg-Bi-CPE via batch injection analysis (100µl of sample is injected toward electrode at potential of -1.2V, this potential is held for another 60 seconds after injection to ensure reduction of Pb and Cd ions at electrode surface). Linear response range is 0.5 to 500nM for both metals, with detection limits estimated to be 1 and 0.5 nM for Cd and Pb, respectively. Zeolite doped carbon paste electrode, modified with Bi film, has been investigated in another study [135]. The working paste is composed of zeolite/graphite powder/silicone oil mixture at optimized 10/190/80 (w/w) ratio. Zeolite (aluminosilicates) is a porous material that has high cation exchange capacity and good thermal stability. Bismuth (at optimal concentration of 0.2mg/l) is co-deposited with Pb and Cd for 120 seconds at -1.2V. The peak current responses obtained from zeolite-Bi-CPE (at metal concentration of 20ppb) are 30% higher than those of bare Bi-CPE. The detection limits are estimated to be 0.08 and 0.1ppb for Cd and Pb, respectively; the linear response range for both

metals is 1 to 20ppb. Reproducibility of analytical signal is expressed as relative standard deviation (RSD) at 20ppb (n=12) as 3.1% for Cd and 2.3% for Pb.

Besides carbon-based, bismuth film can also be used other substrates. For example, successful quantification of Pb and Cd has been reported using Bi film modified silicon-based electrode [136]. Bismuth is sputtered onto a photoresist coated silicon wafer to an optimized thickness of 0.4µm using a thin film deposition system. The sputtered wafer is shaped into an electrode via photolithography. Nafion solution is subsequently spin-coated onto electrode surface. Lead and cadmium are co-deposited on electrode surface at optimal potential of -1.2V for 120 seconds. Relative standard deviations for 8 measurements at 20ppb are 3.8% for Pb and 3.1% for Cd. The detection limit is estimated to be 0.5ppm for both metals. Stripping peak currents of Pb and Cd are stable when upto 10 folds in excess of Mn, Co, Ni, Ca, Mg, and Zn are present.

The discussion of bismuth-base electrode so far only pertains to Bi film modified sensors; however, solid Bi electrode has also been used to quantify Pb [137]. Pre-concentration of lead on solid disk bismuth electrode is carried out at optimized potential of -1.2V for 60 seconds. Two different mode of mass transport enhancement during pre-concentration are investigated: electrode vibration and solution stirring (vibration frequency and stir rate are not specified). It is found that detection sensitivity is enhanced by a factor of two when the electrode is vibrated compare to conventional solution stirring. The detection limit (for vibrated electrode) is estimated to be 1nM, with linear response range from 10nm to 1.5µM and RSD at Pb concentration of 10nm (n=7) is 6%.

As mentioned earlier, besides bismuth, other metallic reagents, such as tin, antimony, gold, etc., have also been investigated as substitutes for mercury. The recent developments of

different modified sensors using these metals as modification reagents to quantify heavy metals are discussed in the following section.

Lead film modified GCE has been shown to be suitable for Cd detection [138]. Lead (at optimal concentration of 1mM) is simultaneously deposited with Cd at optimal potential of -1.3V for 300 seconds onto GCE. Detection limit is calculated as 0.6nM, with stripping peak response linearity range from 2nm to 1µM. Reproducibility of electrode signal is stated in term of RSD as 3.6% for 5 measurements at Cd concentration of 20nM. Surface active surfactants do not influence stripping peak of Cd up to concentration of 5ppm. Furthermore, ten folds excess of Ni, Mn, Zn, Cu, Fe(II) also do not exhibit interfering behavior toward Cd stripping peak. Glassy carbon electrode modified with iridium oxide film has also been shown to be useful in detecting Pb [139]. Iridium oxide film is grown on GCE surface by applying constant potential of 0.84V for 60 seconds to iridium solution (pH=10.5) containing 1.5g/l $IrCl_4.H_2O$. The iridium oxide-GCE is placed in water for 24 hours before first use. Lead is deposited on the modified electrode at potential of -0.52V for 60 seconds. Detection limit is estimated to be 7nM, and relative standard deviation for 10 measurements at Pb concentration of 0.5µM is 2.5%. It is found that up to 100 fold excess of Ni, Co, Cu, Cd, and Fe(II) do not cause significant interference on Pb stripping current response. Antimony has been examined as possible modifying reagent on GCE for analysis of Cd and Pb [140]. The target metals are co-deposited with Sb film (optimized concentration at 0.75mg/l) at optimal potential of -1.5V for 120 seconds at pH=2. Response linearity ranges are 10 to 100ppb and 10 to 120ppb for Cd and Pb, respectively. The detection limits are estimated to be 1.2ppb for Cd and 1.4ppb for Pb. Relative standard deviations for 6 measurements at 50ppb are 2.8% for Cd and 2.6% for Pb. Besides GCE substrate, Sb is also deposited on boron doped diamond (nanoSb-BDD) electrode as nano-particles; this electrode

system has also been shown to be useful in detecting Pb and Cd [141]. Similar to GCE substrate, Sb (optimal concentration of 0.5mg/l) is co-deposited with Pb and Cd onto BDD electrode surface at optimal potential of -1.1V for 120 seconds. However, Sb ions are deposited on BDD electrode as nano-particles rather than film. Stripping peak current responses are found to be linear from 250 to 500ppb for Cd and 50 to 500ppb for Pb. The detections limits are calculated to be 150ppb for Cd and 19ppb for Pb.

Besides lead and antimony, quantification of heavy metals is also possible using tin film modified electrodes. Tin film is deposited on GCE surface and CPE surface (made by mixing 1.5g carbon powder and 1.2ml Nujol oil) simultaneously with cadmium and zinc [142]. The optimal deposition potential and time are -1.5V and 120 seconds. Comparing stripping peak current responses from Sn-GCE and Sb-CPE for Cd, Sn-GCE signal is more well-defined and has flatter baseline; therefore, GCE is the better substrate. Using Sn-GCE, linear response range is 5 to 60ppb for both metals, with the detection limits estimated to be 0.7ppb and 0.9ppb for Cd and Zn, respectively. Relative standard deviations at 20ppb obtained from 8 measurements are 3.6% for Cd and 4.2% for Zn. In a different study, tin film has been further modified with polystyrene to increase the film porosity [143]. It is postulated that by increasing the film porosity, the electrode's internal electro-active area also increases thus the sensitivity is enhanced. Polystyrene spheres (500nm) are spread over a gold electrode surface and allowed to dry for two days. The polystyrene modified gold electrode is submerged in 0.1M tins solution for 15 minutes at constant current of -1.2mA so Sn ions can be deposited on to polystyrene opals, thus forming a porous film. Lead and cadmium are simultaneously deposited on the working electrode surface at optimal potential of -1.2V for 100 seconds. Porous Sn film modified electrode is three times more sensitive compared to nonporous Sn film modified electrode. The

detection limits for Cd and Pb are estimated to be 0.7ppb and 0.5ppb, respectively. Stripping peak current signals for both metals are linear in the range of 20 to 120ppb. Relative standard deviations from 10 measurements at 50ppb are 2.6% for Cd and 3.1% for Pb. Gold film modified screen printed carbon electrode (SPE) has also been used to detect heavy metals [144]. Gold film is deposited on SPE at potential of -0.4V for 240 seconds. After film deposition, the Au-SPE is subjected to constant oxidative potential (0.7V) for 120 seconds to remove any native oxide. The optimal deposition condition for Pb is -1.1V for 120 seconds, while the optimal pre-concentration condition for Hg is 0.3V for 120 seconds. Both Pb and Hg stripping peak current responses are found to be linear in the range of 2 to 16ppb; the detection limits are estimated to be 1.5ppb and 0.5ppb for Hg and Pb, respectively. Reproducibility of analytical signal is quantified in terms of relative standard deviations (n=4) as 3% for Hg and 6% for Pb, both at 10ppb. A mixture of gold, platinum nano-particles and organic nano-fibers (3, 3', 5, 5'-Tetramethylbenzidine (TMB)) has been shown to be suitable modifying reagent for GCE as this electrode system is used to quantify trace level mercury [145]. Gold and platinum nano-particles can be simultaneously reduced with TMB nano-fibers, which have been shown to have excellent coordination capability with transition metals, to create a porous structure/network that has high catalytic property. The solid product of the reaction between 4mM H_2PtCl_6 and 2.5mM TMB is dispersed into ethanol. Ten microliters of this mixture is dropped on glassy carbon electrode surface and the modified electrode is dried at 50 ^{0}C. Gold nano-particles are deposited onto previously modified electrode via cyclic voltammetry (12 cycles in 0.5mM $HAuCl_4$) to form Au/PtNPs-NFs-CPE. Mercury ions are pre-concentrated and reduced on Au/PtNPs-NFs-CPE at optimal potential of 0.5V for 100 seconds. The electrode signal is found to be stable for 30 days. The detection limit is estimated to be 8ppt, with RSD (n=10) at 2ppb as 1.2%. Interference study

reveals that 10 folds excess of Co, Cr (III), Zn, Mn, Fe(II), and Cu have negligible interferening effect on stripping peak of Hg.

c) Organic Polymers/Complexing Ligands Modified Electrodes

Besides metal films, electrochemical sensors can also be modified with organic polymers or complexing ligands that are highly reactive with the target metals. The following section provides a review of recent developments on the specific electrode modification reagents.

Chitosan, a naturally abundant polymer that can binds to transition metals, is used as modifying reagent on screen printed carbon electrode (SPE) to detect Pb, Cu, Cd, and Hg [146]. Homogenized mixture, optimized ink composite, of 0.75g of chitosan, 5g polyvinyl alcohol, and 3g of carbon powder is printed on SPE to make chitosan-SPE. The four target metals are simultaneously deposited onto chitosan-SPE for 30 seconds at potential of -1V. Stripping peak current responses are linear in the range of 20-160ppb for Pb, 20-80ppb for Hg, and 10-200ppb for Cd and Cu. The detection limits are estimated to be 3.4, 5.0, 5.0, and 2.0ppb for Pb, Cu, Cd, and Hg, respectively. Signal reproducibility data (reported for Pb only) in term of relative standard deviation, obtained from 4 measurements, is 4.1% at 50ppb. The interference tolerance level of this electrode system is 100 fold excess of Tl, Zn, Sb, Fe(II), Co, Al, and As. Also, chitosan-SPE is found to be stable for 6 months. Poly (3,4-ethylenedioxythiophene) (PEDOT), poly (aniline-4,4'-diaminodiphenyl sulphone) (poly (ANI-co-DDS)), poly (3,4-ethylenedioxythiophene-diclofenac) (poly (EDOT-co-DCF)) are used as modifying reagents on glassy carbon electrode to quantify Pb, Cd, and Cu [147]. The polymers are individually deposited onto GCE surface via application of linear sweep voltammetry in potential range of -0.6 to 1.3V to the monomer solutions. The target metals are simultaneously deposited onto the polymer modified electrodes at optimal potential of -1.5V for 60 seconds at pH=4. Stripping

analysis reveals that the best sensitivity is obtained with PEDOT modified GCE, whose shelf-life is approximately 20 days; the detection limits estimated with PEDOT modified GCE are 2ppb for Cu and 1ppb for Pb and Cd. The linear response range for all three metals with PEDOT modified GCE is 3 to 200ppb. Poly (ANI-co-DDS) modified GCE shows worst sensitivity as the detection limits are in the order of part per million. Another polymer that has been used as modifying reagent on GCE for metal detection is polycyclodextrin [148]. Cyclodextrin molecular structure resembles a basket cavity, i.e. a receptor-like feature, in which the metals ions can affine. Two different cyclodextrin (CD) polymers are used, alpha and beta, which have six and seven D-glucopyranose units, respectively. The monomers (at 0.01M) are individually electro-polymerized onto GCE via cyclic voltammetry (30 cycles of potential range 1.3 to -0.85V). Lead and cadmium are co-deposited onto polymer modified GCE at optimal potential of -0.9V for 60 seconds. Preliminary cyclic voltammetric analysis reveals that beta-CD-GCE exhibits better analytic performance than alpha-CD-GCE. The detection limits are estimated for alpha-CD-GCE to be 0.63μM for Pb and 2.5μM for Cd; similarly, the detection limits estimated for Pb and Cd using beta-CD-GCE are 0.71μM and 0.21μM, respectively. Lead and cadmium detection using *p-tert*-butylthiacalix [4]arene (TCA) modified GCE has also been reported [149]. TCA belongs to thiacalix class ligand that offers excellent metal complexing ability. TCA film is built onto GCE surface by vertical dipping at surface pressure of 24mN/m. The modified electrode is air dried for 30 minutes before first use. Lead and cadmium are co-deposited at optimal potential of -1.2V for 5 minutes at pH=4.8. Compare to bare GCE, significantly higher sensitivity in stripping peak signal is obtained with TCA-GCE. The detection limits are calculated for Cd as 20nM (linear response range of 0.2 to 50μM), and for Pb as 8nM (linear response range of 0.1 to 25μM). Relative standard deviations from 4 measurements at 1μM are 3.2% for Cd and 2.9% for

Pb. The cation interference tolerance level for TCA-GCE is 1000 folds excess of Zn, Fe(II), Co, Ni, Ag, and 100 folds excess of Hg, Cu. Poly(phenol red) is another GCE modifying reagent that has been reported to be capable of detecting lead [150]. Phenol red is postulated to complex with metal ions via sulfur functional group. Poly(phenol red) (PPR) film (5mM monomer solution) is deposited onto GCE surface by the application of cyclic voltammetry for 60 segment at potential range of 0 to 2V in pH=7. Lead is pre-concentrated onto PPR-GCE at optimal potential of -0.8V for 120 seconds at pH=2.5. Cyclic voltammetric study further reveals that the redox process for Pb at PPR-GCE is reversible. Lead stripping current response is linear in the range of 5 to 500nM, with detection limit estimated to be 2nM. Relative standard deviation for 10 experiments at Pb concentration of 50nM is 4.4%. Five hundred folds excess of Na, Mg, Mn, Cr(III) and 200 folds excess of Zn, Co, Ni, Cu, Cd, and Ca do not appear to significantly interfere with Pb stripping peak signal.

Beside GCE, organic complexing reagents can also be used on carbon paste electrodes (CPE). The detection of mercury using poly (vinyl sulfonic acid) (PVSA) modified CPE has been investigated [151]. In order to form the working paste, a mixture of 1.9ml methyl-trimethoxysilane, 1.5ml ethanol, 1.5ml water, 0.2ml 11M HCl, 0.25ml 10% polyethylene glycol, and 1g of PVSA is ultra-sonicated for 2 minutes before 2.7g of carbon powder is added. Mercury is pre-concentrated onto electrode surface by immersing the electrode in Hg solution (at pH=3) for 8 minutes. The pre-concentrated Hg ions are subsequently reduced by applying a potential of -0.3V for 60 seconds. At Hg concentration of 1μM, the stripping peak current obtained from PVSA-CPE is 44 times higher than that of bare CPE. The peak current response is found to be linear from 50nM to 50μM, with the detection limit estimated to be 15nM. Reproducibility of analytical signal is reported as relative standard deviation for 20 measurements at 100nM as

4.3%. A different study reported the use of keratin (from chicken feathers) as a modifying reagent in CPE for quantification of Pb [152]. The chicken feathers are cleaned, sun-dried, ground and the powder is oven-dried. The feather powder is then mixed with carbon powder and Nujol oil to form the working paste, the optimal amount of feather is 8%. Lead is pre-concentrated onto feather-CPE at optimal potential of -1.5V for 300 seconds. Detection limit for Pb is estimated to be 0.12ppm, with linear response range of 0.5 to 5ppm. Relative standard deviation for 10 measurements is calculated to be 4.5% at Pb concentration of 1ppm. The feather-CPE shelf-life is estimated to be 5 months. Interference study reveals that up to 10 folds excess of Cr(III), Cd, Zn, Co, Ni, and Mg do not interfere with Pb stripping peak signal. Another organic ligand incorporated CPE that has been reported to be promising in detection of Pb and Cd is diacetyldioxime modified carbon paste electrode (DADO-CPE) [153]. Diacetyldioxime can complex with metal ions via its NOH functional group. The working paste is composed of 10mg diacetyldioxime, 50mg carbon powder, and 20µl paraffin oil. Lead and cadmium are co-deposited onto DADO-CPE at optimal potential of -1.1V for 5 minutes at pH=5.The stripping current responses are linear in the range of 0.1 to 15µM for Pb and 0.25 to 25µM for Cd. The detection limits are estimated to be 10nM and 4nM for Pb and Cd, respectively. Relative standard deviations for 6 measurements at 0.5µM are 2.9% for Pb and 3.2% for Cd. Cation interference tolerance level for this electrode system is 4000 folds excess of Ca, Zn, Mg, Mn, and 400 fold excess of Co, Fe(II), Cu.

d) Porous Silica-based Electrodes

As mentioned earlier, high porosity on electrode surface is often desired as high porosity means large electro-active surface area which leads to higher sensitivity. In order to increase the porous density of an electrochemical sensor's surface, most of the time, a modifying reagent with

porous property is used. Silica gel, with high porous property and excellent physical stability, is often the choice [154, 155].

Dipyridyl nano-porous silica gel (DPSG) modified carbon paste electrode has been shown to be useful in detecting mercury [156]. The working paste is made by mixing 150mg DPSG, 600mg graphite powder, and 250mg paraffin oil. Optimal pH range for deposition of Hg is 3 to 4 and optimal potential and time are -0.2V for 450 seconds. At 80nM, stripping peak current of DPSG-CPE is almost 10 times higher than that of bare CPE. The reproducibility of analytical signal is expressed in term of relative standard deviation (RSD), which is calculated to be 5% for 6 measurements at Hg concentration of 40nM. Detection limit is estimated to be 8nM, and linear response range is 20 to 100nM. Furthermore, 50 folds excess of Pb, Zn, Cd, Cu, Ni, and 500 folds excess of Cr(III), Co, Fe(II), Mn show little interference on Hg stripping peak. Carbamoylphosphonic acid on mesoporous silica (CAMS) is another silica gel based modifying reagent that has been used on CPE for quantifying Cd and Pb [157]. The mixture of acetamide phosphonic acid and mesoporous silica gel is homogenized with carbon powder and mineral oil to form working electrode paste (20% CAMS, 80% carbon paste). Cation exchange property of acetamide phosphonic acid coupled with high electro-active surface area of porous silica gel is proposed to enhance sensitivity of the CPE. Pre-concentration of metal ions onto modified electrode surface is done in open circuit for 20 minutes. The metal ions adsorbed are reduced via electrolysis at potential of -1V for 60 seconds. Linearity range of current response is 10 to 200ppb for both metals, with detection limit estimated to be 10ppb. Relative standard deviation for 7 measurements at Pb concentration of 50ppb is 5%.

Carbon paste electrode modified with zirconium phosphate porous silica gel (SiZrPH) has been shown to be capable of detecting Pb at nano-molar concentration [158]. The SiZrPH is

made by refluxing 50g silica gel, 11.6g $ZrCl_4$ in 300ml ethanol for 8 hours. Twenty five grams of solid product is shaken in 200ml 0.1M phosphoric acid for 10 hours. The precipitate, after being oven-dried for 4 hour at 100 ^{0}C, is mixed with 0.6g of carbon powder and 0.25g of paraffin oil to make the working paste. Open circuit pre-concentration of Pb ions onto electrode surface is carried out for 2 minutes; the metal ions are subsequently reduced at potential of -1V for 1 minute. Detection limit for Pb, with linear response range of 2.5nM to 50nM, is estimated to be 0.35nM. Relative standard deviation for 7 measurements at Pb concentration of 10nM is 4.2%. Interference effect on Pb stripping peak signal due to Zn, Co, Cr(III), Mg, Mn (at 2000 fold excess) and 200 folds excess of Ni, Cd is negligible. Besides carbon paste electrode, porous silica can also be used to modify screen printed electrode (SPE) as quantification of Pb using mesoporous silica nano-particles modified SPE has been reported [159]. Functionalized nano-particle mesoporous silica (FNPMS) is prepared by reacting calcined tetraethylorthosilicate/ Tergitol NP-9 suspension with 5-mercapto-1-methyltetrazole. The resulting FNPMS is oven-dried at 110 ^{0}C for 4 hours. Carbon powder, mineral oil, and dried FNPMS (at 3:1:1 (w/w) ratio) are mixed together to form working paste. The paste is printed on SPE to form FNPMS-SPE. Lead ions are pre-concentrated onto modified SPE surface for 5 minutes with no applied potential. The accumulated ions are subsequently reduced at -1.2V for 120 seconds. With response linearity range of 1 to 30ppb, the detection limit is estimated to be 0.1ppb. Reproducibility of analytical signal is expressed in term of relative standard deviation (n=3) as 5% at Pb concentration of 20ppb.

e) Other Novel Electrodes

One of these novel electrodes is the silver-methylcrylate carbon paste composite electrode [160]. The main component of this electrode is the carbon-based paste which is made

by mixing methylcrylate resin, graphite powder, and silver powder at optimized weight percentage ratio of 60:20:20. The silver-methylcrylate carbon paste composite electrode is dried at room temperature for approximately six hours before first use. Lead ions are pre-concentrated and reduced on the electrode surface at optimized constant potential of -1.2V for 200 seconds. Stripping voltammetric analysis of Pb at this electrode reveals that the range of signal linearity is 10 to 200ppb, the detection limit is estimated to be 3ppb. Another electrode system that has been developed to quantify Cd is the boron doped diamond (BDD) electrode [161]. The working BDD disked is made by vapor deposition of boron doped diamond particles on graphite substrate. Cadmium ions is deposited and reduced at the electrode surface by applying optimized potential of -1.8V for 60 seconds at pH=4.8. This pre-concentration step is ultrasound assisted using optimized intensity of 155Wcm^{-2}. Ultrasound assisted deposition is found to enhance stripping detection limit for Cd (3.9 nM) by a factor of 6 compare to silent deposition. The presence of surface active substance interference (Triton X), up to 3µM, does not significantly affect stripping peak magnitude. In a separate study, BDD electrode is also used to quantify Zn and Cu [162]. The optimized deposition potential for both metals is -1.3 V for 180 seconds. Compare to pure Zn stripping peak, the peak current of Zn stripping is severely suppressed when Cu was co-deposited. This phenomenon is attributed for the fact that Cu ions have higher affinity to electrode surface than Zn ions, thus outcompeted Zn ions in the deposition process.

Solid silver working electrode is also studied in stripping analysis of Pb and Cd [163]. Solid silver electrode is used to quantify Cd and Pb in horseradish roots. Using subtractive square wave anodic stripping voltammetric (SWASV) analysis, with optimal deposition potential at -0.8V for 100 seconds, the concentrations for Pb and Cd in plant material are determined to be 2.13 ±0.2 and 3.56 ±0.25ppm, respectively. Thallium is found to effect stripping peak of Cd

significantly at concentration greater than 1/12 of Cd concentration. Closely related is the silver-gold alloy working electrode, which was also investigated in a separate study to quantify Pb and Cd [164]. It is found that 50/50 (w/w) Ag-Au alloy electrode's, which is made by melting exact quantities of Ag and Au, behavior is intermediate of pure gold and silver electrodes. Furthermore, it is found that the Ag-Au alloy electrode is more suitable to quantify Tl in the presence of Pb and Cd than individual quantification of Pb and Cd via voltammetric stripping analysis. Another novel electrode developed for quantification of Cd is carbon paste electrode made with peroxide oxidized activated carbon [165]. Pristine activated carbon powder is oxidized by treatment of 30% peroxide and ultrasonication for 10 hours. The peroxide oxidized activated carbon (200mg) is oven dried at 120 ^{0}C before mixing with 600mg regular graphite powder and 240µl paraffin oil to form the paste. Cadmium is pre-concentrated on electrode surface for 120 seconds at optimal potential of -1.1V. Compare with peroxide oxidized activated carbon modified carbon paste electrode (H_2O_2-AcC-CPE), unoxidized activated carbon modified carbon paste electrode stripping peak current magnitude is approximately 12 times smaller at Cd concentration of 0.5µM. The detection limit of H_2O_2-AcC-CPE is estimated to be 5nM with linearity response range from 0.05 to 5µM. In term of signal reproducibility, the relative standard deviation at Cd concentration of 0.5µM for 10 measurements is 6.8%. Interference study reveals that 10,000 folds excess of Al, Zn, Ca, Fe (II), 1000 folds excess of Pb, Ni do not significantly affect striping peak magnitude of Cd. Unmodified edge plane pyrolytic graphite electrode (EPPGE), which was mentioned earlier, is also utilized to detect trace level of Cd and Pb [166]. Pyrolytic carbon is produced by heating hydrocarbons to decomposition temperature and let graphite crystallized during cooling process. Edge plane sites, which are highly reactive, are created by cutting layered highly ordered pyrolytic graphite sheets to make steps [167].

Cadmium and lead are pre-concentrated on electrode surface at optimal potential of -1.2V for 240 seconds at pH=4.6. With response linearity range of 2 to 20 ppb, the detection limits for Cd and Pb are estimated to be 0.3 and 0.2 ppb, respectively. Another electrochemical sensor that has been shown to be promising in detection of Pb is nitrogen doped tetrahedral amorphous carbon (Ta-C:N) on silica substrate [168]. Ta-C:N film is coated on silica substrate by introducing pure graphite target in filtered cathodic vacuum arc deposition chamber with optimal nitrogen flow rate of 20 standard cubic centimeter per minute (SCCM). The optimal deposition potential and time for Pb ions for this electrode are -1.4 V and 120 seconds. This electrode system has also been shown to be useful in quantification of mercury and copper.

Another novel electrode that is useful to quantify Pb and Cd is the barium hydrogen phosphate carbon paste electrode (BHP-CPE) [169]. Alkali and alkali earth metal phosphates are known for their catalytic and ion exchange properties. Barium hydrogen phosphate powder, made by reacting $BaCl_2.2H_2O$ with K_2HPO_4 for 1 hour, is mixed with carbon powder and Nujol oil at optimal ratio 3:77:20 (w/w) for 30 minutes to make the working paste. Optimal deposition potential for both Pb and Cd is -1.2V at pH=7 for 300 seconds. With linear response range from 10nM to 80nM for both metals, the detection limits are estimated to be 1.5 nM and 3nM for Cd and Pb, respectively. Reproducibility of electrode response is quantified in terms of relative standard deviations (n=8) at 50nM as 3.6% for Cd and 4.0% for Pb. In addition, 1000 folds excess of Na, Ca, Ba, Sr, 100 folds excess of Sn, Co, and 10 folds excess of Ni show no interference with stripping peak current of Pb and Cd. Graphite-epoxy composite electrode, which was mentioned earlier, also has been shown to be capable of detecting Pb at part-per-billion level [170]. The electrode paste is made by mixing graphite power and epoxy resin at 1:4 (w/w) ratio with hardener. The electrode is cured for a week at 40 ^{0}C before first use. Lead is

pre-concentrated at electrode surface at optimized potential of -1.4V for 60 seconds at pH=4. The detection limit is estimated to be 10ppb and the linear response range is 50 to 500ppb. Relative standard deviation at Pb concentration of 100ppb (n=4) is 21%. Another electrode system that has been utilized to study trace level of Pb is the titanium carbide (TiC) composite electrode [171]. The TiC mixture is made by mixing titanium powder, activated carbon powder, and phenol-formaldehyde resin under 50 KPa pressure. The paste is dried and hot pressed at 2100 ^{0}C to form solid TiC electrode. The electrode is shown to be electrochemically stable for one week. Relative standard deviation for 5 measurements at 20 nM of Pb is 2%. The electrode stripping response is linear in the range of 10 to 100nM; the detection limit is estimated to be 2nM. Moreover, interference tolerance level for TiC electrode is 100 folds excess of Cd, Co, Ni, Zn, Cu, 10 folds excess of Sb, and 5 folds excess of Se. And lastly, multi-walled carbon nanotubes (MWCNTs) modified glassy carbon electrode has been used to detect Pb and Cd at trace level [172]. Modifying MWCNTs mixture is made by ultrasonicating 5mg of MWCNTs, 5mg of dihexadecyl hydrogen phosphate, and 5ml of water. Five microliters of this mixture is coated onto GCE to make MWCNTs-GCE. Lead and cadmium are simultaneously deposited onto MWCNTs-GCE surface at optimal potential of -1.2V for 5 minutes at pH=4.5. At metals'concentration of 0.5µM, the stripping peak current responses obtained with MWCNTs-GCE are approximately 5 times higher than those obtained with bare GCE. The detection limits are estimated to be 6nm for Cd and 4nM for Pb, with linear response range of 20nM to 10µM for both metals. Analytical signal reproducibility is expressed in terms of relative standard deviations from 10 measurements as 4.2% for Cd and 4.5% for Pb at 0.5µM.

II. Experimental

1) Materials

Methyltrimethoxysilane (MTMOS), Ti(IV) isopropoxy, Zr(IV) propoxy, Tween 80, Tween 20, Ammonium Tetraflouroborate (ATFB),$Pb(NO_3)_2$, $Cd(NO_3)_2$.$4H_20$, $K_2Fe(CN)_6.3H_2O$, Triton-X, Cetyl trimethylammonium bromide (CTAB), $NaCH_3COO$, KNO_3, KCl, Hydrated nitrate salts of Mg, Ca, Fe, Cu, Co, Ni, were purchased from Sigma-Aldrich. Concentrated H_2SO_4, HNO_3, glacial Acetic acid, and Isopropanol were from Wright State Lab Store. Capillary tubes (1.5-1.8 mm I.D., 10cm, borosilicate glass opened both ends) were from Kimble Chase. Graphite powder (7-11 micron, 99%) was from Alfa Aesar. Standard reference Pb solution (1000 ppm) and Cd solution (100 ppm) were from Hach- Lange. Cellulose acetate syringe filters (0.22 micron) and syringes were from Cole-Parmer.

2) Apparatus

Bioanalytical System Epsilon potentiostat was used to conduct all CV and SWASV experiments. Utilizing three electrodes electrochemical cell, the Ag/AgCl (3 M NaCl) reference electrode and the platinum wire auxiliary electrode were employed for all voltammetric measurements. Furthermore, all CV and SWASV experiments were carried out at room temperature. In addition, all SWASV experiments were done with stirring during the pre-concentration step, followed by anodic stripping step after 5 seconds quiet time, with stripping square wave frequency = 25 Hz, square wave amplitude = 25 mV, and ΔE step = 5mV.

ICP-OES measurements were obtained with ICP-OES (Agilent 710 series) and morphological characterization of the electrode surface was studied by an electron scanning

microscope (SEM, Philips XL 30 ESEM-FEG) and X-ray photoelectron spectroscopic system (XPS, PHI 5400, Mg X-ray).

3) Chemicals

For optimization electrode synthesis parameters as well as estimation of kinetic parameters, 0.01 M Pb in 0.1 M ATFB and 0.01 M Cd in 0.1 M ATFB solutions were used. For estimation of electrode surface area, 0.001 M $K_2Fe(CN)_6$ in 0.1 M ATFB solution was used. Acetate buffers (made by titrating appropriate volume of 0.1 M sodium acetate into 0.1 M acetic acid) and 1 M HNO_3 were used to adjust pH in CV experiments. pH adjustment in all SWASV measurements were done using 1 M HNO_3. For optimization of SWASV parameters, Pb and Cd solutions of $1x10^{-7}$ M were used.

With respect to interference analysis via SWASV, baseline signals were obtained with 100 ppb Pb and Cd solutions. For surface active substances interference analysis, solutions of Triton-X and CTAB at 1000, 500, 200, 100, 50, 20, 10, and 1 fold excess of Pb or Cd (weight to weight ratio) were used. Similarly, for cations interference analysis, solutions of Ca, Mg, Ni, Fe, Co, and Cu at 2000, 1500, 1000, 500, 200, 100, 50, and 20 folds excess of Pb or Cd (w/w ratio) were used.

River water and well water from Saigon, Vietnam, and river water from the Great Miami river in Dayton, Ohio, were used in the study. These water samples were syringe-filtered using 0.22 micron cellulose acetate filters. Appropriate amounts of KNO_3 were added to the filtered water samples to make 1 M solution, then 1 M HNO_3 was added to adjust the solutions' pH to 3. The acidified solutions were spiked with Pb or Cd standard reference to make 100 ppb solution. Analysis of Pb and Cd in spiked river water and well water samples, using SWASV and ICP-

OES, were done via multiple standard additions. Standard solutions of Pb and Cd (at 4 ppm) were added in increment of 0.15 ml to 10 ml of test solution.

4) Sample calculations

a) Electrode surface area estimation

$$I_p=269\ n^{3/2}\ AD^{1/2}\ Cv^{1/2}$$

Plotting I_p versus $v^{1/2}$ to obtain linear fit, and then using the slope to calculate surface area:

$A=slope/(269*n^{3/2}*D^{1/2}*C) = 2.02x\ 10^{-5}/\ (269*1*0.0028*0.001) = 0.027$ cm

(slope = $2.02x\ 10^{-5}$, n=1, D=7.6E-6 cm^2/s, C= 0.001 M)

b) Estimation of electron transfer coefficient (α)

Plotting potential versus natural log of current in the rising portion of the cathodic peak to obtain linear fit (simple Tafel plot); the slope of this fit is equaled -αnF/RT.

For Pb, α = slope / (-nF/RT) = -34.57/ (-[2*96, 485.34]/ [8.314*298]) = 0.44

(slope = -34.57, n=2, F= 96,485.34 sA/mol, R= 8.314 J/Kmol, T= 298K)

c) Estimation of heterogeneous electron transfer rate constant (k_0)

Measuring the potential separation (ΔE_p) at different scan rates (20-120 mV/s), then use the working curved which related ΔE_p to Ψ[23, 24] in order to estimate Ψ values, and then use the following equation to estimate k_0 at each scan rate, then average to obtain the overall k_0 value.

$$k_0 = \Psi\ (\pi Dv)^{1/2}[(nF)/(RT)]^{1/2}$$

For Pb, at v= 20 mV/s and Ψ= 0.68, then:

$k_0 = 0.68*(3.14*1.38x\ 10^{-5}*0.02)^{1/2} * ([2*96, 485.34]/ [8.314*298])^{1/2} = 5.59x\ 10^{-3}$ cm/s

(π= 3.14, D= $1.38x\ 10^{-5}$ cm^2/s, n=2, F= 96,485.34 sA/mol, R= 8.314 J/Kmol, T= 298K)

d) Detection limit estimation

Using 3-sigma method, the current magnitudes (at interested analyte's oxidative potential) from 10 independent blanks are converted to concentration values using the linear fit equation obtained in linear calibration range study, the average "blank" concentration plus three times the standard deviation of the "blank" concentration is the detection limit.

For SWASV of Pb, the average "blank" concentration is calculated to be 0.245 ppb using the lower concentration linear calibration equation (Current = 1.2*Concentration +1.65)

Detection limit = 0.245 + 3*0.078 = 0.479 ppb (1 sigma = 0.078)

e) Concentration calculation from multiple standard additions

The current is related to the concentration as followed:

$I_u = K*C_u$

$I_{u+s} = K*[(V_uC_u+C_sV_s)/(V_u+V_s)]$

$I_{u+s}*(V_u+V_s) = K*V_uC_u + K*C_sV_s$

(I_u is the current response from testing solution, I_{u+s} is the current response from testing solution + added standard, V_u is the testing solution volume, V_s is the volume of standard added, C_u is the concentration of the interested analyte in testing solution, C_s is the concentration of standard, and K is an arbitrary constant, which will be dropped during the calculation process).

By multiplying the current reading (I_{u+s}) to the total liquid volume (sum of testing solution volume and volume of standard added) ($V_u + V_s$), this product is plotted versus the volume of standard added (V_s) to obtain a linear fit.

At y= 0, we have $V_uC_u = C_sV'_s$, in which V'_s is the x-intercept (or – y-intercept/slope).

For SWASV analysis of Pb in river water (trial 1), the linear fit equation is y= 1526x + 388.7

$C_u = -V'_sC_s/ V_u = -[(-388.7/1526)*4000]/10 = 101.9$ ppb

(C_s = 4000 ppb, V_u = 10 ml)

f) Relative standard deviation calculation

Relative standard deviation (RSD), expressed as a percentage, is the ratio of the standard deviation to the average, which is used as a measurement of the reproducibility of an experiment. For 10 independent SWASV runs of Pb at 100ppb, the average measurement is 6.06×10^{-5}A and the standard deviation is calculated to be 1.53×10^{-6}. The RSD is calculated to be:

$RSD = (1.53 \times 10^{-6} / 6.06 \times 10^{-5}) * 100\ \% = 2.52\ \%$

III. Results and Discussion

1) Optimization of electrode synthesis parameters

a) Optimization of heating temperature and duration

For optimization of heating conditions, the following temperatures were chosen: 290 ^{0}C, 375 ^{0}C, 452 ^{0}C, and 525 ^{0}C, and the selected heating durations were: 10, 20, and 30 minutes. The electrode carbon paste used for heating optimization had the following composition: 1.5 mL MTMOS + 0.3 mL 1 M H_2SO_4 + 0.5 mL Iso-propanol +Ti isopropoxy/Zr propoxy (0.3 mL each) + 3 g Carbon. Heating is known to help with the annealing process as well as developing the electrode crystalline surface structure [1-4]. The range of heating temperature above was selected because too low of a temperature would not be sufficient to develop the surface structure, while too high of a temperature would lead to surface cracking thus damaging the electrode surface [173, 174]. For the same reasons, the heating durations above were selected. By running cyclic voltammogram (CV) of the different electrodes heated at different temperature/duration combinations in 0.01 M Pb and 0.01 M Cd solutions (in 0.1 M ATFB supporting electrolyte), the oxidative current magnitudes were collected and compared. For each heating condition combination, data from multiple different electrodes were collected.

Figure 1A and 1B illustrated that, for both heavy metals, the overall trend appeared to be increasing heating time meant lower response (this can be understood as the result of overheating). Asides from this general trend, no other obvious correlation can be observed. Furthermore, at the heating combination 375 ^{0}C /10 min, the electrode response appeared to be optimum for both heavy metals, but for cadmium it was much more obvious compared to lead. Therefore, 375 ^{0}C /10 min was selected to be the optimal heating condition combination for the TiO_2/ZrO_2 carbon paste composite working electrode [181].

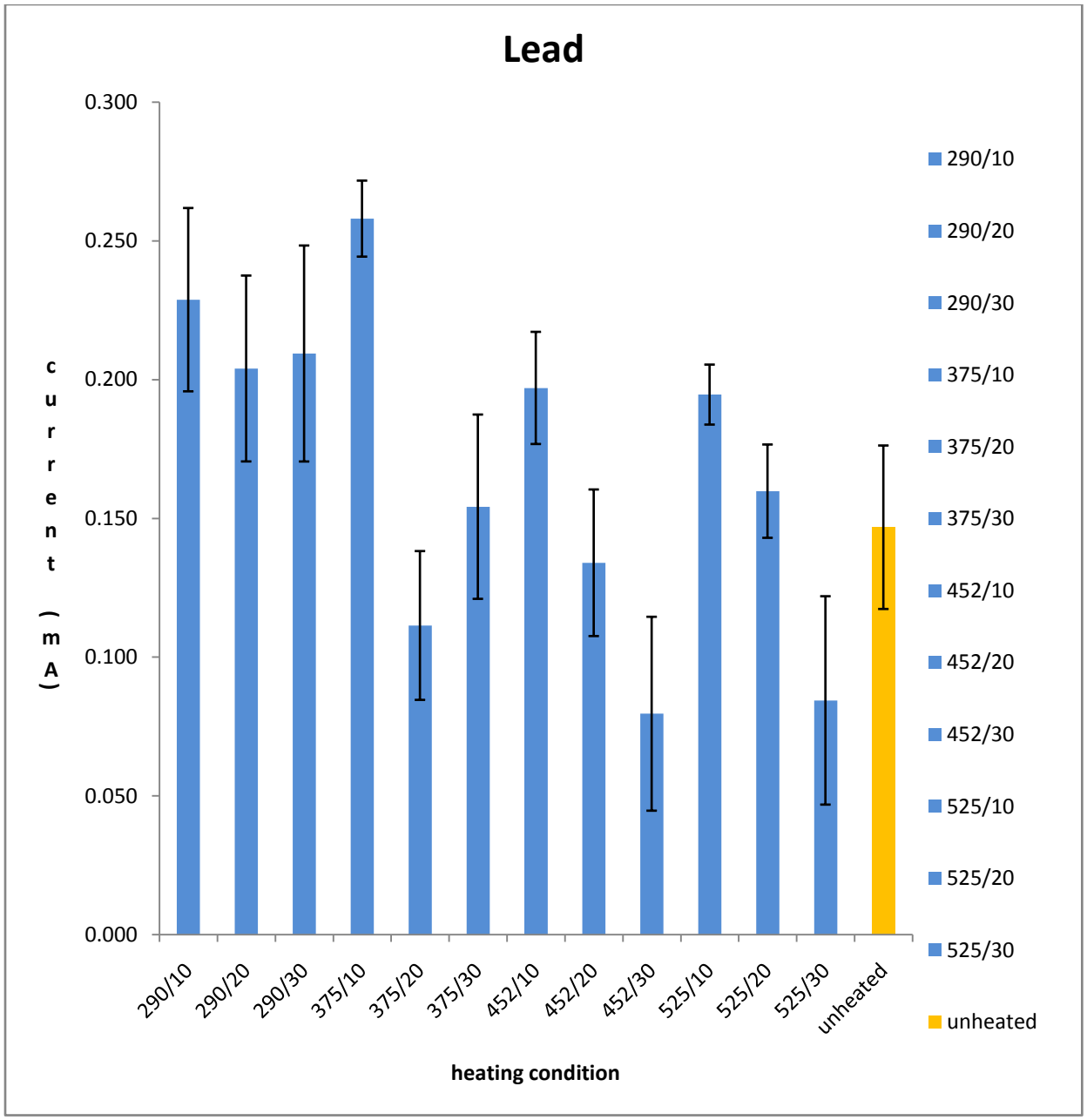

Figure 1A: Heating optimization data for Pb (0.01 M Pb in 0.1M ATFB), error bars represented ± 1σ.

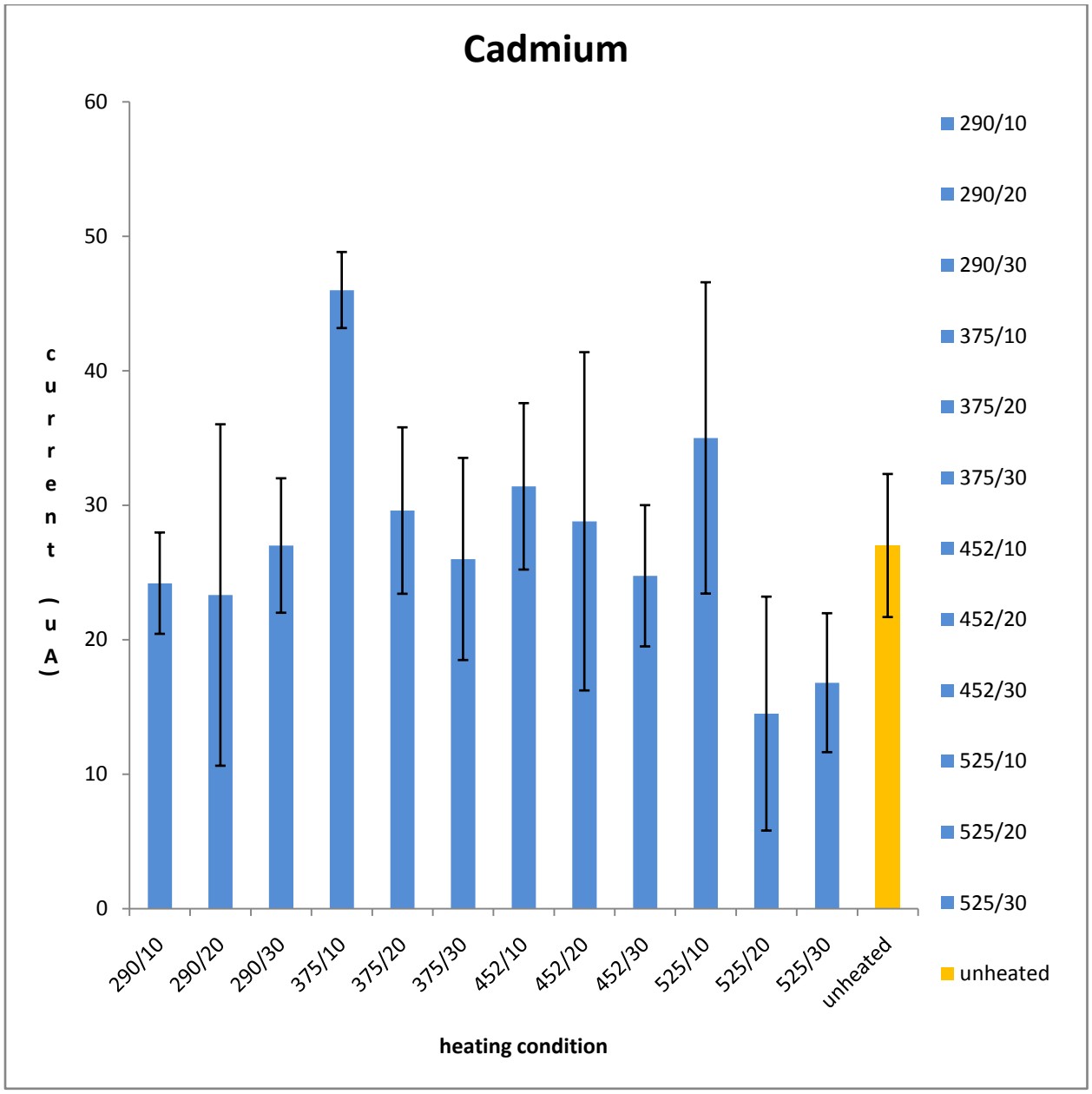

Figure 1B: Heating optimization data for Cd (0.01 M Cd in 0.1M ATFB), error bars represented ± 1σ.

b) Optimization of TiO_2/ZrO_2 ratio and surfactant application

The next parameter of optimization was the ratio of TiO_2 and ZrO_2. For this step the following TiO_2/ZrO_2 ratios (volume: volume) were chosen: (2:1), (1:1), (1:2), TiO_2 only, and ZrO_2 only (constant total volume of 0.6 mL). For the control electrode, 0.6 mL of high-quality water is used instead of TiO_2 or ZrO_2. For surfactant variability, two surfactants were chosen (Tween 20 and Tween 80), which are both polysorbate surfactants. These surfactants were found to improve the crystalline process of TiO_2 and ZrO_2 after heating and help homogenizing the sensor surface thus enhancing the electrocatalytic activity of the electrode surface [8, 9, 175]. For applications of these surfactants, two different methods of applications were tested. The first method was dipping of the electrode into the surfactants before heating, and the second method was direct incorporation of the surfactants (0.5 mL) into the carbon paste composite. The electrodes prepared via dipping into surfactants appear to be burned at the surface after heating. All electrodes were heated at optimal heating conditions previously established (375 ^{0}C for 10 min). Similar to optimization of heating condition, the oxidative current magnitude data from multiple independent different electrodes were collected and compared by running CV in 0.01 M Pb and 0.01 M Cd (in 0.1 M ATFB) solutions.

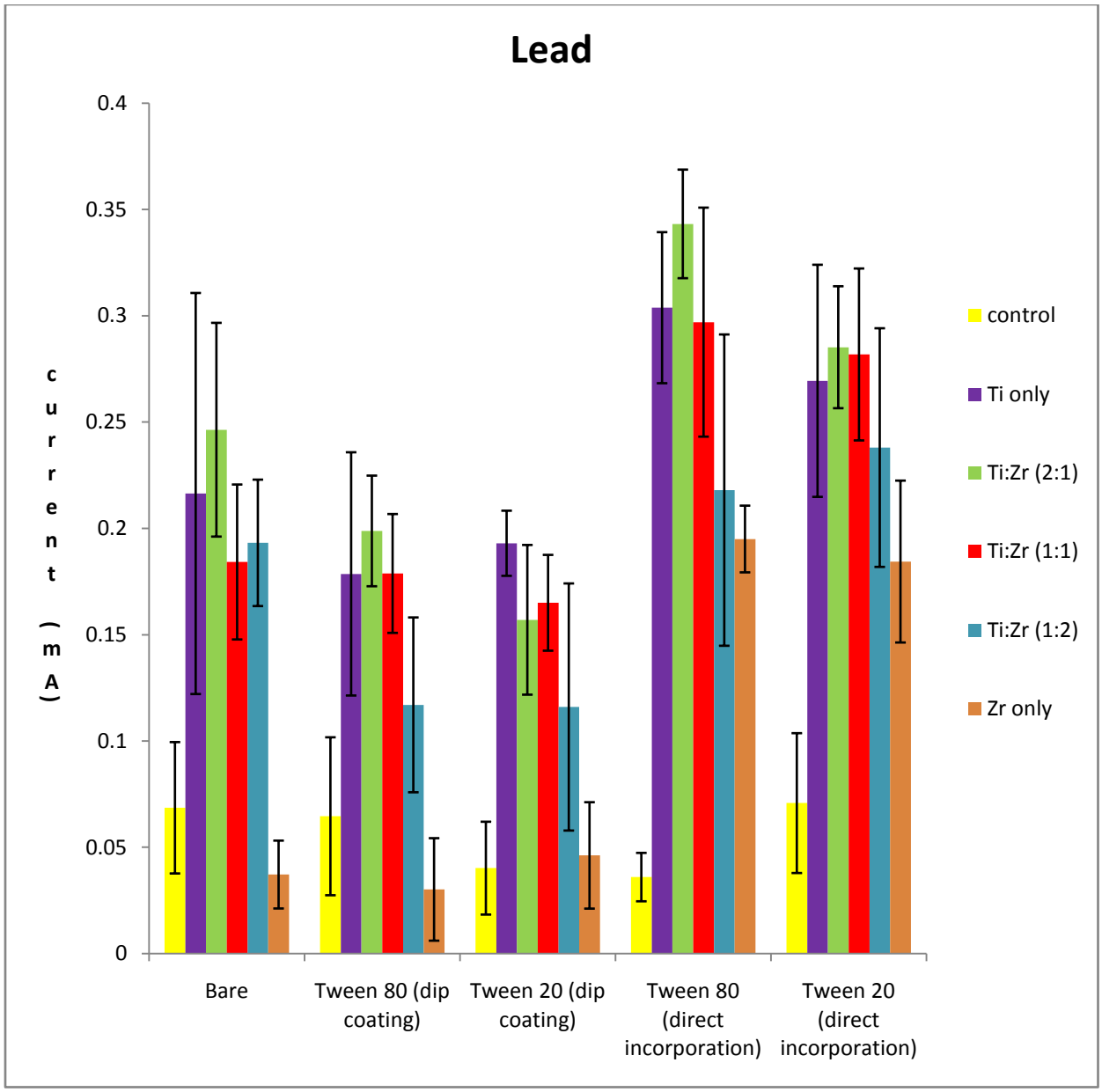

Figure 2A: TiO_2/ZrO_2 ratio and surfactant application optimization data for Pb (0.01 M Pb in 0.1M ATFB solution), error bars represented ± 1σ.

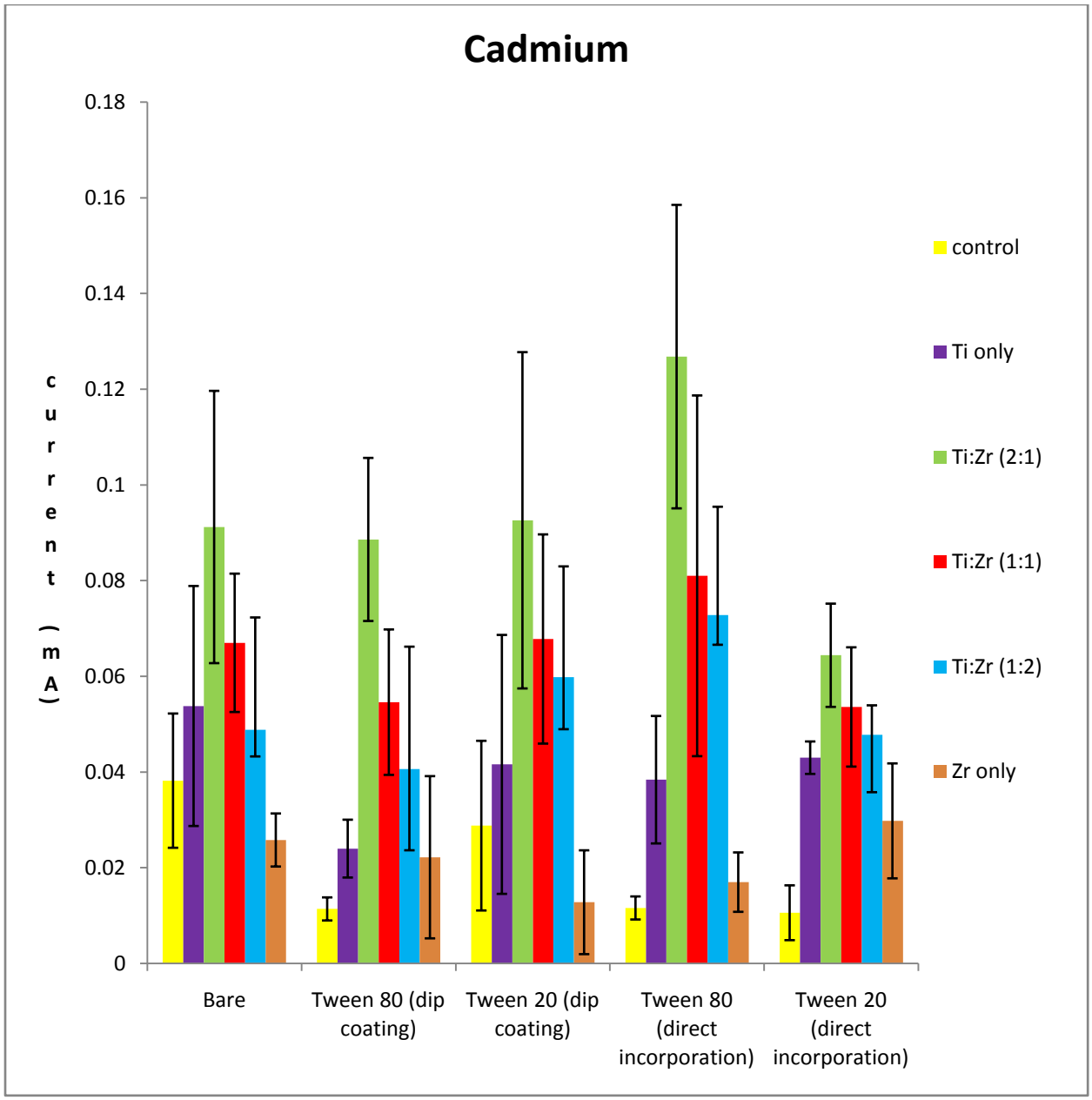

Figure 2B: TiO_2/ZrO_2 ratio and surfactant application optimization data Cd (0.01 M Cd in 0.1M ATFB solution), error bars represented ± 1σ.

From the data in Figure 2A and 2B, it is observed that, for lead and cadmium, the electrodes that were modified with TiO_2 and (or) ZrO_2 appeared to be more sensitive than the control ones (control- without TiO_2 or ZrO_2; bare- no Tween 80 or Tween 20). Furthermore, the general trend, with a few exceptions, was that the sensitivity appeared to be best for TiO_2/ZrO_2 (2:1) compared to other ratios of (1:1), (1:2), TiO_2 only, then lastly ZrO_2 only, regardless of surfactant application. For Pb, it was more apparent that surfactant application via direct incorporation into carbon paste was better, but the same conclusion cannot be drawn for Cd data, Figure 2B. Asides from the trend mentioned previously, no other correlation was observed. Overall, the electrode made with TiO_2/ZrO_2 (2:1) and Tween 80 (0.5 mL) directly incorporated appeared to be most sensitive for both metals. Therefore, 2:1 TiO_2/ZrO_2 ratio and Tween 80 (0.5 mL) direct incorporation was selected as the optimal modification quantity [181].

c) Optimization of TiO_2/ZrO_2 Tween 80 volume loading

Once the TiO_2/ZrO_2 ratio as well as surfactant type and surfactant application method were optimized, the total volume of TiO_2, ZrO_2 and loading volume of Tween 80 would be the next parameters to be optimized. Using the optimal ratio of TiO_2/ZrO_2 (2:1) the total volumes were varied from 0.3 mL to 1.2 mL (increasing at 0.3 mL increment). Also, the volume loading of Tween 80 were varied from 0.5 mL to 1 mL (increasing at 0.25 mL increment). Using CV, the oxidative current magnitude data were collected and compared (0.01M Pb and 0.01M Cd (in 0.1M ATFB) solutions).

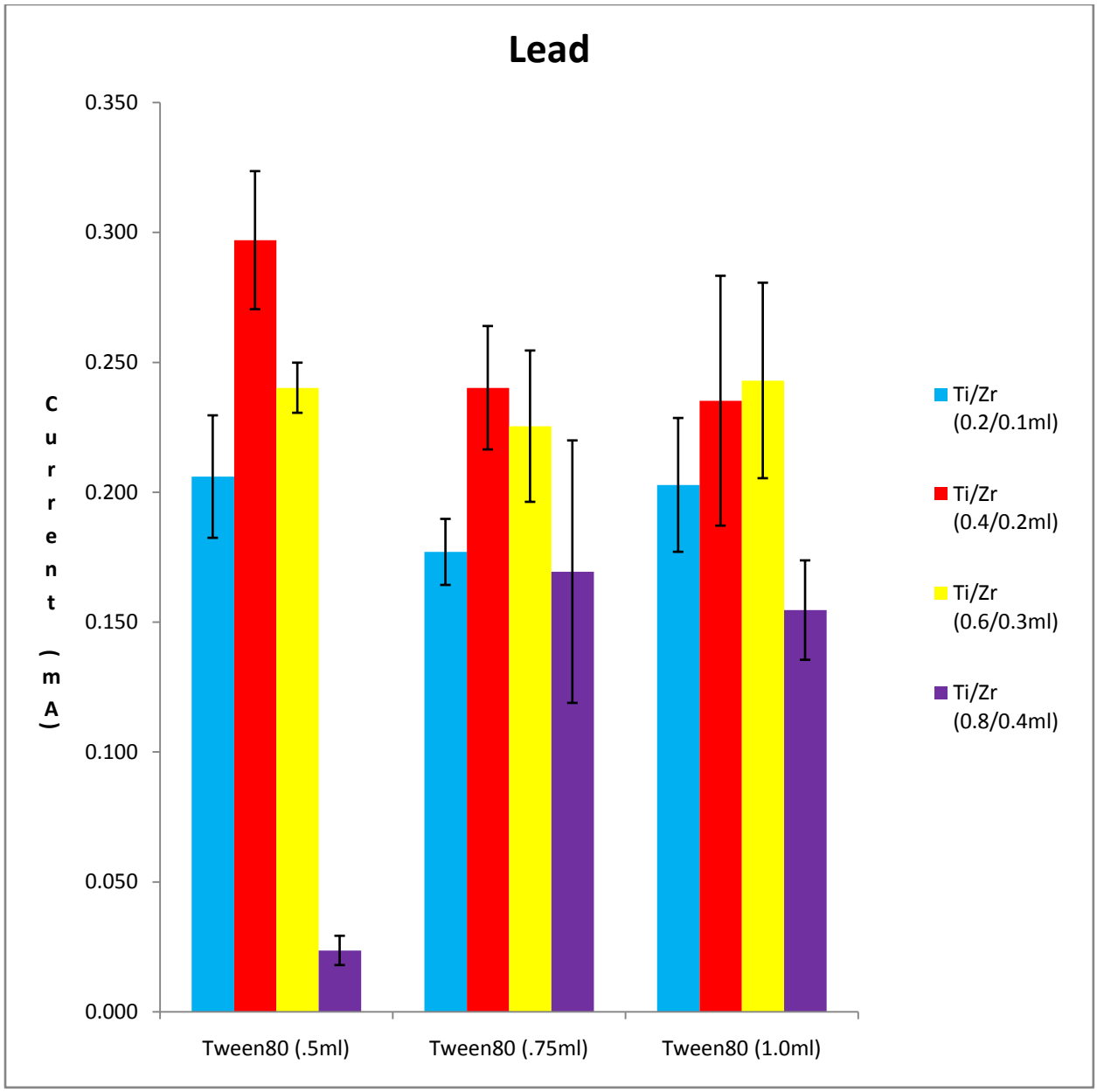

Figure 3A: TiO_2/ZrO_2 /Tween 80 volume loading optimization data for Pb (0.01 M Pb in 0.1 M ATFB), error bars represented ± 1σ.

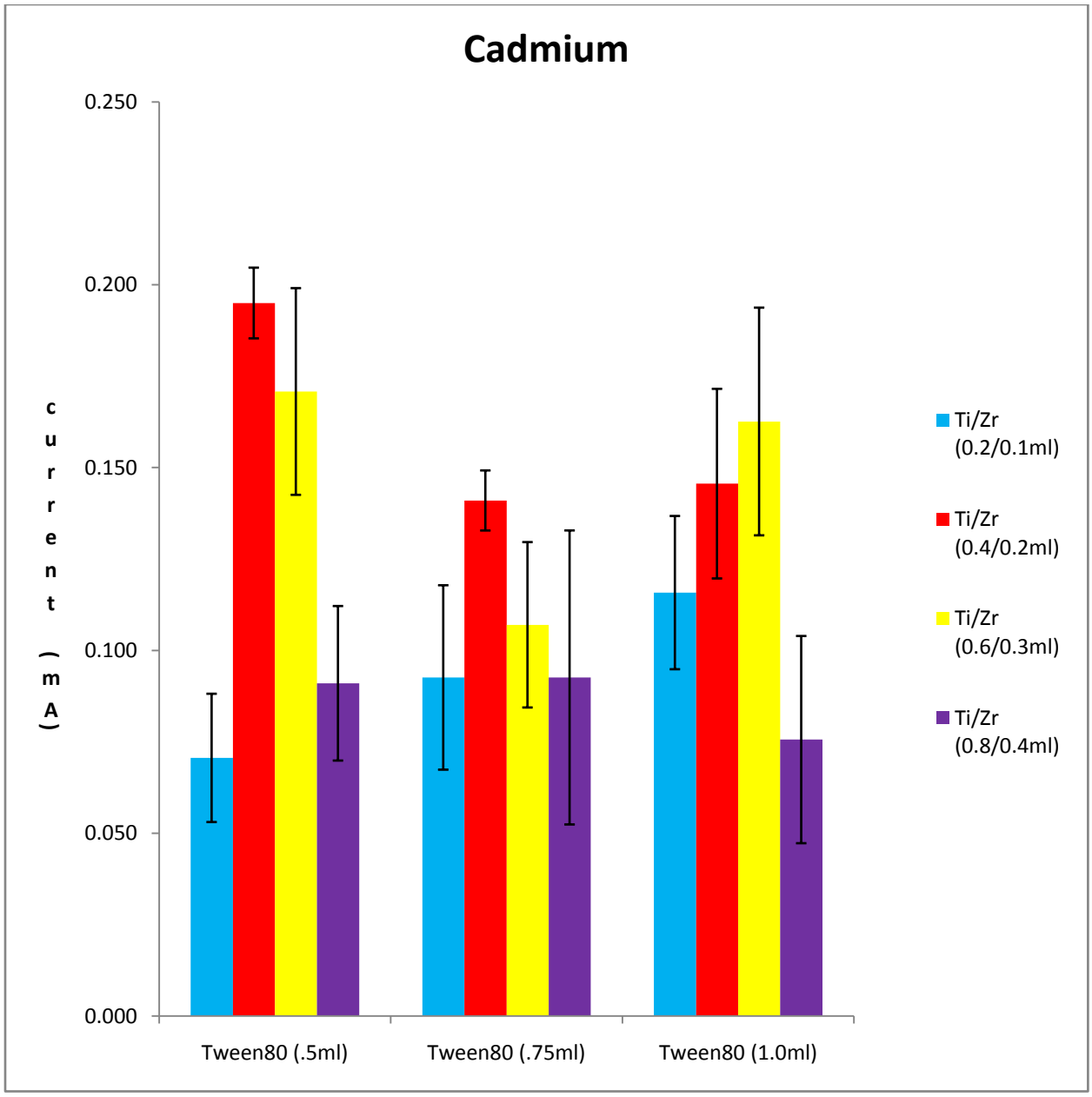

Figure 3B: TiO_2/ZrO_2 /Tween 80 volume loading optimization data for Cd (0.01 M Cd in 0.1 M ATFB), error bars represented ± 1σ.

According to data presented in Figure 3A and 3B, it is observed that, for both Pb and Cd, at Tween 80 volume of 0.5 mL and 0.75 mL, the response was best for TiO_2/ZrO_2 total volume of 0.6 mL. While at Tween 80 volume of 1mL, the response appeared to be best at TiO_2/ZrO_2 total volume of 0.9 mL. One important factor to note was that, for increasing TiO_2/ZrO_2 total volume, the carbon paste became much thicker and harder to pack. No obvious correlation between the total TiO_2/ZrO_2 volume and surfactant volume loading was seen. Overall, the electrodes made with total TiO_2/ZrO_2 volume of 0.6 mL and 0.5 mL Tween 80 were the most sensitive for both metals; therefore, this combination of TiO_2/ZrO_2 /Tween 80 volume loading was chosen for subsequent electrode synthesis [181].

From the electrode synthesis optimization data discussed above, the optimally modified TiO_2/ZrO_2/Tween 80 carbon paste composite electrode is prepared as followed:

3 g of graphite powder were added into a mixture of 1.5 mL MTMOS, 0.3 mL 1 M H_2SO_4, 0.5 mL isopropanol, 0.4 mL Ti(IV) isopropoxy, 0.2 mL Zr(IV) propoxy, and 0.5 mL Tween 80. This mixture is thoroughly mixed in a borosilicate glass vial to form a homogenous carbon paste material. A copper wire (0.5 mm O.D., 12.5 cm long) is inserted into the capillary tube, the copper wire serves as the electrical contact component. The carbon paste mixture above was manually packed into the capillary tube with the copper wire and allowed to be set at room temperature. After 15 minutes of setting time, the carbon paste electrode was heated for optimized results at 10 minutes at 375 ^{0}C and allowed to be cooled and set naturally at room temperature for 24 hours before utilized.

2) Estimation of the optimal TiO_2/ZrO_2/Tween 80 carbon paste composite electrode surface area

The electrode surface was estimated using Randles-Sevcik equation [82, 83, 85]:

$$I_p=269\ n^{3/2}\ AD^{1/2}\ Cv^{1/2}$$

In which I_p represents peak current, n is the number of electron transfer, C is the solution concentration, A is the electrode surface area, D is the diffusion coefficient, and v is the scan rate. Using the reference compound potassium hexacyanoferrate (II) at 0.001M, CV's of this solution were obtained at various scan rates (from 50 to 200 mV/s, at 25 mV/s increment increase). By measuring the anodic peak current, which reflected the oxidation of $Fe(CN)_6^{4-}$ to $Fe(CN)_6^{3-}$, at various scan rates and by plotting these peak current magnitude vs. square root of the scan rate, a linear fit with the electrode surface area equal to slope/(269*$n^{3/2}$*$D^{1/2}$*C) was obtained.

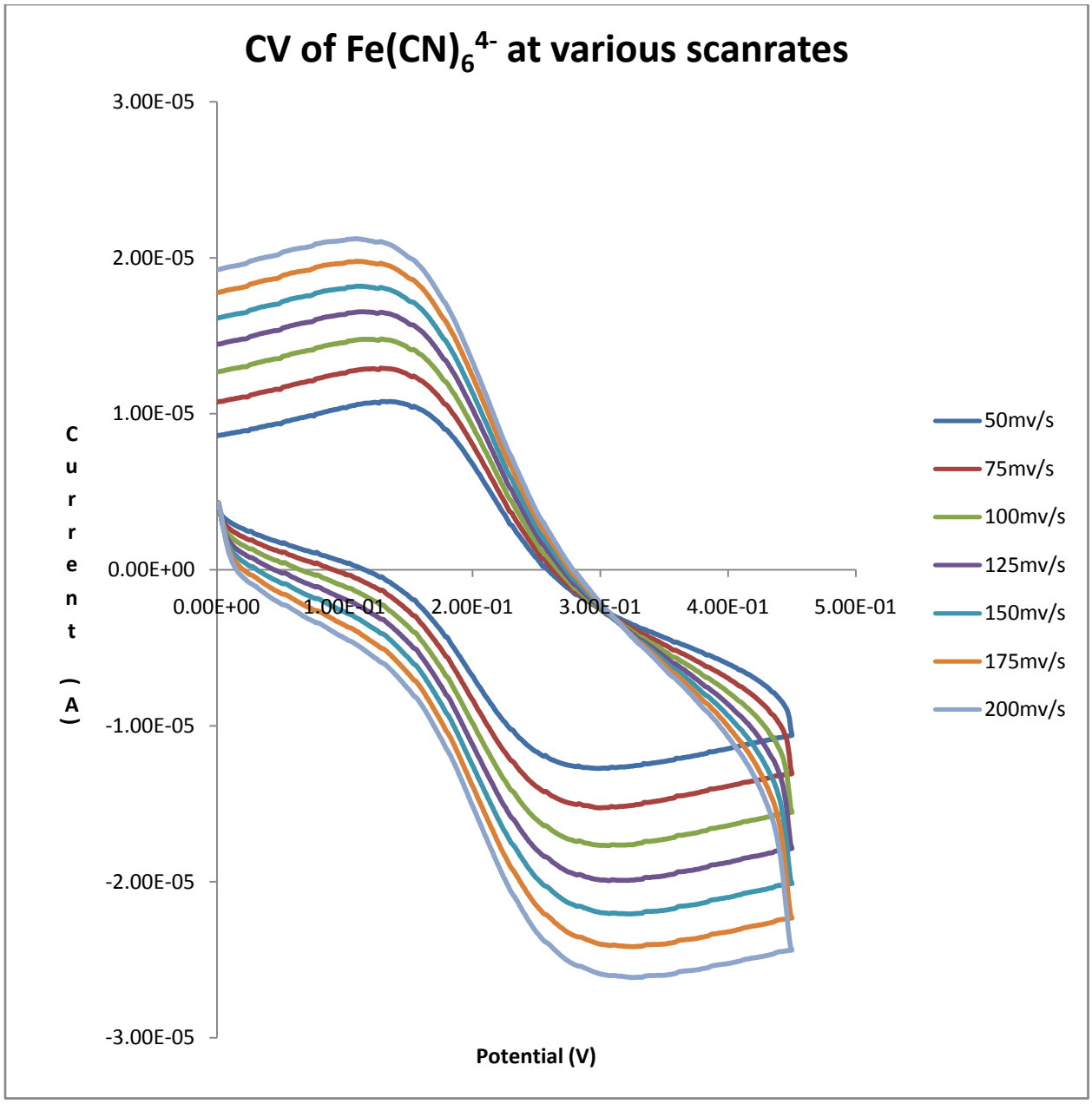

Figure 4A: CV of 1mM $Fe(CN)_6^{4-}$ (in 0.1 M ATFB) at various scan rates (50-200 mV/s).

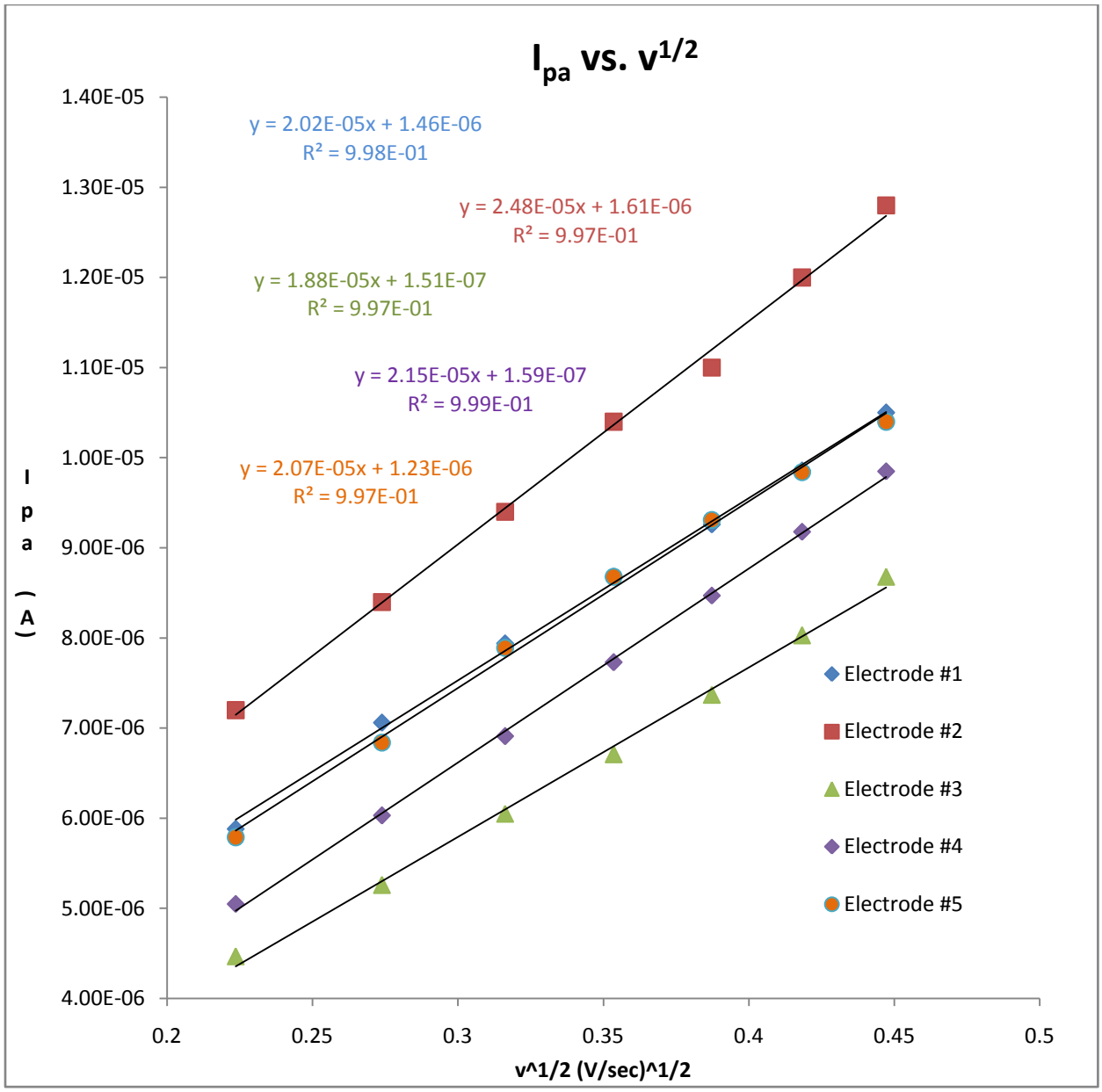

Figure 4B: Plot of I_{pa} versus $v^{1/2}$ of five different electrodes.

From the data presented in Figure 4A and 4B, the average estimated electrode surface area is calculated to be 0.028 (±0.003) cm^2 (D=7.6E-6 cm^2/s [176], n=1). This value is acceptable because with the assumption of a flat surface, the average electrode area would be approximately 0.021 cm^2 (assuming the average opening diameter of the capillary tube to be 0.165cm). The increase in electrode surface area could be accounted for the presence of surface micro-structures [181].

3) Estimation of kinetic parameters- electron transfer coefficient (α) and heterogeneous electron transfer rate constant (k_0).

The simple Tafel plots (Figure 6A and 6B) were constructed by plotting the potential versus natural log of current in the rising portion of the cathodic branch. These plots would be approximately linear with the slope equal to -αnF/RT, in which alpha is a kinetic parameter known as the electron transfer coefficient. From this relationship, the electron transfer coefficients for Pb and Cd redox systems (n=2), using the optimal TiO_2/ZrO_2/Tween 80 carbon paste composite electrode, were estimated to be 0.44 and 0.33, respectively. These results were reasonable as visual inspection of the voltammogram indicated that the cathodic branch of the voltammogram was much broader compared to the anodic branch. The slow scan rate of 20 mV/s was chosen because at this scan rate the redox process would still be predominantly kinetic dependent, while at higher scan rates, the redox process would become more diffusion control as indicated by the broadening of both the anodic and cathodic peaks (Figure 5A and 5B) [181].

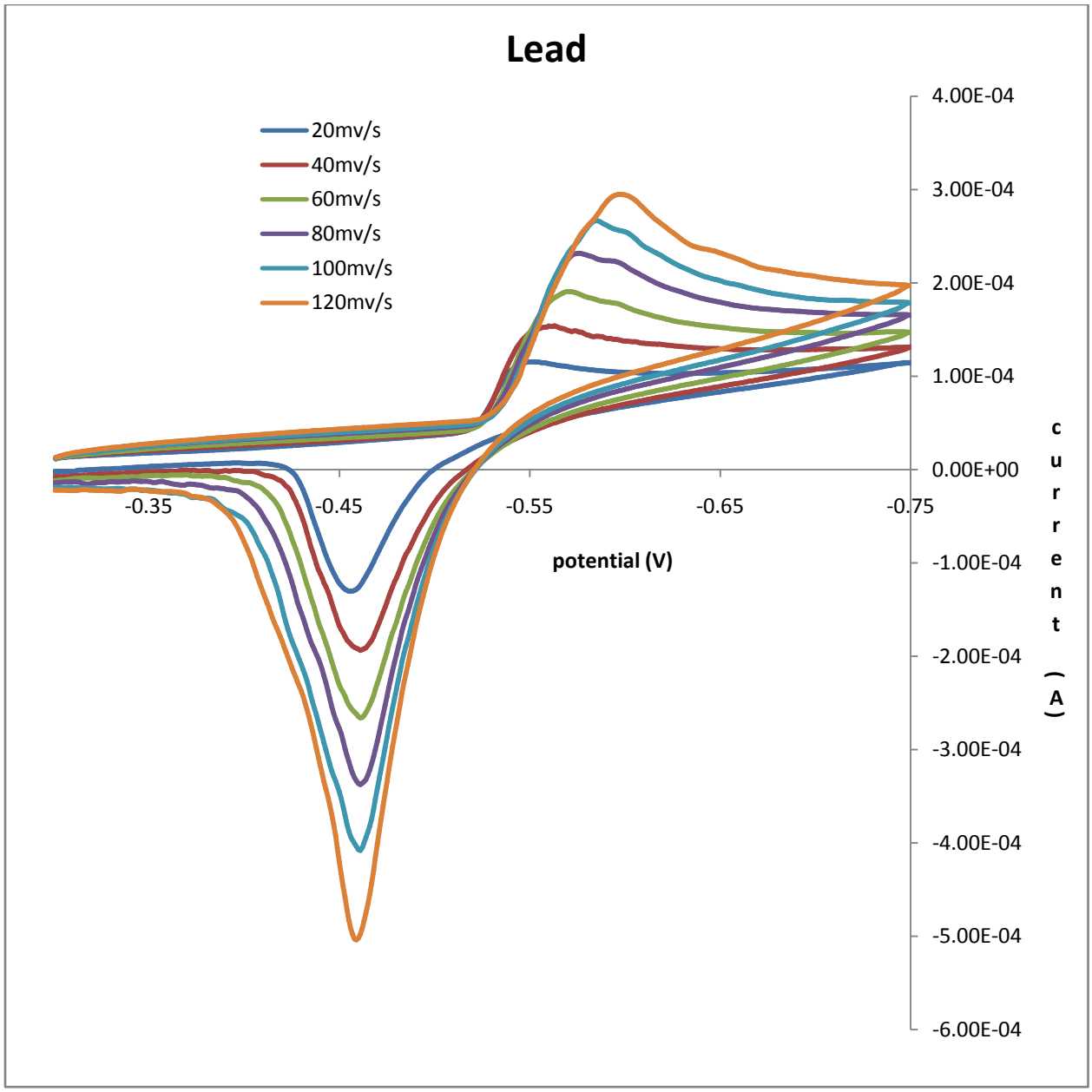

Figure 5A: CV of 0.01 M Pb (in 0.1 M ATFB) at various scan rates (20-120 mV/s).

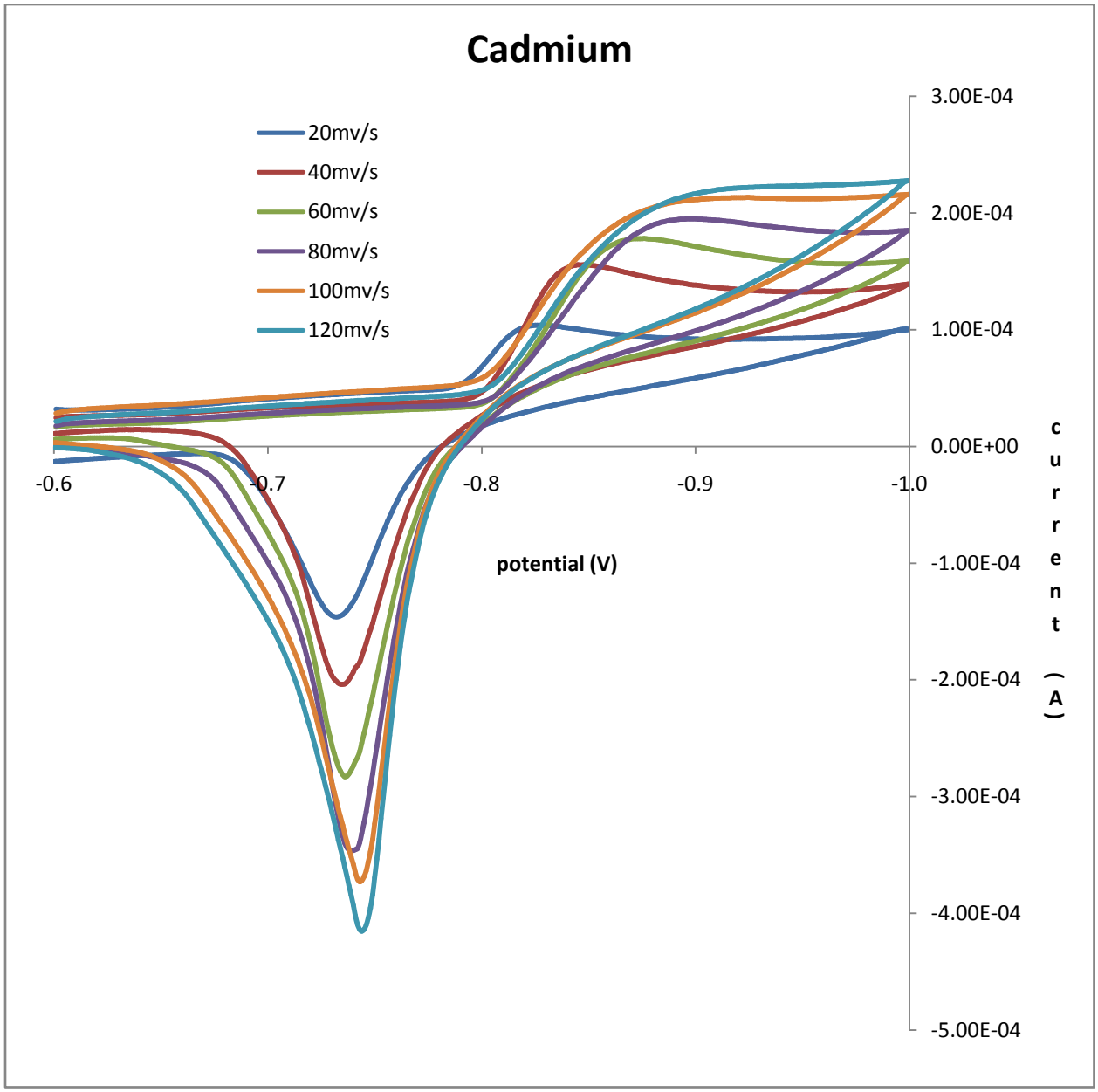

Figure 5B: CV of 0.01 M Cd (in 0.1 M ATFB) at various scan rates (20-120 mV/s).

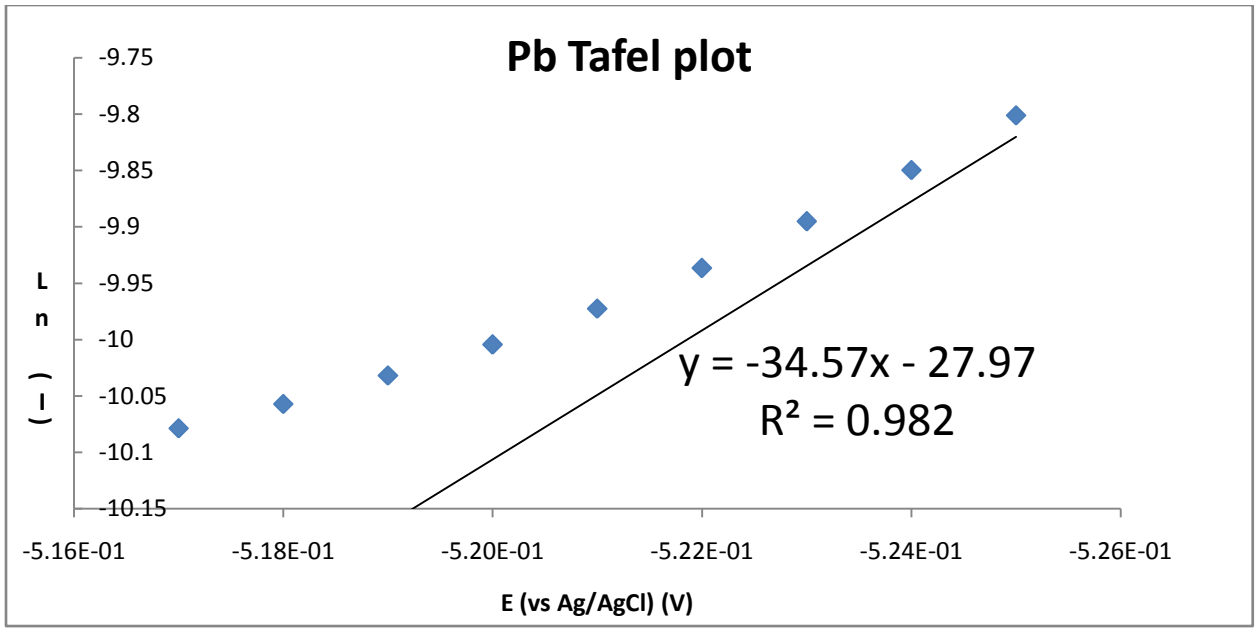

Figure 6A: Tafel plot of Pb.

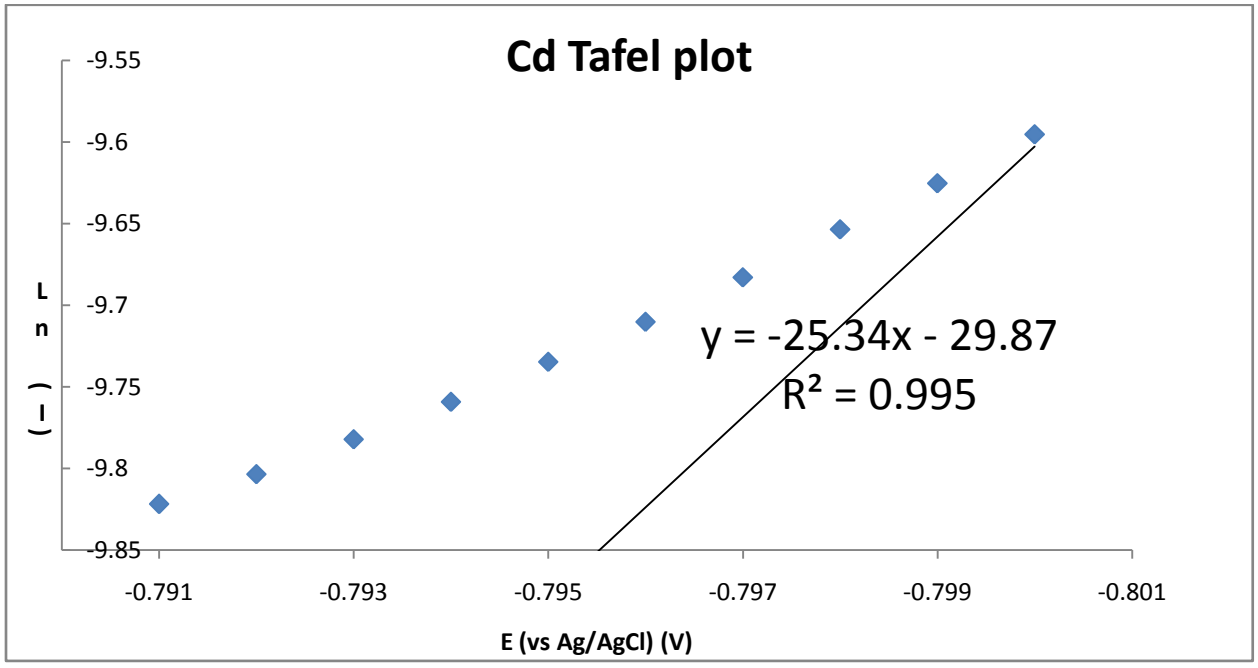

Figure 6B: Tafel plot of Cd.

Using the method described by Nicholson [177], the heterogeneous electron transfer rate constant of a redox couple can be estimated. This parameter reflected the rate of electron transfer between the redox system and the electrode surface (at formal potential). Furthermore, this parameter would be quite useful in determining the reversibility of a redox couple under specific conditions. Nicholson had published the relationship between the electron transfer rate constant and the function psi (Ψ). Working curve of this function psi relates to ΔEp has been published [177, 178] to be used for estimation of k_0 by measuring ΔEp and relating that to psi at various scan rate. Using the optimal TiO_2/ZrO_2 carbon paste composite working electrode, k_0 values were estimated to be $2.42x10^{-3}$ and $5.64x10^{-3}$ (cm/s) for Cd and Pb, respectively. The diffusion coefficients used for k_0 calculations for Pb and Cd ions were from Valente [179] and Macero [180]. These results indicated that both Pb and Cd redox systems at the new electrode surface were quasi-reversible under the current experimental setup/ conditions as redox couples with k_0 values between $2x10^{-2}$ and $3x10^{-5}$ cm/s would be classified as quasi-reversible [84].

4) Optimization of pH

From Figure 7, it was observed that, at pH of 1and 7, the respond for Cd detection was not observable. This could be due to hydrogen and hydroxide ion activity at large negative potential, which resulted in sufficiently large charging background current that masked the oxidation peak current. This problem, however, was not as severe for Pb as the potential range for redox of Pb is not as negative compared to that of Cd. Overall, it was observed an increase in peak current magnitude as pH increases from 1 to 3, at pH of 3, the electrode appeared to be most sensitive. Furthermore, beyond pH of 3, the peak current magnitude decreased gradually with increasing pH. From these results, the functional pH range of the novel working electrode

for detection of Pb would be between 1 and 7, while the functional pH range for Cd would be between 2 and 6, with the optimal pH appeared at 3 for both metals [181].

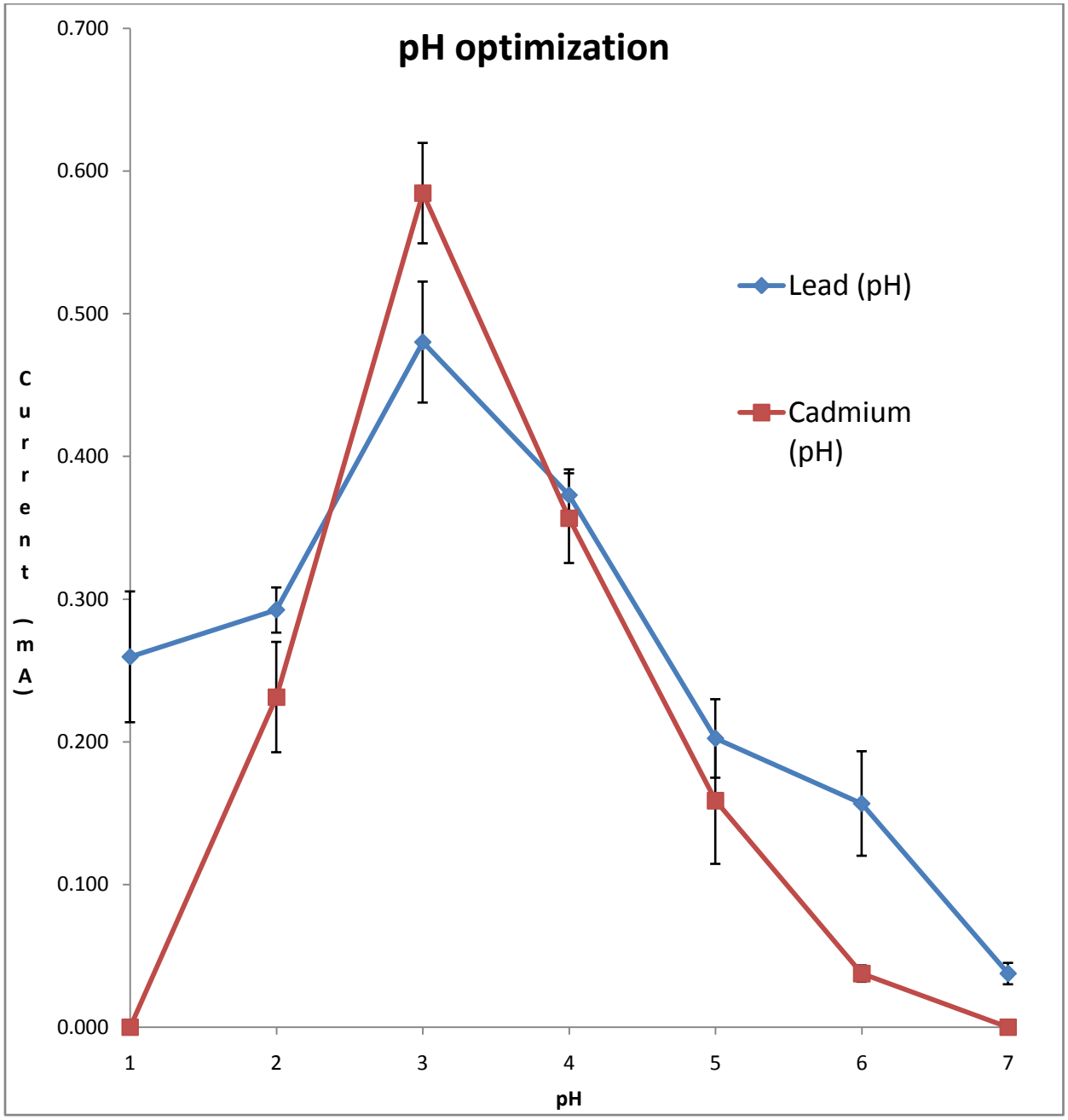

Figure 7: Oxidative current variation with pH, pH adjustment using acetate buffers and 1 M HNO_3, error bars represented ± 1σ.

5) Performance/sensitivity comparison between the optimal TiO_2/ZrO_2/Tween 80 carbon paste composite electrode and the unmodified carbon paste electrode (CPE).

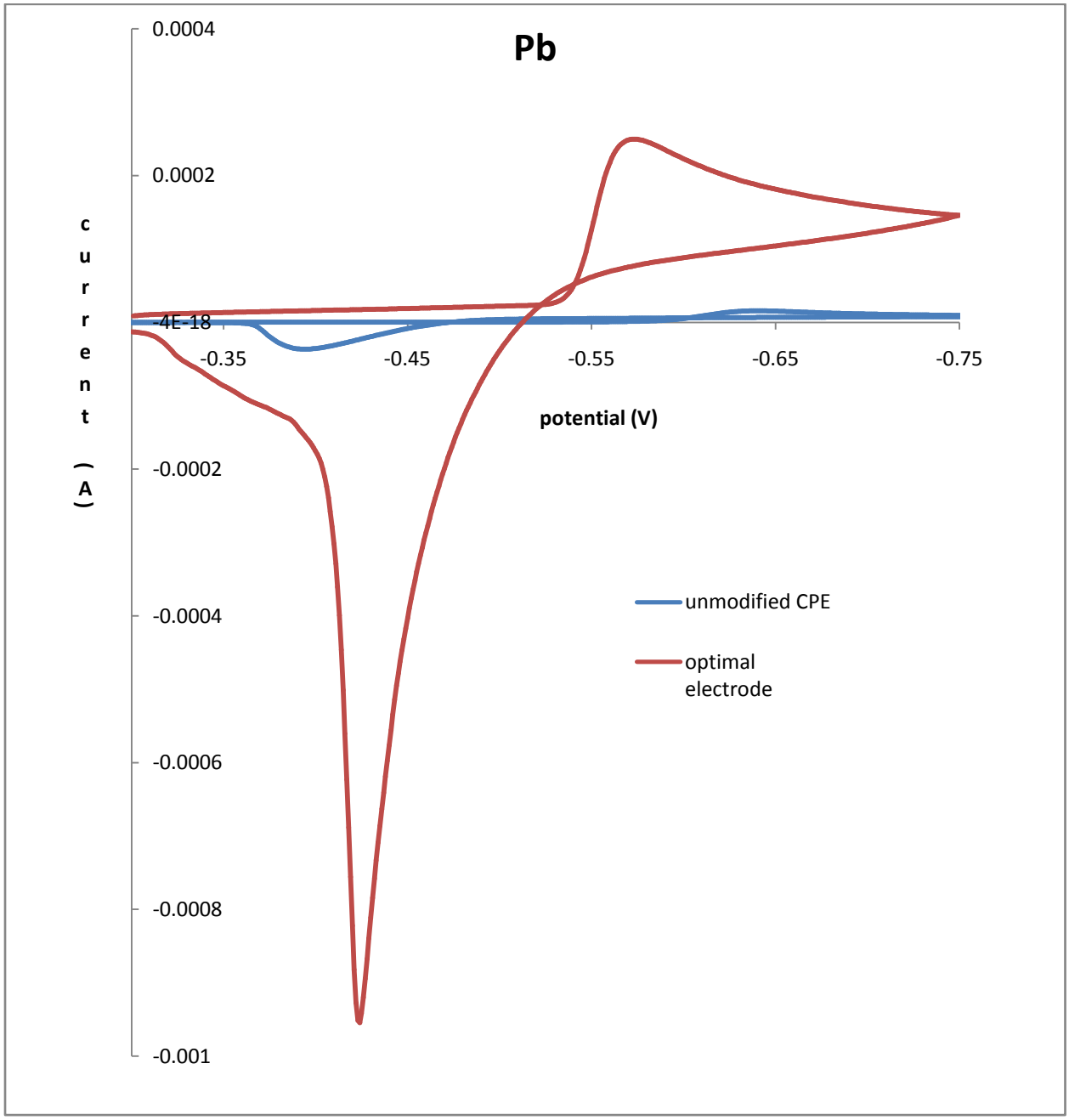

Figure 8A: Comparison between optimal TiO_2/ZrO_2/ Tween 80 carbon paste composite electrode and unmodified CPE for Pb detection(0.01 M Pb, scan rate 100 mV/s, pH=3).

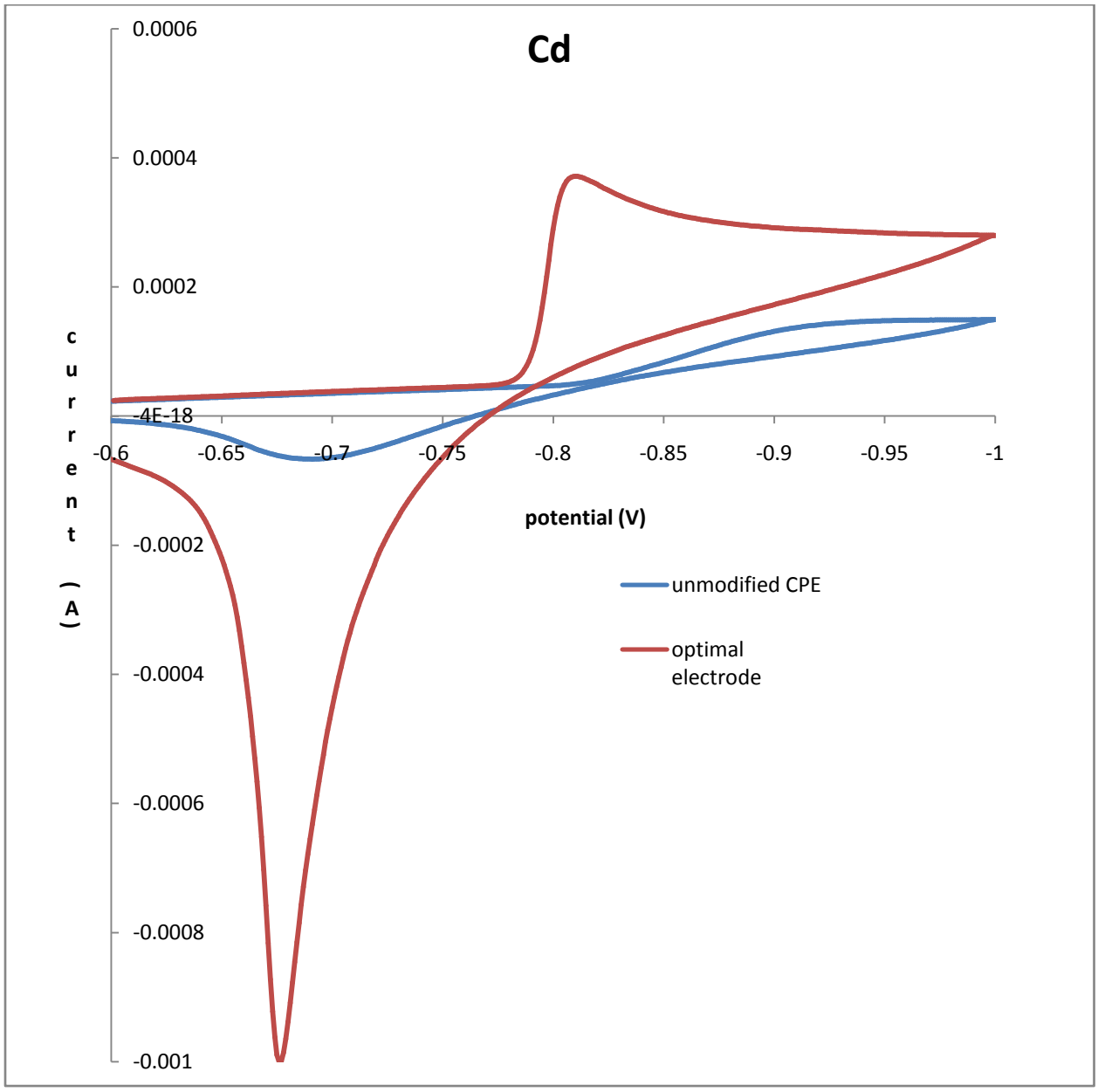

Figure 8B: Comparison between optimal TiO_2/ZrO_2/ Tween 80 carbon paste composite electrode and unmodified CPE for Cd detection(0.01 M Cd, scan rate 100 mV/s, pH=3).

From Figure 8A and 8B, it can be seen that the sensitivity, for both metals, of the optimal TiO_2/ZrO_2/Tween 80 carbon paste composite electrode was much higher compared to that of the unmodified CPE (prepared without TiO_2, ZrO_2, and Tween 80.) Furthermore, when the optimal electrode was used, reversibility of both redox couples (Pb and Cd) appeared to be very much improved (smaller peak potential separations) compared to when the unmodified CPE was employed. This data supported our hypothesis that the present of TiO_2/ZrO_2/Tween 80 helped improve the electrode performance/sensitivity by enhancing the electro-catalytic activity of the modified electrode surface [181].

6) Linear response range and detection limit of Pb and Cd using CV

Figure 9A, 9B, and 10 illustrated the range of linear detection for these heavy metals with the TiO_2/ZrO_2 carbon paste composite electrodes. Thus, using the optimal TiO_2/ZrO_2 carbon paste composite electrode, the linear response ranges were found to be from $1x10^{-2}$ M to $1x10^{-5}$ M for Pb and from $1x10^{-2}$ M to $5x10^{-5}$ M for Cd via cyclic voltammetric analysis. Moreover, from 10 independent blanks, the detection limit of Pb and Cd were estimated to be $7.6x10^{-6}$ M and $1.1x10^{-5}$ M, respectively. The detection limits were estimated using 3 sigma method, which the detection limit equal to blank signal plus 3 times the blank standard deviation [181].

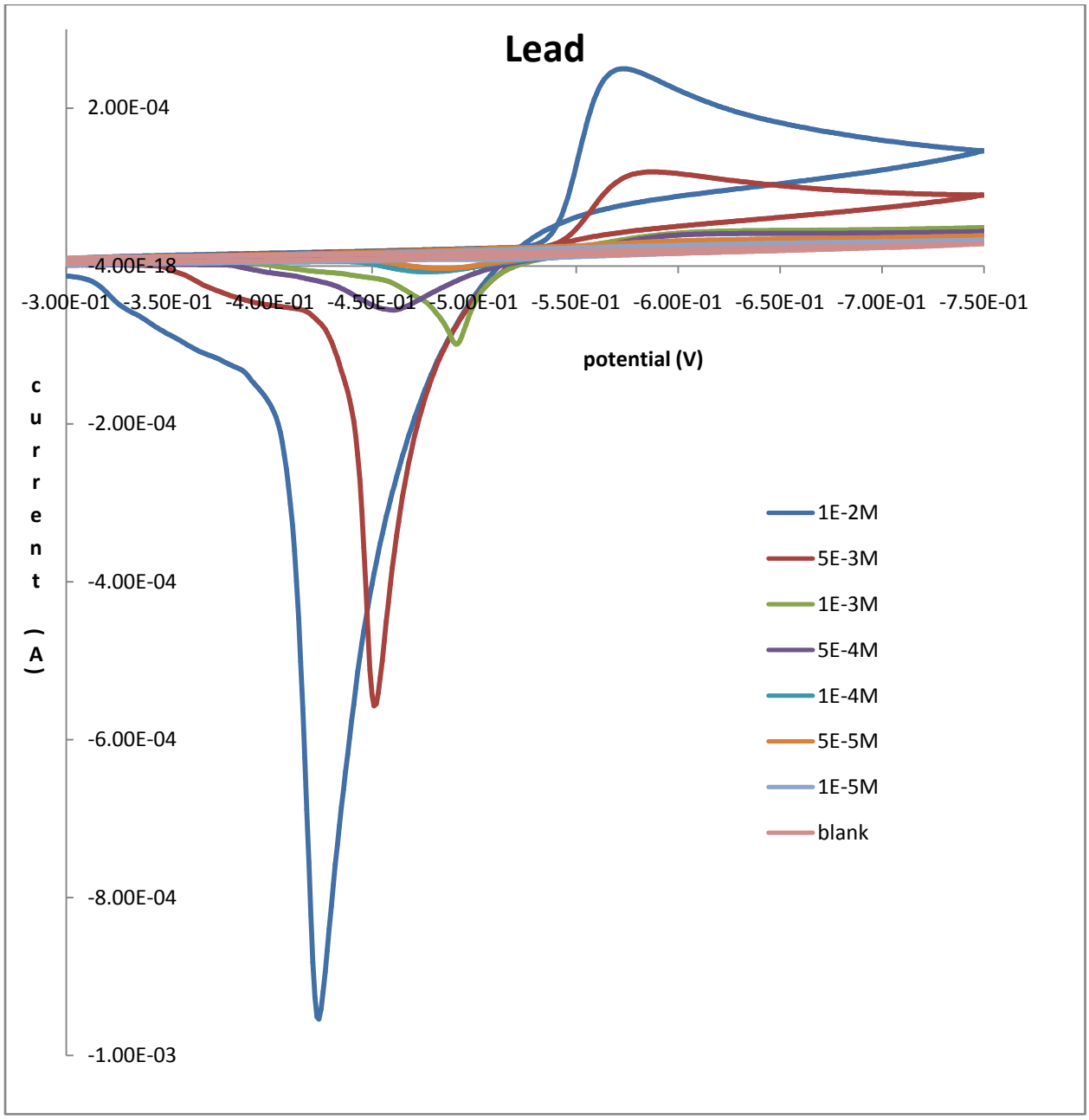
Lead
2.00E-04
-4.00E-18
-2.00E-04
-4.00E-04
-6.00E-04
-8.00E-04
-1.00E-03
-3.00E-01
-3.50E-01
-4.00E-01
-4.50E-01
-5.00E-01
-5.50E-01
-6.00E-01
-6.50E-01
-7.00E-01
-7.50E-01
potential (V)
current (A)
1E-2M
5E-3M
1E-3M
5E-4M
1E-4M
5E-5M
1E-5M
blank

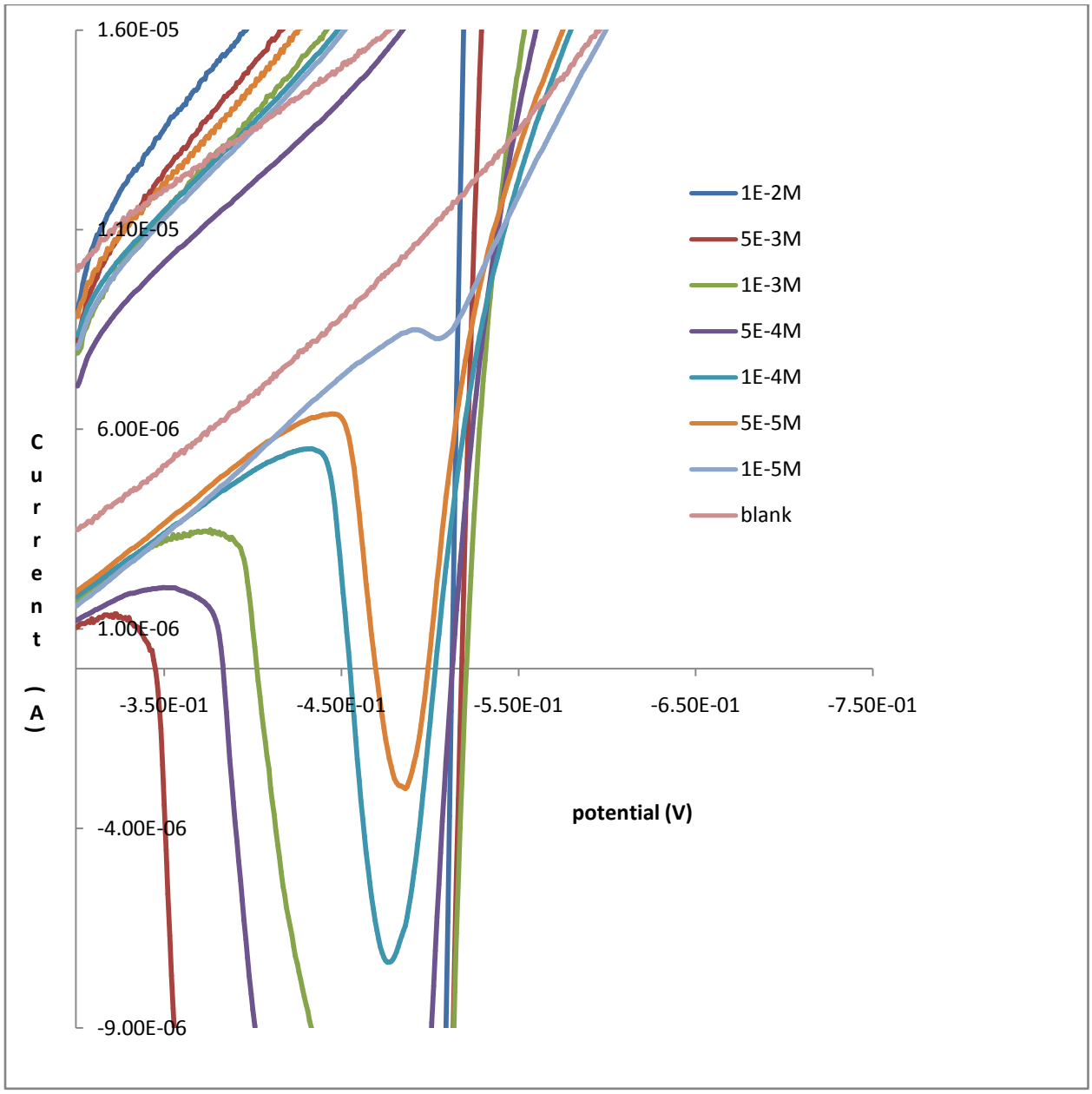

Figure 9A: CV of Pb at different concentrations (full and zoomed in), scan rate 100 mV/s, pH=3.

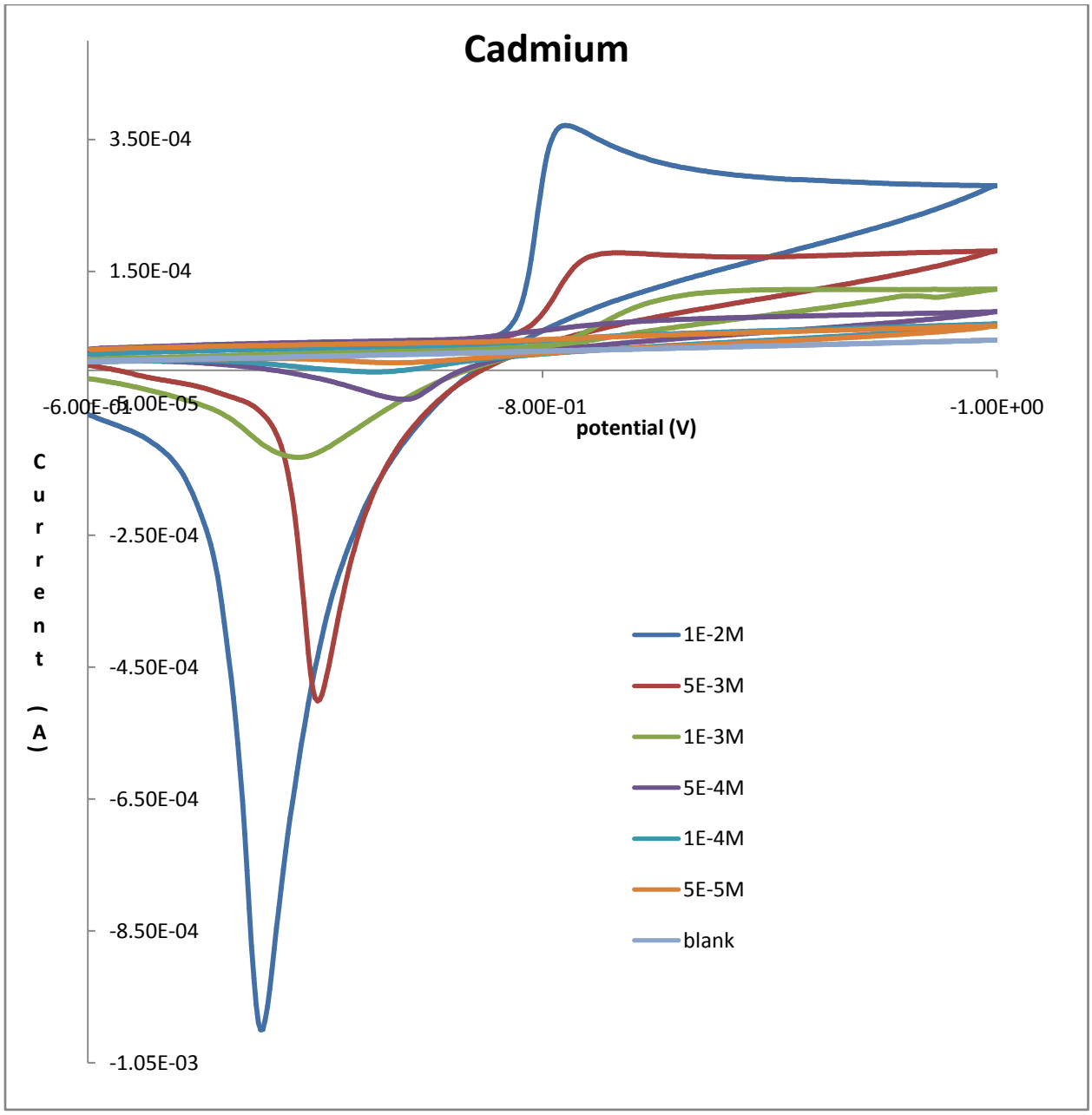
Cadmium
3.50E-04
1.50E-04
-6.00E-01
-5.00E-05
-8.00E-01
-1.00E+00
potential (V)
Current (A)
-2.50E-04
-4.50E-04
-6.50E-04
-8.50E-04
-1.05E-03
1E-2M
5E-3M
1E-3M
5E-4M
1E-4M
5E-5M
blank

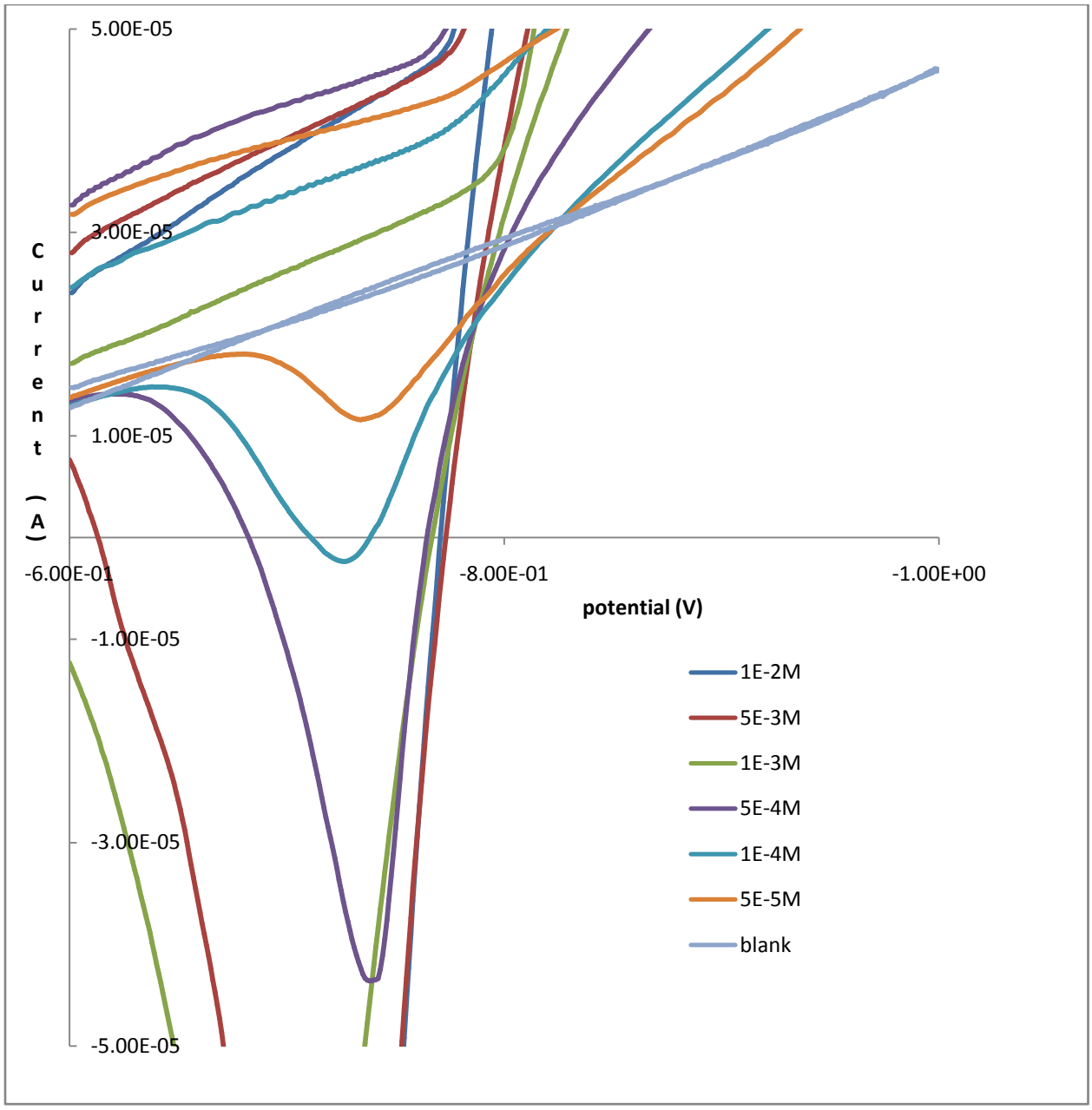

Figure 9B: CV of Cd at different concentrations (full and zoomed in), scan rate 100 mV/s, pH=3.

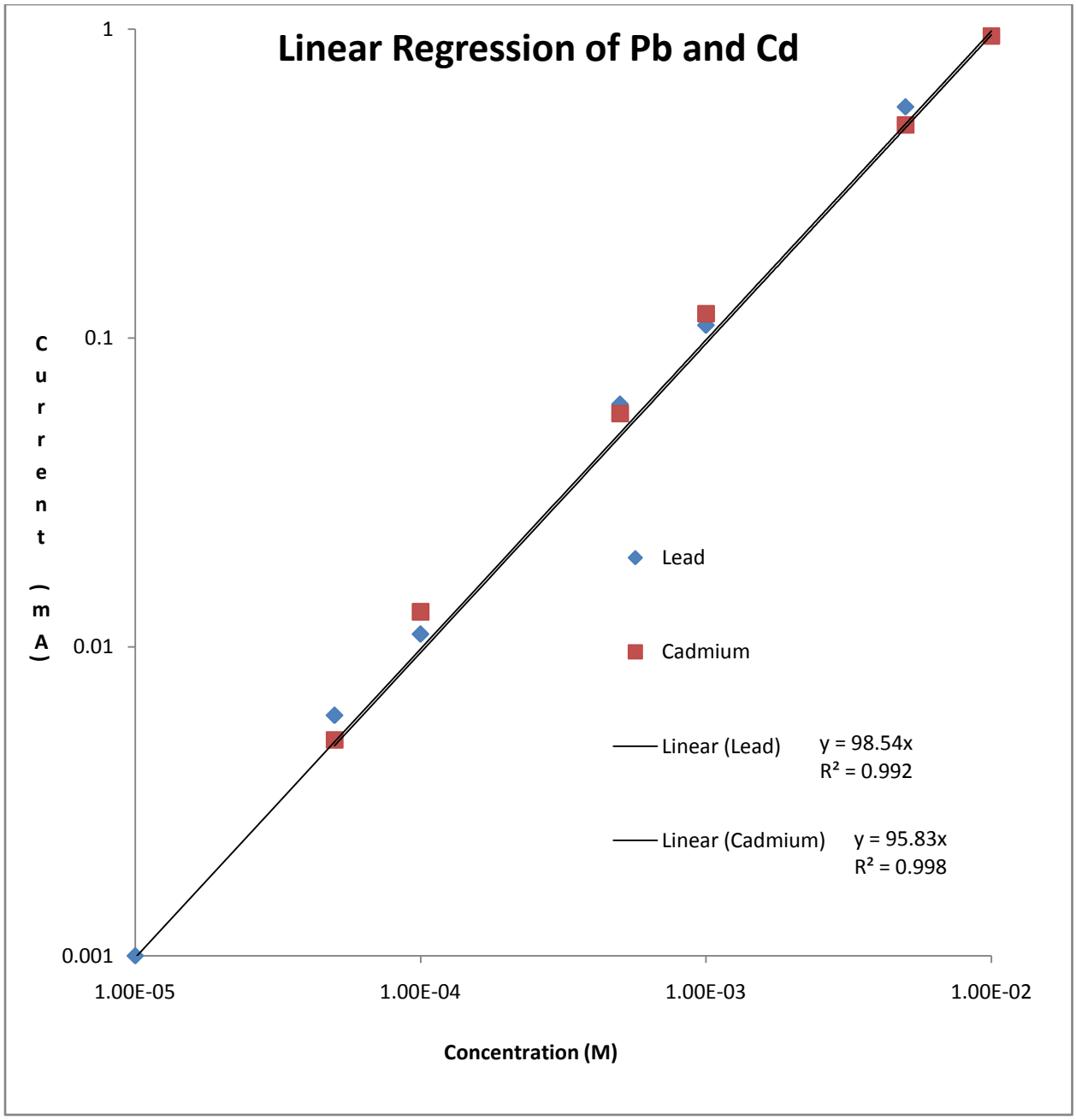

Figure 10: Linear response plot of Pb and Cd (oxidative peak current vs. metal ion concentration) in log-log scale.

7) Optimization of SWASV analysis parameters

As previously mentioned, due to its susceptibility to charging current, the sensitivity of CV analysis is typically limited to micro-molar concentration. Therefore, in order to quantify Pb and Cd at trace (ppb) level, a more effective electro-analytical method must be employed. For this reason SWASV, with its selective sampling nature and effective pre-concentration technique, is utilized for quantitative analysis of Pb and Cd. However, prior to SWASV analysis to quantify the linear calibration ranges and detection limits of Pb and Cd using the TiO_2/ZrO_2 carbon paste composite working electrode, three important square wave stripping parameters must be optimized. These are: supporting electrolyte concentration (KNO_3 is the chosen supporting electrolyte for this study), pre-concentration potential, and pre-concentration time (all subsequent SWASV analysis were carried out at the optimal pH of 3, as previously established).

a) Optimization of supporting electrolyte concentration

Supporting electrolyte is a vital component in controlled-potential analysis as supporting electrolyte reduces internal solution resistant and eliminates electro-migration. In SWASV, inorganic salts, such as potassium chloride or nitrate, are often used as supporting electrolyte when water is the main solvent due to the inert nature these inorganic salts [82]. For this study, $KNO_3$was selected to be the supporting electrolyte for SWASV analysis of Pb and Cd. Asides from KNO_3, other types of supporting electrolyte, including ammonium tetrafluoroborate, acetate buffer, and KCl were also tested. Overall, SWASV data obtained with KNO_3 was most favorable; therefore, this salt was chosen as the supporting electrolyte for subsequent analysis. The range of supporting electrolyte concentration tested was 0 to 1.5 M. From Figure 11, it was observed that the peak current increased sharply for both metals when KNO_3 was added, compared to that when there is no KNO_3 present. Furthermore, the stripping peak current

magnitude increased with increasing concentration of KNO_3, up to 1 M, for both Pb and Cd. At KNO_3 concentrations greater than 1 M, the stripping peak current magnitudes appeared to attenuate. This could be due to the fact that, at KNO_3 concentration greater than 1 M, the potassium salt began to act more as an interfering source than a supporting electrolyte. Overall, 1M KNO_3 gave the optimal response for both metals; therefore, this supporting electrolyte concentration was chosen for all subsequent SWASV analysis [182].

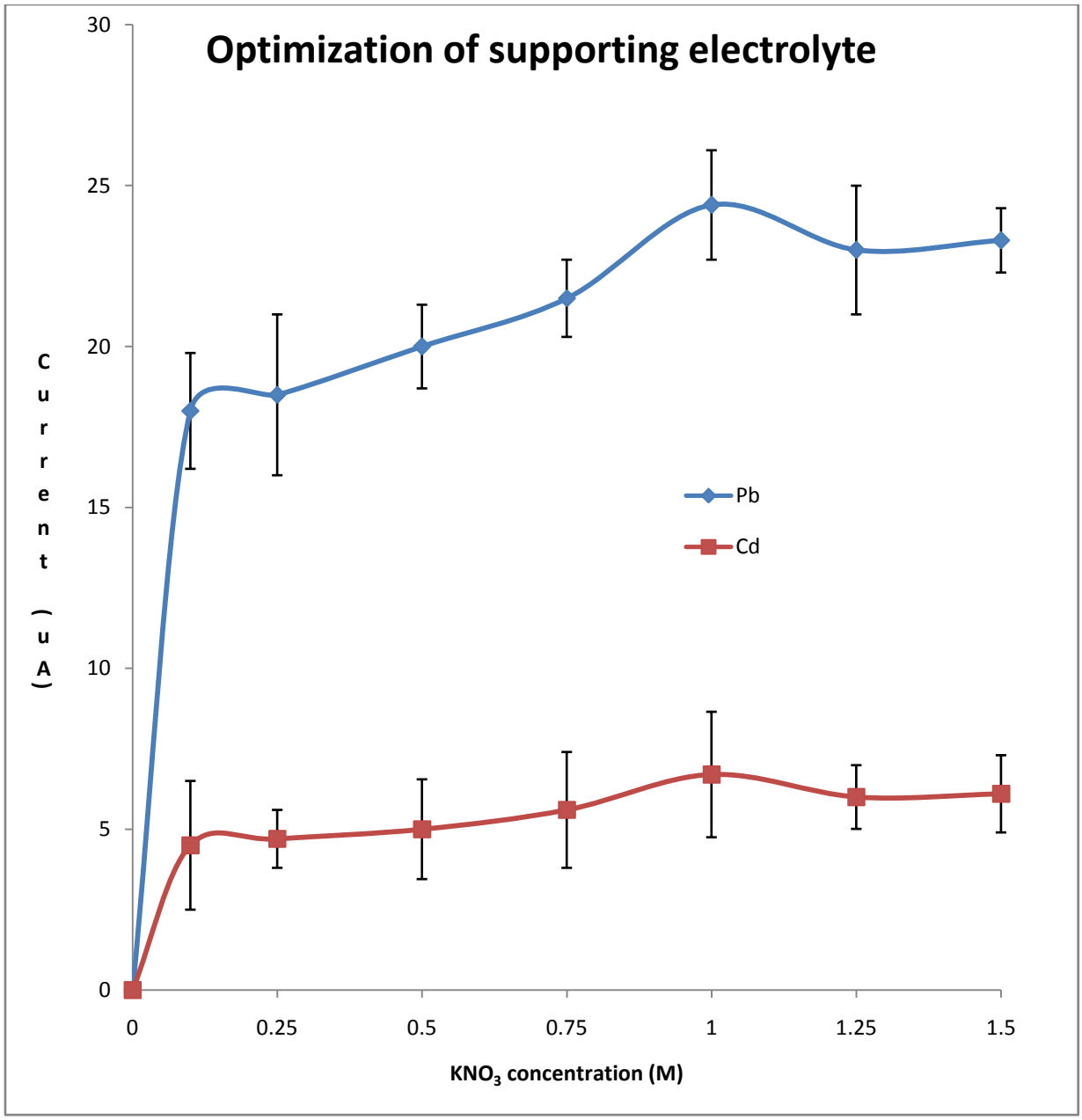

Figure 11: SWASV analysis, optimization of KNO_3 supporting electrolyte concentration, error bars represented ± 1σ.

b) Optimization of pre-concentration potential

The second SWASV analysis parameter to be optimized was pre-concentration potential. The range of deposition potential selected was -1000 to -1300 mV. This range of deposition potential was chosen because for potential more positive than -1000 mV, pre-concentration of Cd may be incomplete, and for potential more negative than -1300 mV, severe hydrogen evolution can influence the efficiency of the pre-concentration process. From Figure 12, for both Pb and Cd, it can be seen that the stripping peak current magnitudes increased with increasing deposition potential, up to -1200mV. For deposition potential of -1250 mV and -1300 mV, hydrogen evolution became profound as formation of bubbles at the electrode surface was observed. In addition, the sensitivity of SWASV analysis appeared to decrease for deposition potential more negative than -1200 mV; therefore, pre-concentration potential of -1200 mV was selected to be the optimal deposition potential for all subsequent SWASV analysis [182].

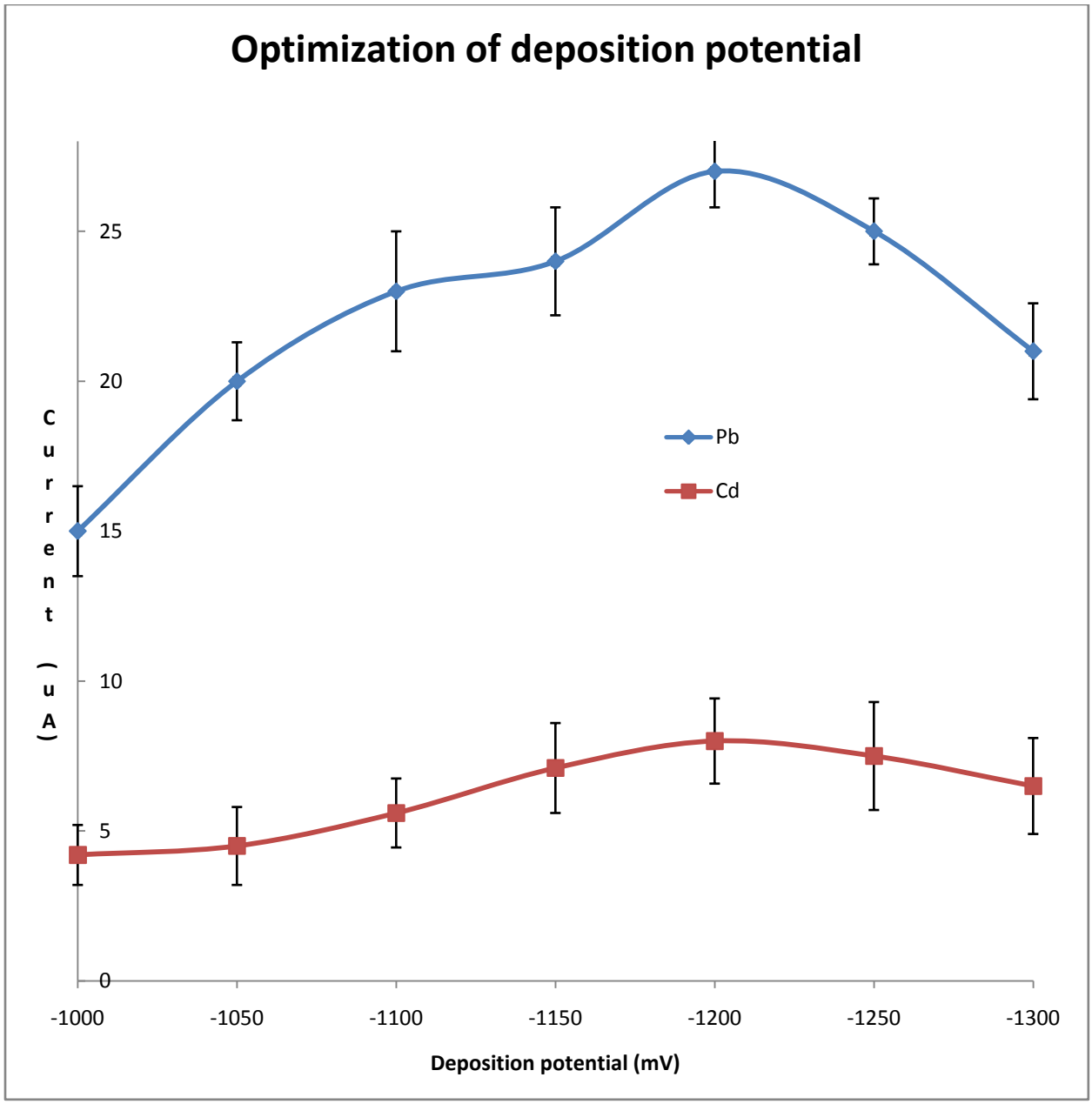

Figure 12: SWASV analysis, optimization of pre-concentration potential, error bars represented ± 1σ.

c) Optimization of pre-concentration time

In addition to supporting electrolyte concentration and pre-concentration potential, deposition time was also optimized for SWASV analysis of Pb and Cd. The tested deposition times ranged from 60 to 300 seconds. Due to the possibility of electrode surface decay, no deposition period longer than 300 seconds was tested. As illustrated in Figure 13, overall, for both metals, increasing deposition time corresponded to increasing peak current magnitudes, up to 120 seconds. For pre-concentration time beyond 120 seconds, enhancement of peak current magnitude was not observed. From this result, pre-concentration time of 120 seconds was used for all subsequent SWASV analysis [182].

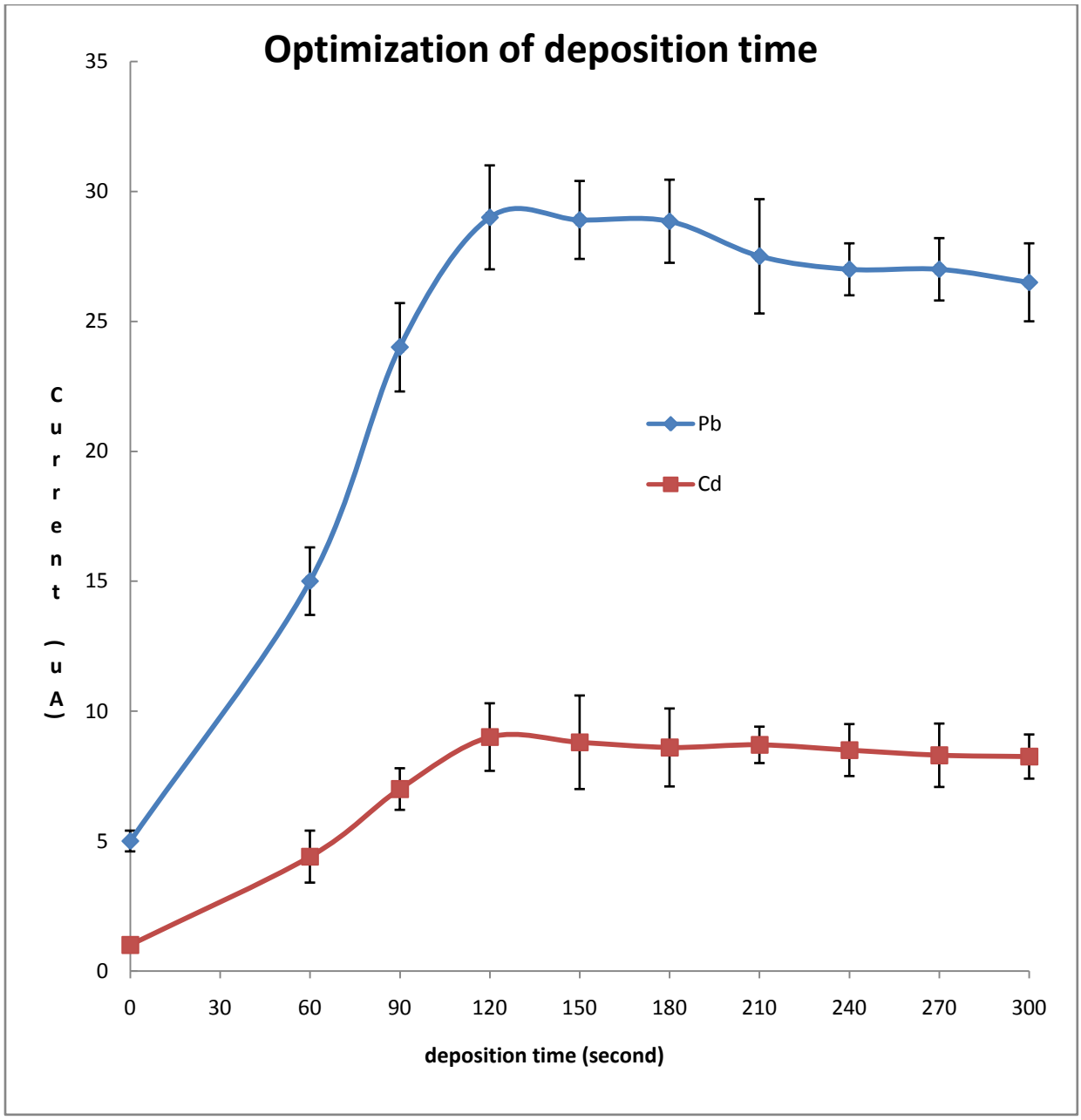

Figure 13: SWASV analysis, optimization of pre-concentration time, error bars represented ± 1σ.

8) SWASV analysis of Pb and Cd utilizing TiO_2/ZrO_2 carbon paste composite electrode

a) SWASV analysis of Pb

In this study, SWASV analysis for Pb was performed in the concentration range between 1 to 200 ppb (Figure 14A and 14B). Regression analysis revealed that there were two different linear calibration ranges for Pb (Figure 15). The first linear concentration range was from 1 to 40 ppb, with linear regression equation estimated as: $y = 1.201x + 1.650$ ($R^2 = 0.997$). From the slope of the linear calibration equation, the sensitivity for Pb detection using TiO_2/ZrO_2 carbon paste composite electrode at the above concentration range was 1.2 µA/ppb. The second linear calibration range spanned from 40 to 200 ppb, with the best-fitted linear regression equation being: $y = 0.72x + 20.04$ ($R^2 = 0.997$). From the slope, the sensitivity of Pb detection for the concentration range between 40 to 200 ppb was estimated to be 0.72 µA/ppb. In addition, reproducibility of SWASV peak signal for Pb was investigated by measuring 10 independent trials at 100 ppb; this analysis revealed that the response for Pb was acceptably reproducible as the relative standard deviation was calculated to be 2.5% (Figure 16). Moreover, using the lower concentration range linear calibration equation and 3-sigma method, the detection limit for Pb was estimated to be 0.48 ppb (estimation based on 10 independent blank measurements).

It was also observed that the stripping potential of Pb appeared to shift in the positive direction as the concentration of Pb increased. This phenomenon could be rationalized as the layer of Pb being deposited onto the electrode surface became thicker, higher potential would be required to oxidize the analyte from the electrode surface [182].

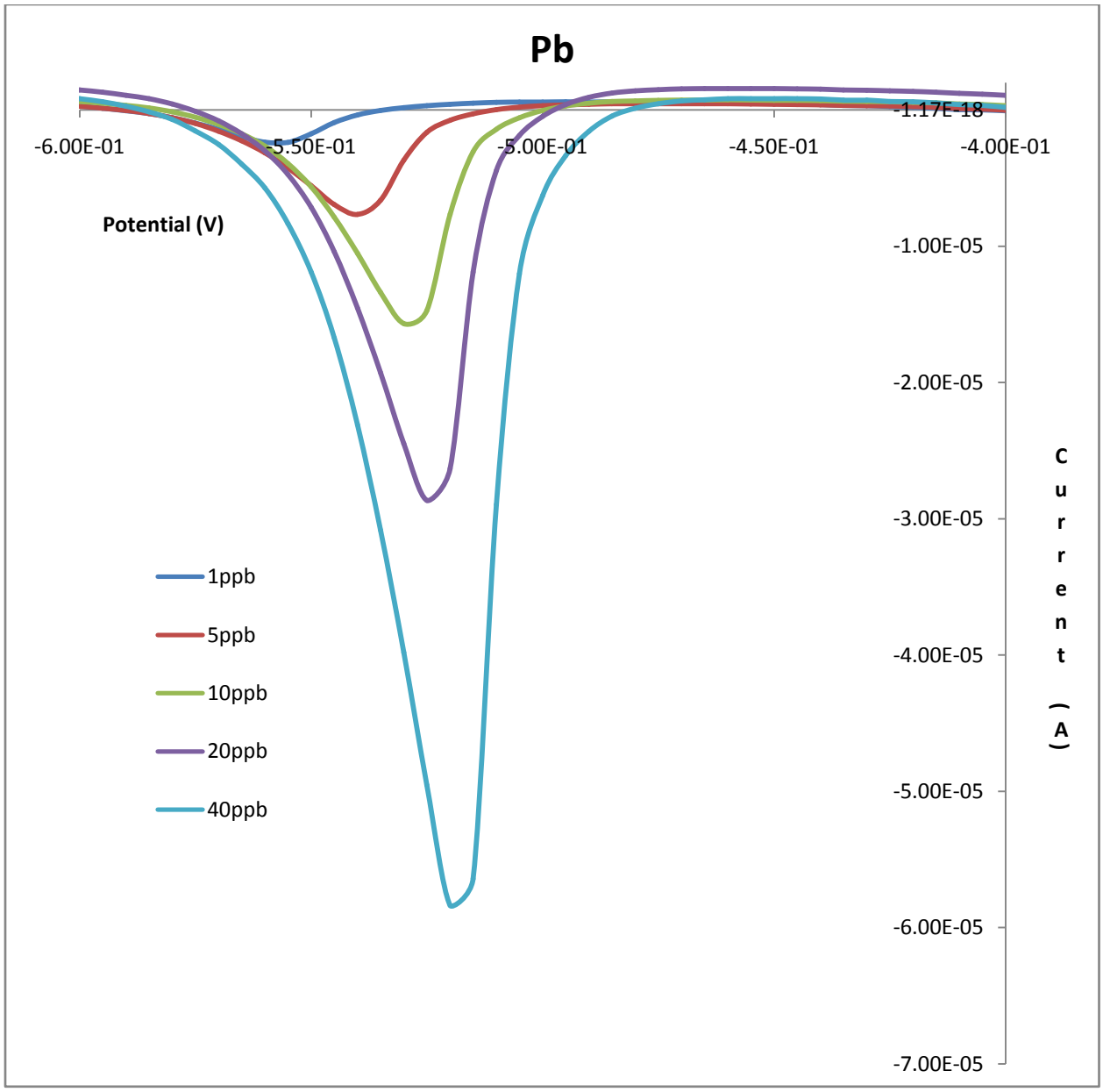

Figure 14A: SWASV analysis of Pb in concentration range 1 to 40 ppb.

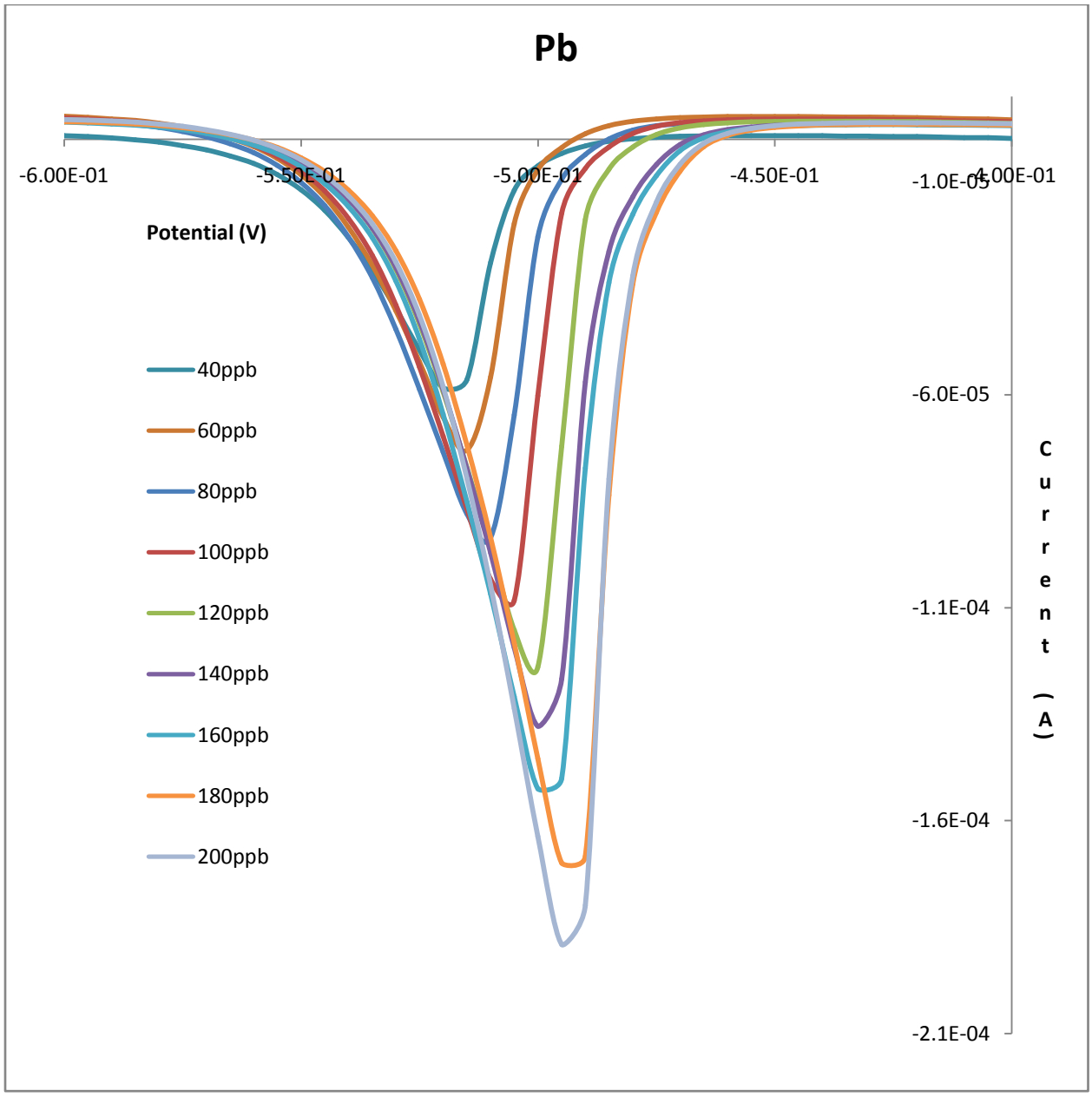

Figure 14B: SWASV analysis of Pb in concentration range 40 to 200 ppb.

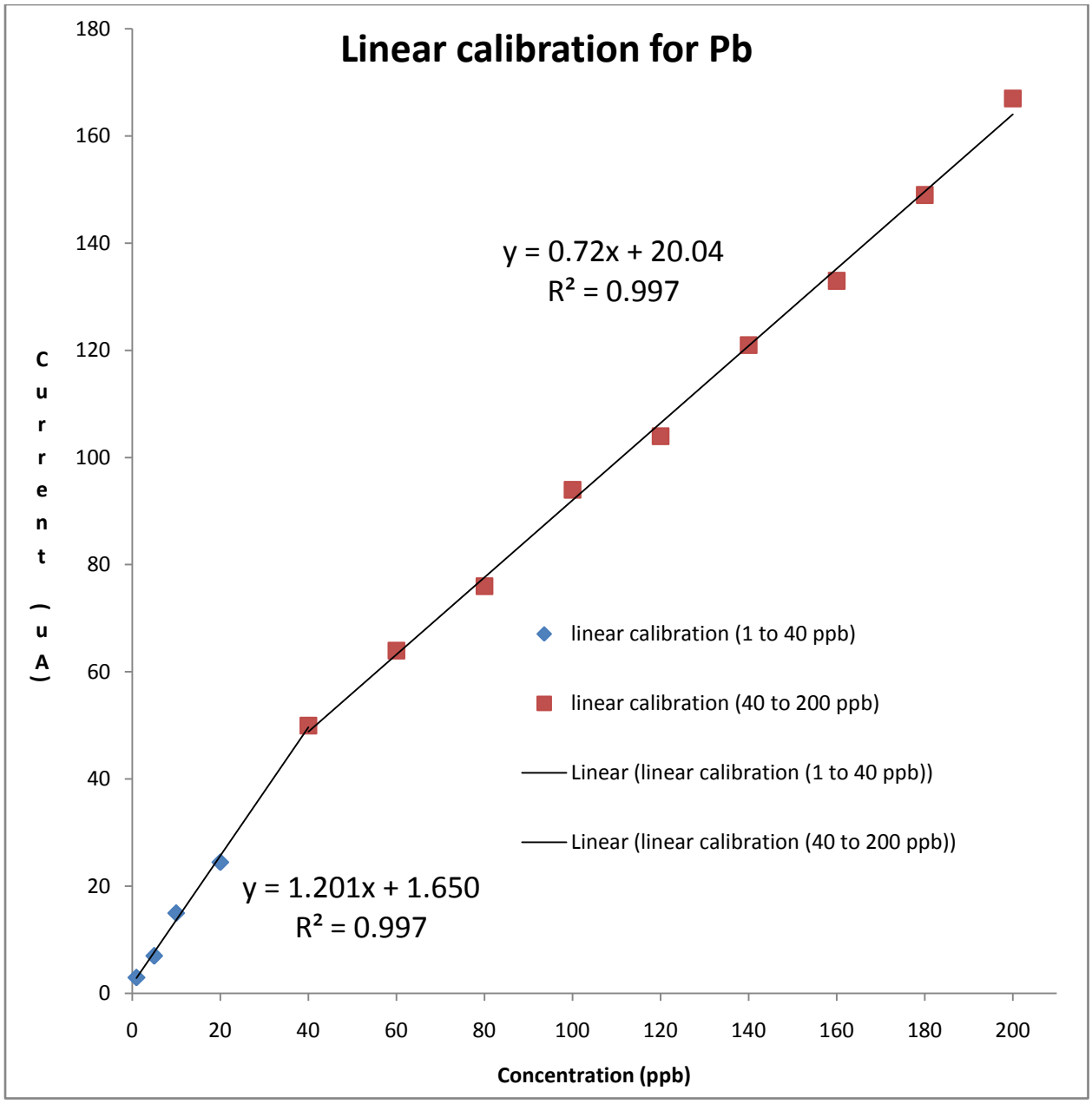

Figure 15: Linear calibration plot for SWASV analysis of Pb.

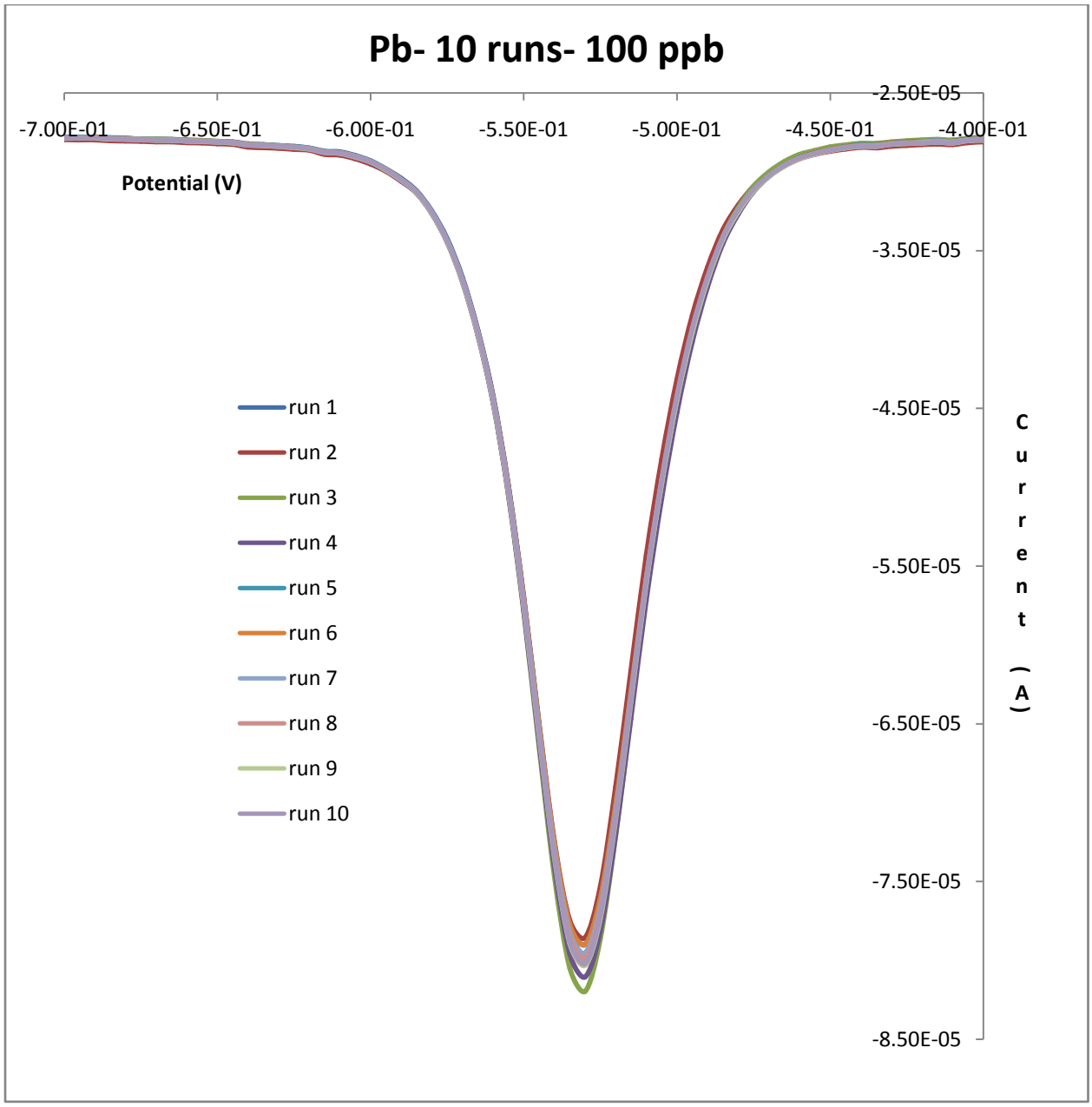

Figure 16: SWASV of Pb at 100 ppb, 10 independent runs.

b) SWASV analysis of Cd

Similarly to Pb, SWASV analysis for Cd was also performed in the concentration range between 1 to 200 ppb (Figure 17A and 17B). Linear calibration analysis also revealed that there were two different linear calibration ranges for Cd (Figure 18). From 1 to 60 ppb, the first linearity calibration range was observed, with linear regression equation estimated as: $y = 0.604x + 1.357$ ($R^2 = 0.995$). From the slope of the linear calibration equation, the sensitivity for Cd detection, using TiO_2/ZrO_2 carbon paste composite electrode at the above concentration range, approximately equaled 0.6 µA/ppb. The second linear concentration range was found to be between 60 to 200 ppb, with the linear regression equation being: $y = 0.367x + 14.43$ ($R^2 = 0.996$). From the slope, the sensitivity of Cd detection for the concentration range between 40 to 200 ppb was estimated to be 0.37 µA/ppb. Also, similar to Pb analysis, SWASV peak signal reproducibility for Cd was investigated by measuring 10 independent trials at 100 ppb; this analysis revealed that the response for Cd was also acceptably reproducible as the relative standard deviation was calculated to be 3.8% (Figure 19). Furthermore, from lower concentration range linear calibration equation and application of 3-sigma method, the detection limit for Cd was estimated to be 0.77 ppb (estimation based on 10 independent blank measurements). Similar to Pb analysis, shifting of Cd peak potential in the positive direction as Cd concentration increased was also observed; however, such potential shift was not as dramatic as in the case of Pb [182].

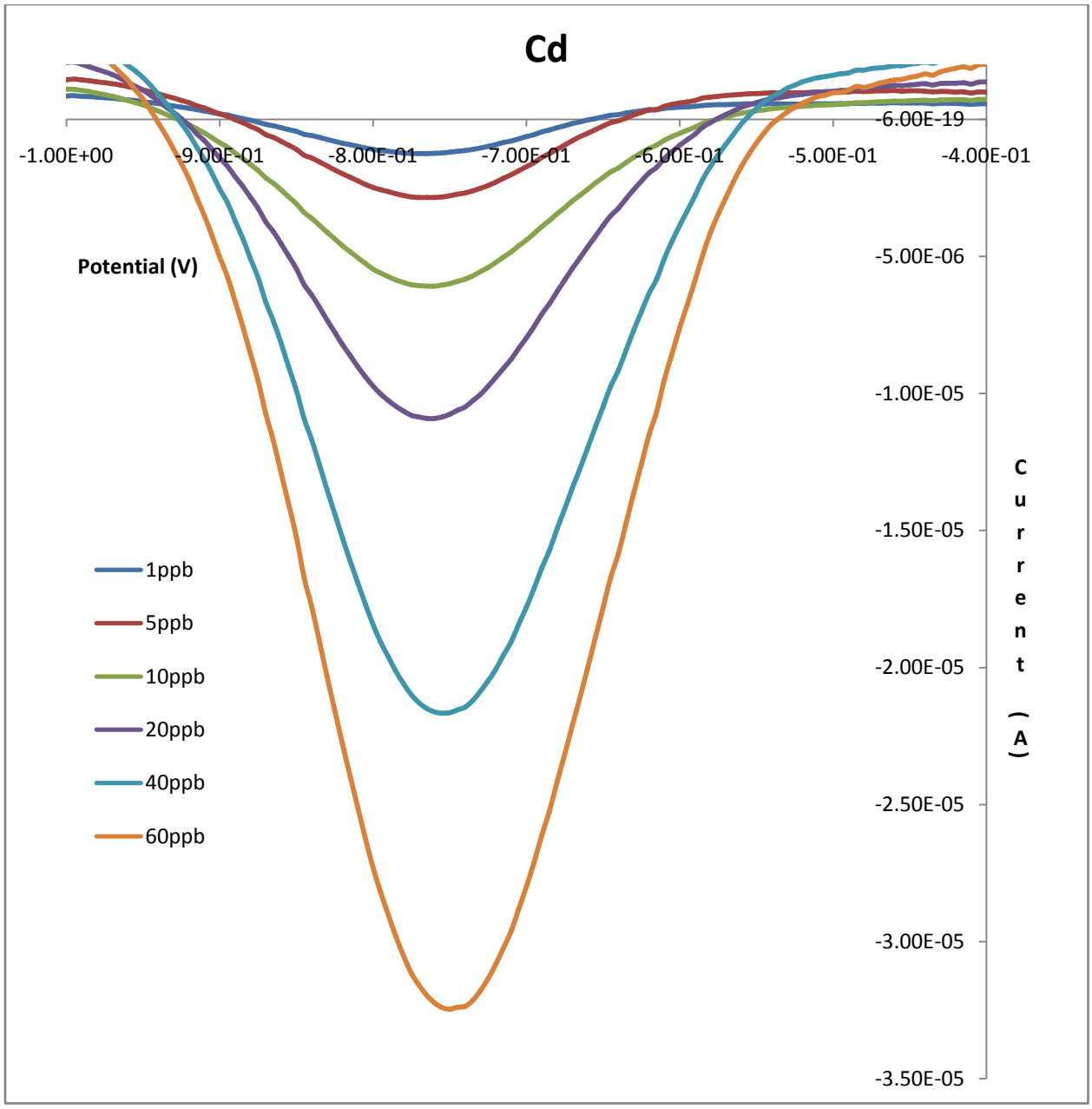

Figure 17A: SWASV analysis of Cd in concentration range 1 to 60 ppb.

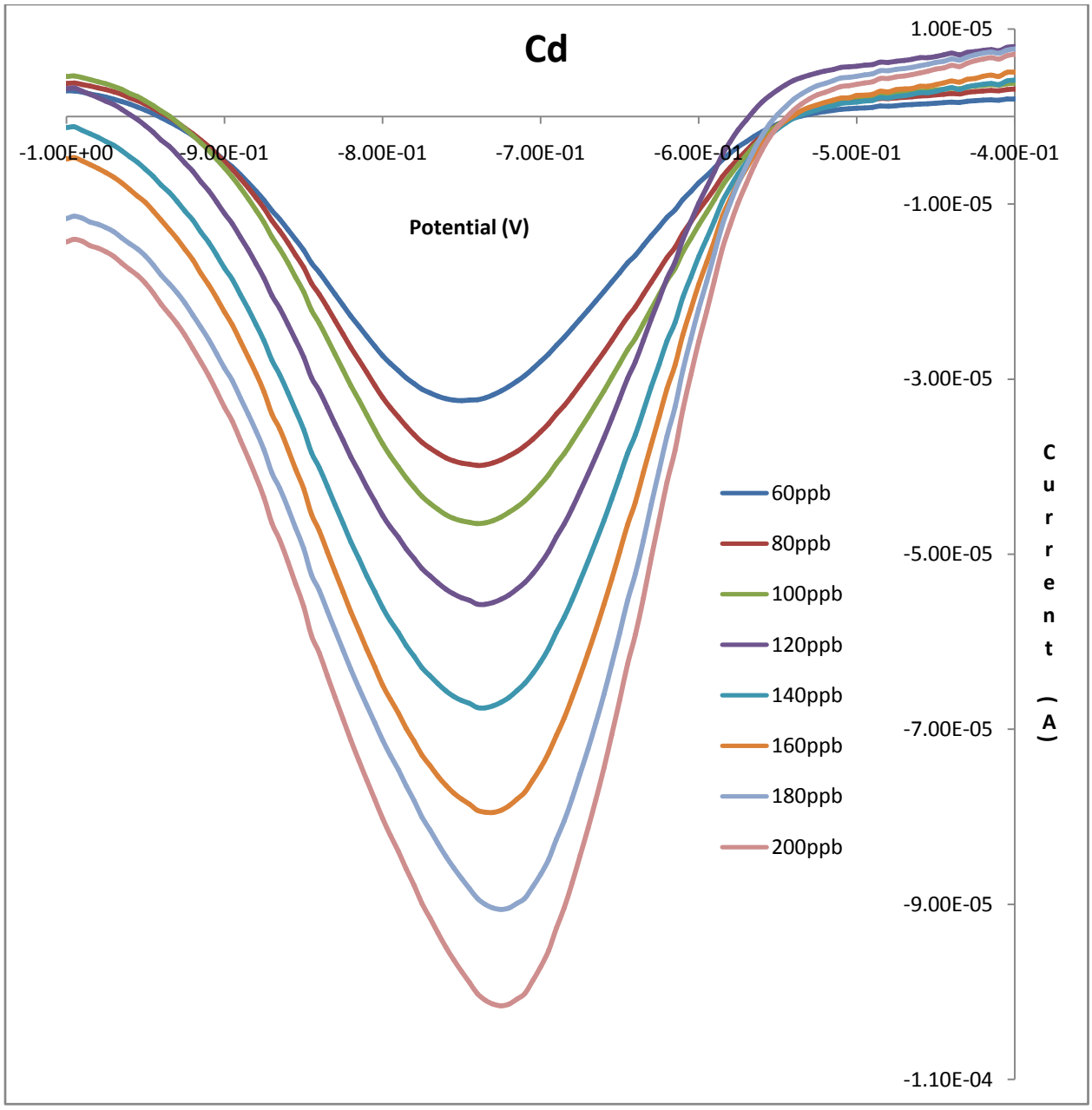

Figure 17B: SWASV analysis of Cd in concentration range 60 to 200 ppb.

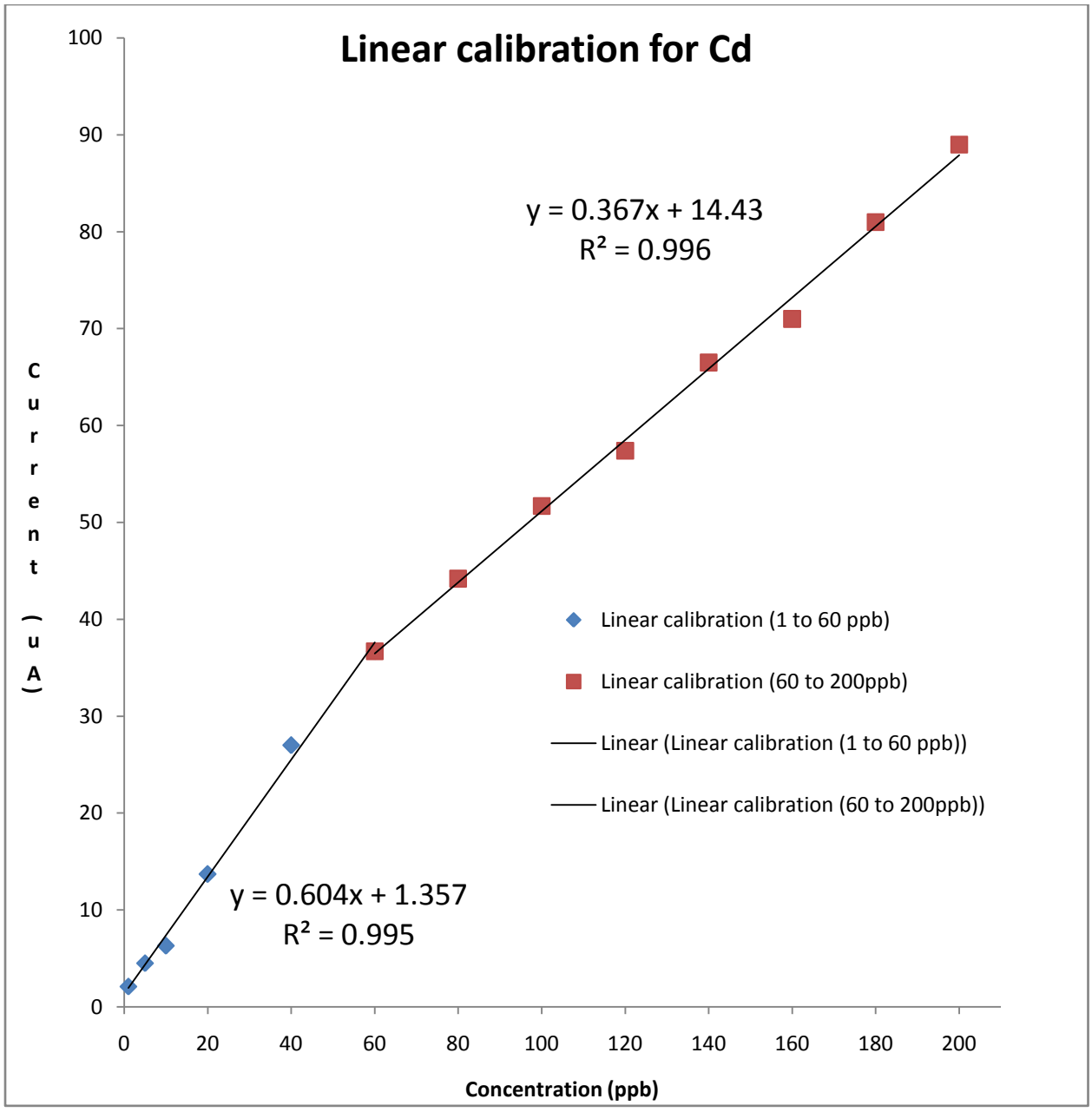

Figure 18: Linear calibration plot for SWASV analysis of Cd.

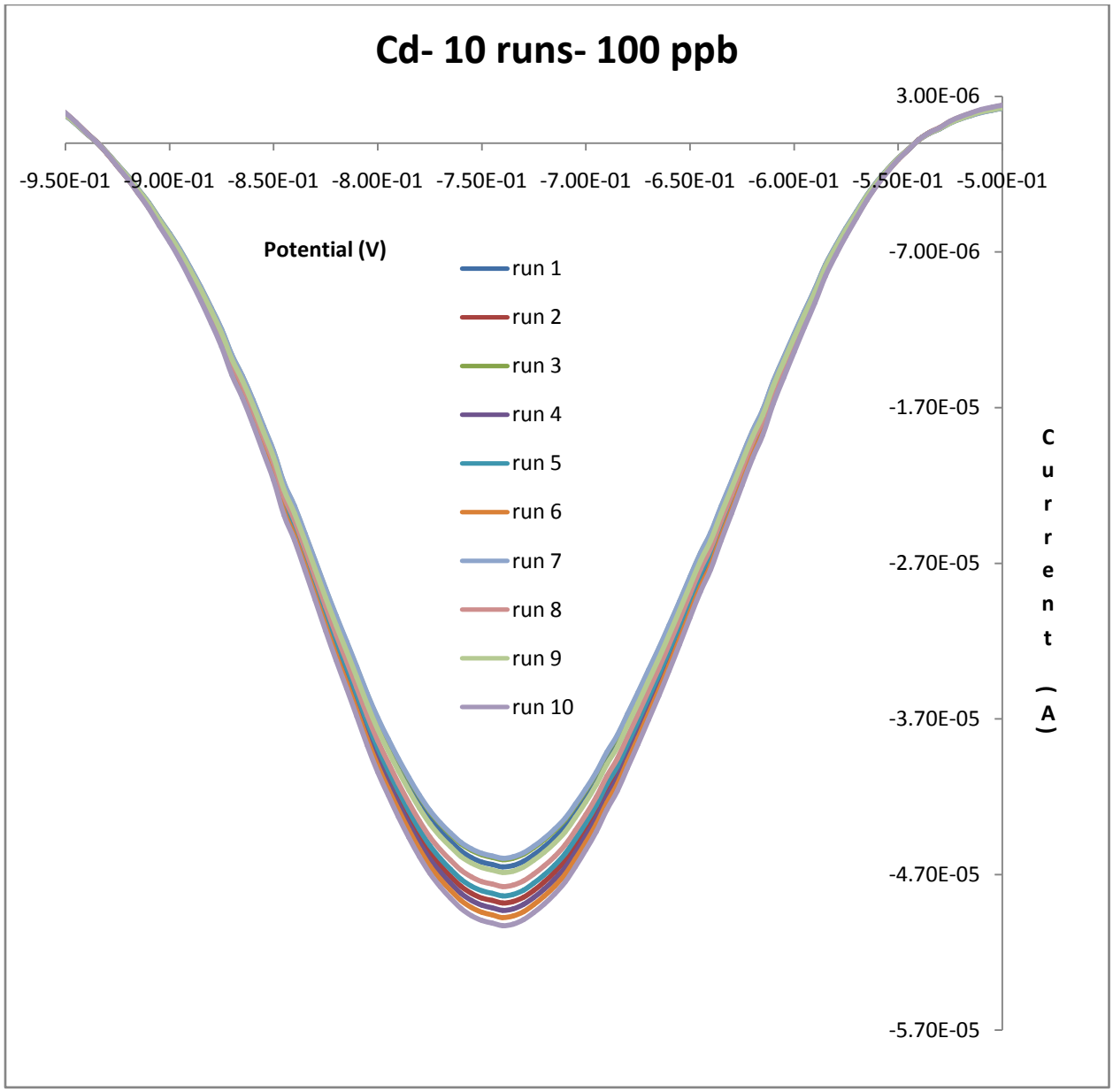

Figure 19: SWASV of Cd at 100 ppb, 10 independent runs.

c) SWASV analysis of Pb and Cd simultaneously

In addition to SWASV analysis for the individual metal, simultaneous Pb and Cd detection via SWASV analysis was also investigated (Figure 20A and 20B). Like individual metal analysis, Pb and Cd simultaneous detection also appeared to have two different linear calibration ranges (Figure 21); the first range lied between 1 to 60 ppb, while the second range was from 60 to 200 ppb. With respect to the lower concentration linear calibration range, the linear regression equations were $y = 3.258x + 4.643$ ($R^2 = 0.998$) and $y = 0.672x + 2.516$ ($R^2 = 0.992$) for Pb and Cd, respectively. From the linear regression slopes, the estimated sensitivity for Pb was 3.26 µA/ppb and 0.67 µA/ppb for Cd in the concentration range of 1 to 60 ppb. Regarding the upper concentration linear calibration range, the linear regression equations were estimated to be: $y = 1.781x + 94.02$ ($R^2 = 0.998$) and $y = 0.300x + 24.82$ ($R^2 = 0.997$) for Pb and Cd, respectively. Similarly, from the linear calibration slopes, the estimated sensitivity for Pb was 1.78 µA/ppb and 0.3 µA/ppb for Cd in the concentration range of 60 to 200 ppb. Overall, the sensitivity for Cd detection did not differ significantly when comparing between individual analysis and with Pb presence. However, we observed an increase (approximately 2.5 folds enhancement) in the sensitivity of Pb detection when being analyzed in the presence of Cd compared to that of individual Pb analysis. At high concentrations of Cd, distortions to the stripping peaks of Cd were observed. A possible explanation for this issue is the surface stability variation over numerous continuous cycles over time [182].

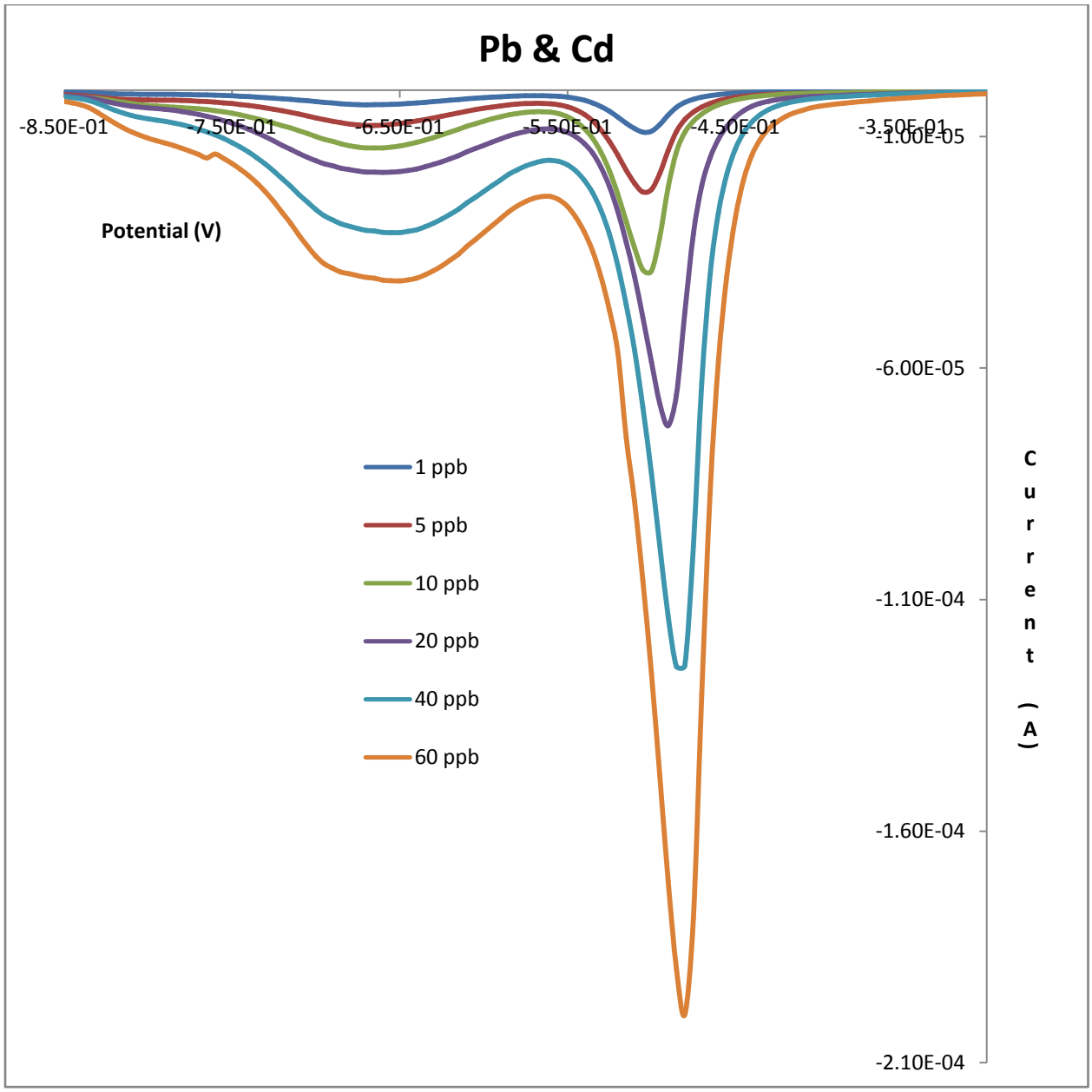

Figure 20A: Simultaneous SWASV analysis of Pb and Cd in concentration range 1 to 60 ppb.

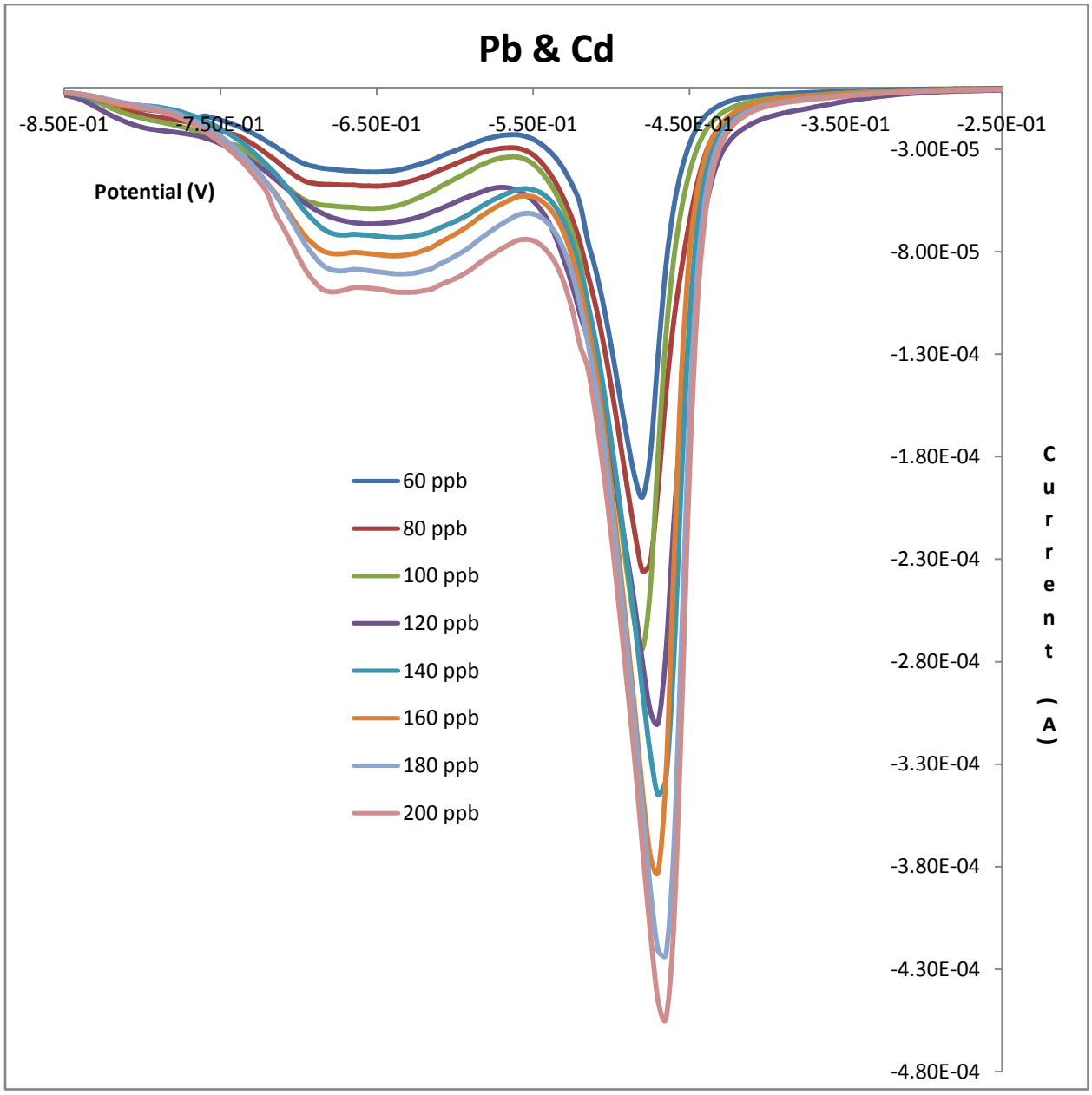

Figure 20B: Simultaneous SWASV analysis of Pb and Cd in concentration range 60 to 200 ppb.

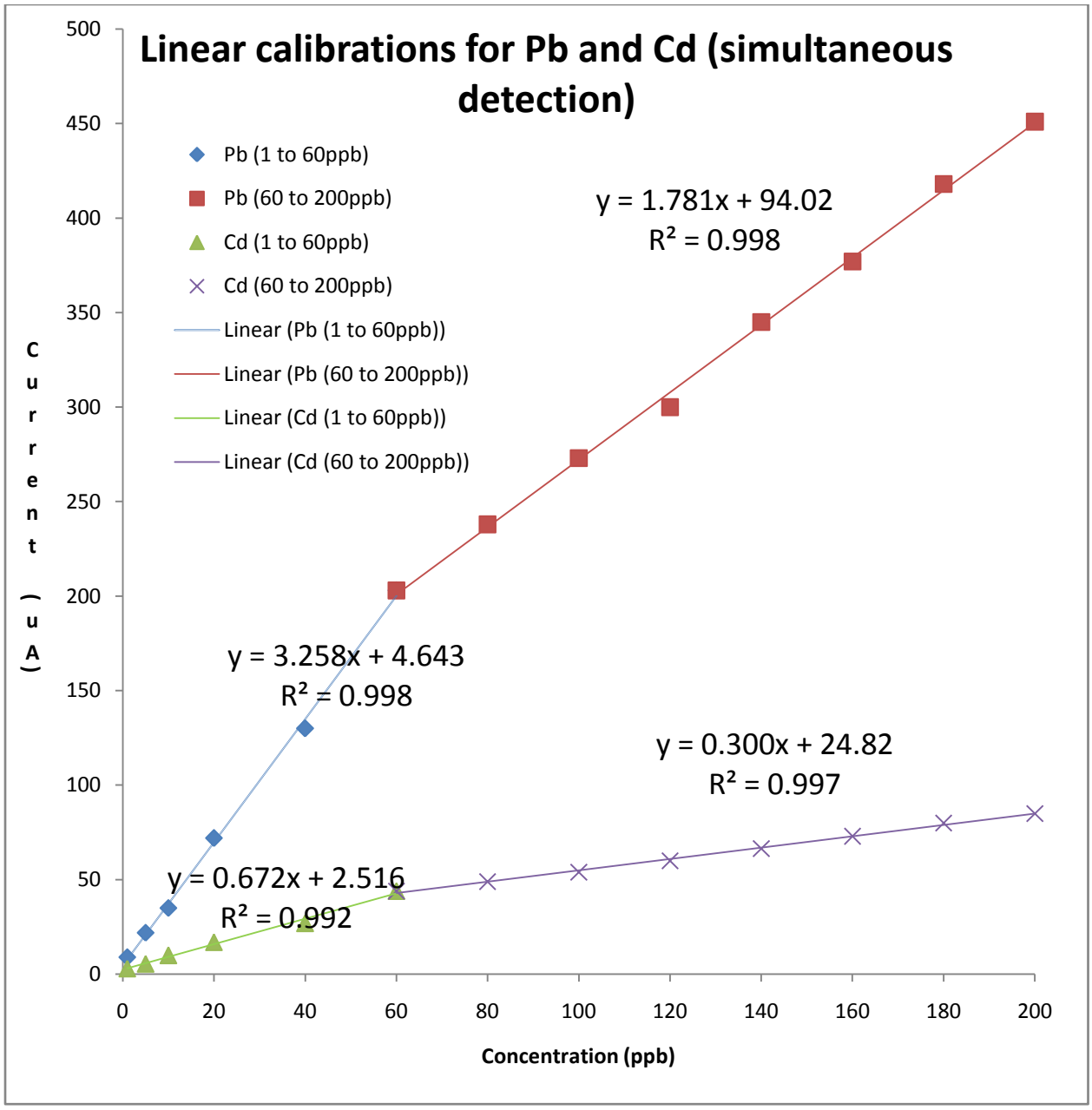

Figure 21: Linear calibration plot for simultaneous SWASV analysis of Pb and Cd.

As observed in both individual and simultaneous analysis of Pb and Cd, unified linearity throughout the entire testing concentration range was not seen, but rather splitting in linear calibration ranges was obtained. In addition, the sensitivities of the electrode toward detection of the analytes were better in the lower concentration ranges compared to that of the upper concentration ranges. This phenomenon is not uncommon in electro-analytical chemistry, particularly in heavy metal analysis.

d) Analysis of river water and well water sample, and certified standard reference waste water

In order to evaluate the performance of the TiO_2/ZrO_2 carbon paste composite electrode for real world application, SWASV of Pb and Cd was performed in river water and well water samples. Three different water samples (river water and well water from Saigon, Vietnam, and river water from the Great Miami River in Dayton, Ohio) were used in this study. The water samples were filtered with 0.22 micron cellulose acetate syringe filter (Cole Parmer), appropriate amount of supporting electrolyte was added prior to acidification with HNO_3. Spiking of the water samples with Pb and Cd was done prior to SWASV analysis. For analytical purposes, square wave stripping analysis of the metals was done via multiple standard additions, and the accuracy of the assays was cross-checked with ICP-OES. Table 1 summarized the results of river waters and well water analysis via SWASV and ICP-OES. Overall, the data obtained with SWASV agreed very well with that of ICP-OES (none of the measurements differed more than 5%), these results demonstrated the proposed sensor's potential for real world application [182].

In addition to river and well water samples, SWASV analysis was also carried out on certified standard reference waste water (purchased from High-Purity Standards), which has a known amount of Pb (1.00 ppm) and Cd (0.250 ppm). After micro-filtration, the waste water sample was diluted accordingly (by a factor of 10 for Pb analysis, and a factor of 2.5 for Cd

analysis) with acidified water solution that contained appropriate amount of supporting electrolyte. In a similar manner to river and well water samples analysis, multiple standard additions was used for certified standard reference waste water analysis. Figure 31A &B and Figure 32A &B illustrated the results for particular experiment. From this data, the concentrations of Pb and Cd, in the original certified standard reference waste water sample, were calculated to be 0.97 (±0.03) ppm and 0.244 (± 0.021) ppm, respectively. This corresponded to a 97% recovery for Pb and 98% recovery for Cd, assuming the certified concentration value is absolutely correct. From the results of SWASV analysis of certified standard reference waste water sample, the potential for real world application of the newly developed electrode is further confirmed.

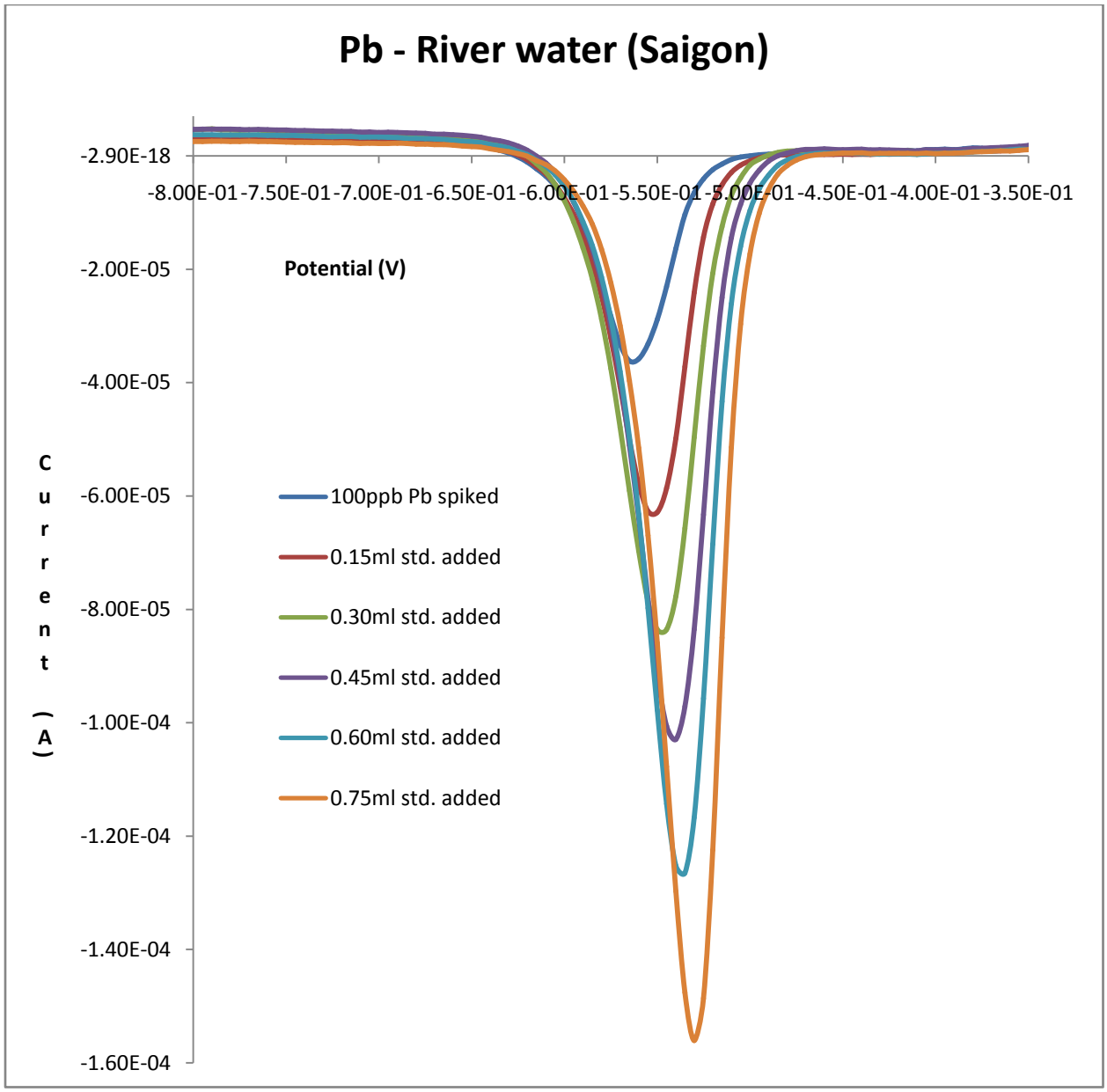

Figure 22A: SWASV analysis of Pb in river water sample from Saigon, Vietnam.

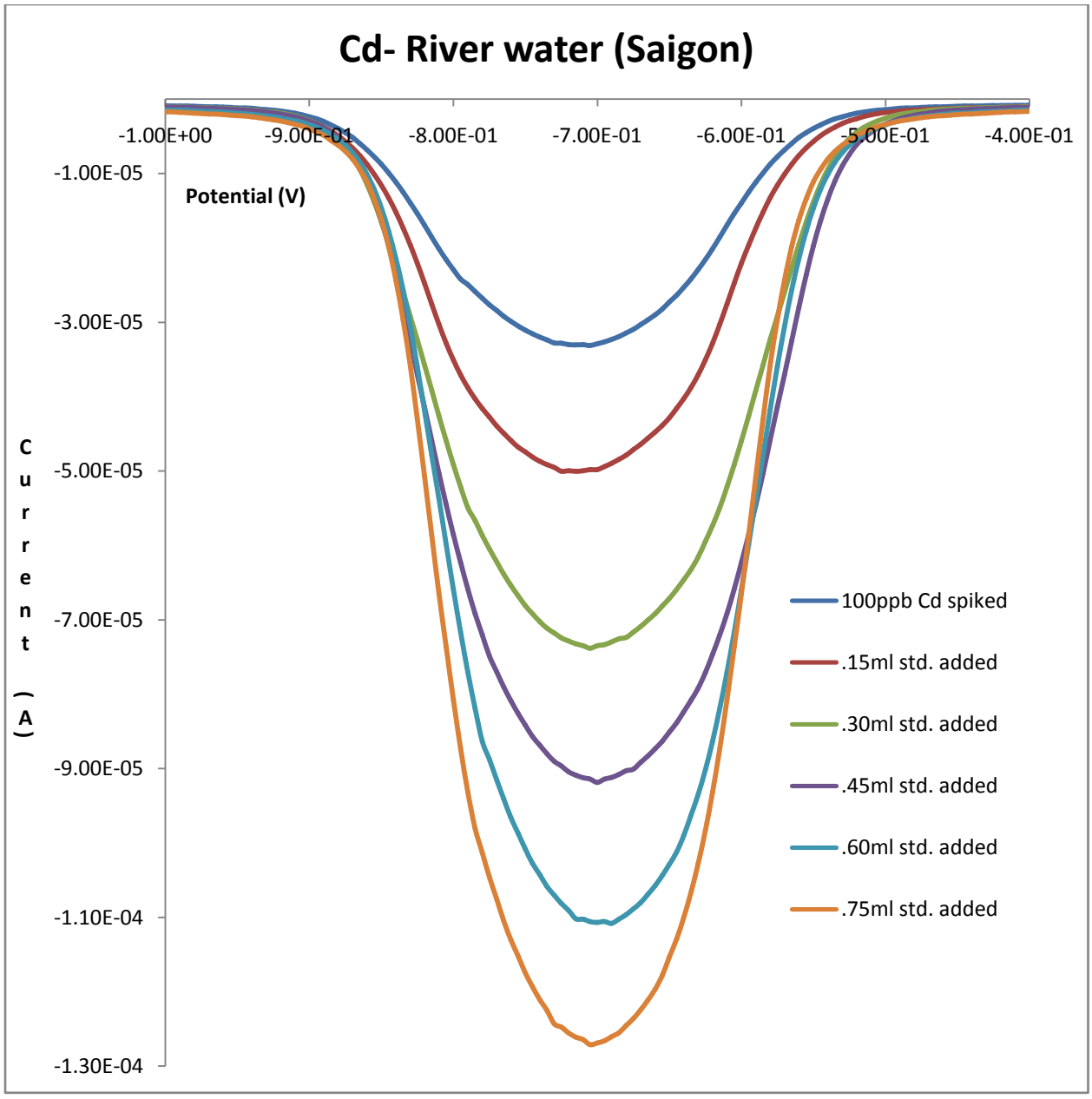

Figure 22B: SWASV analysis of Cd in river water sample from Saigon, Vietnam.

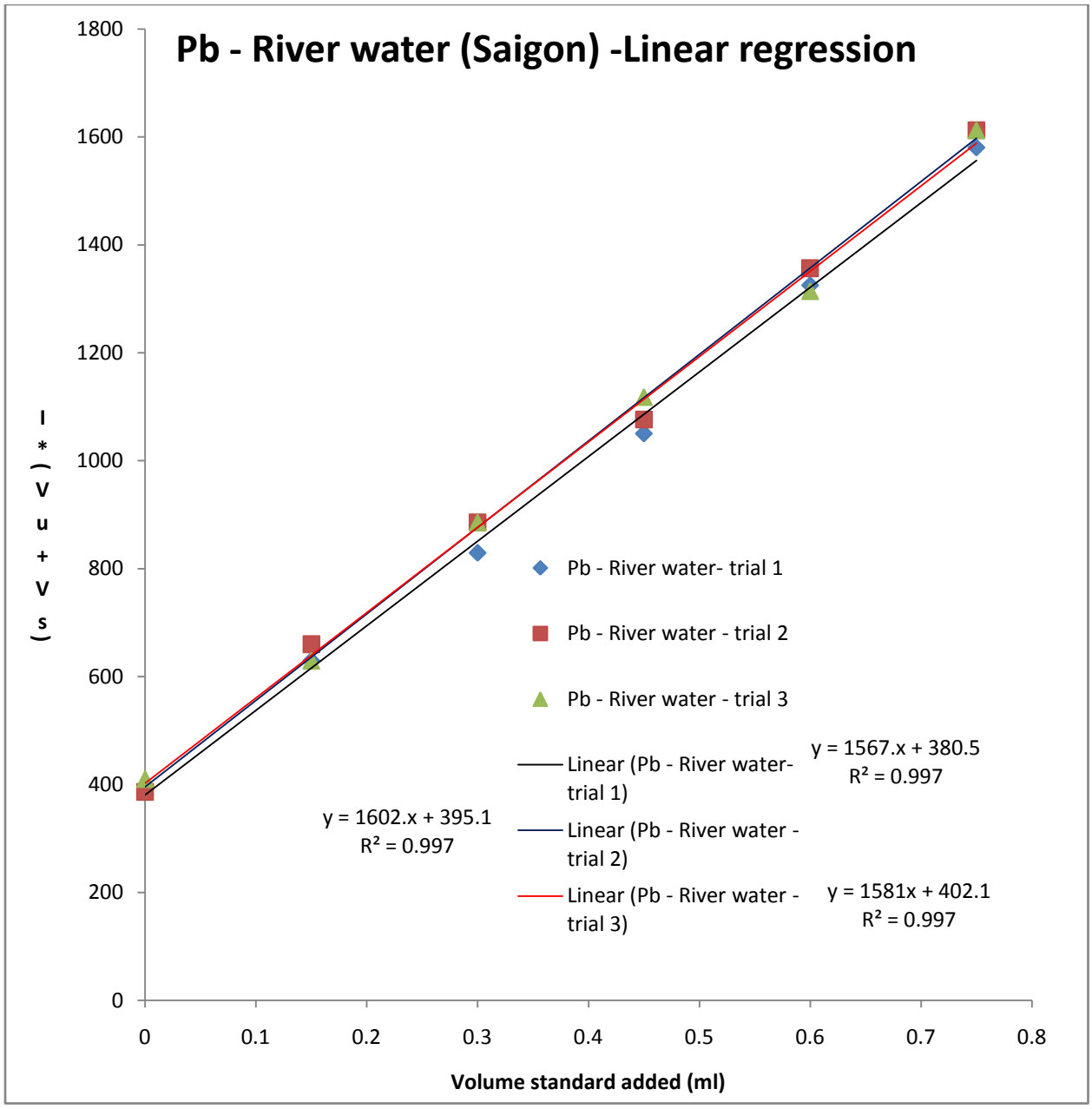

Figure 23A: Linear regression analysis for Pb SWASV results in river water sample from Saigon, Vietnam.

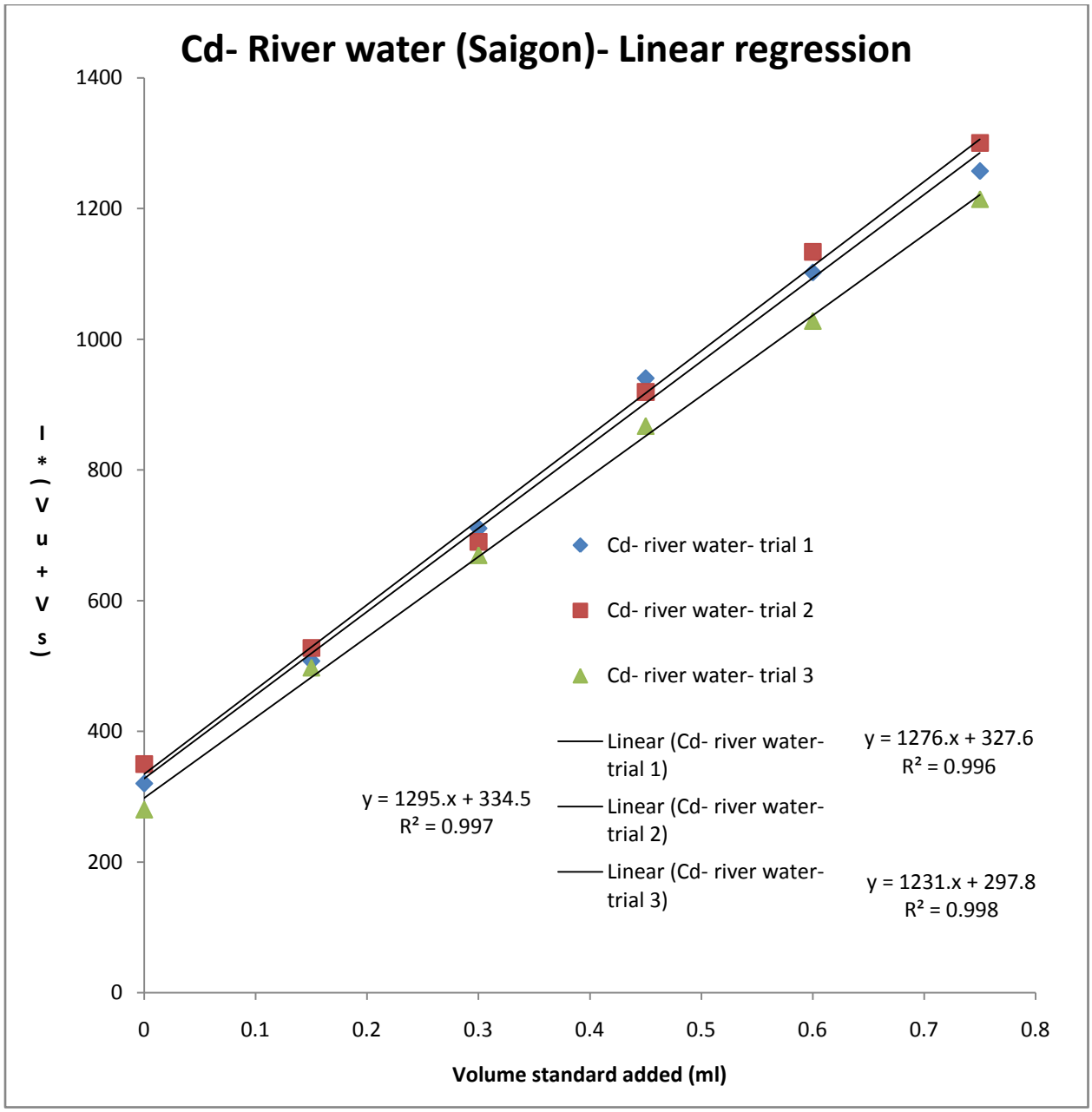

Figure 23B: Linear regression analysis for Cd SWASV results in river water sample from Saigon, Vietnam.

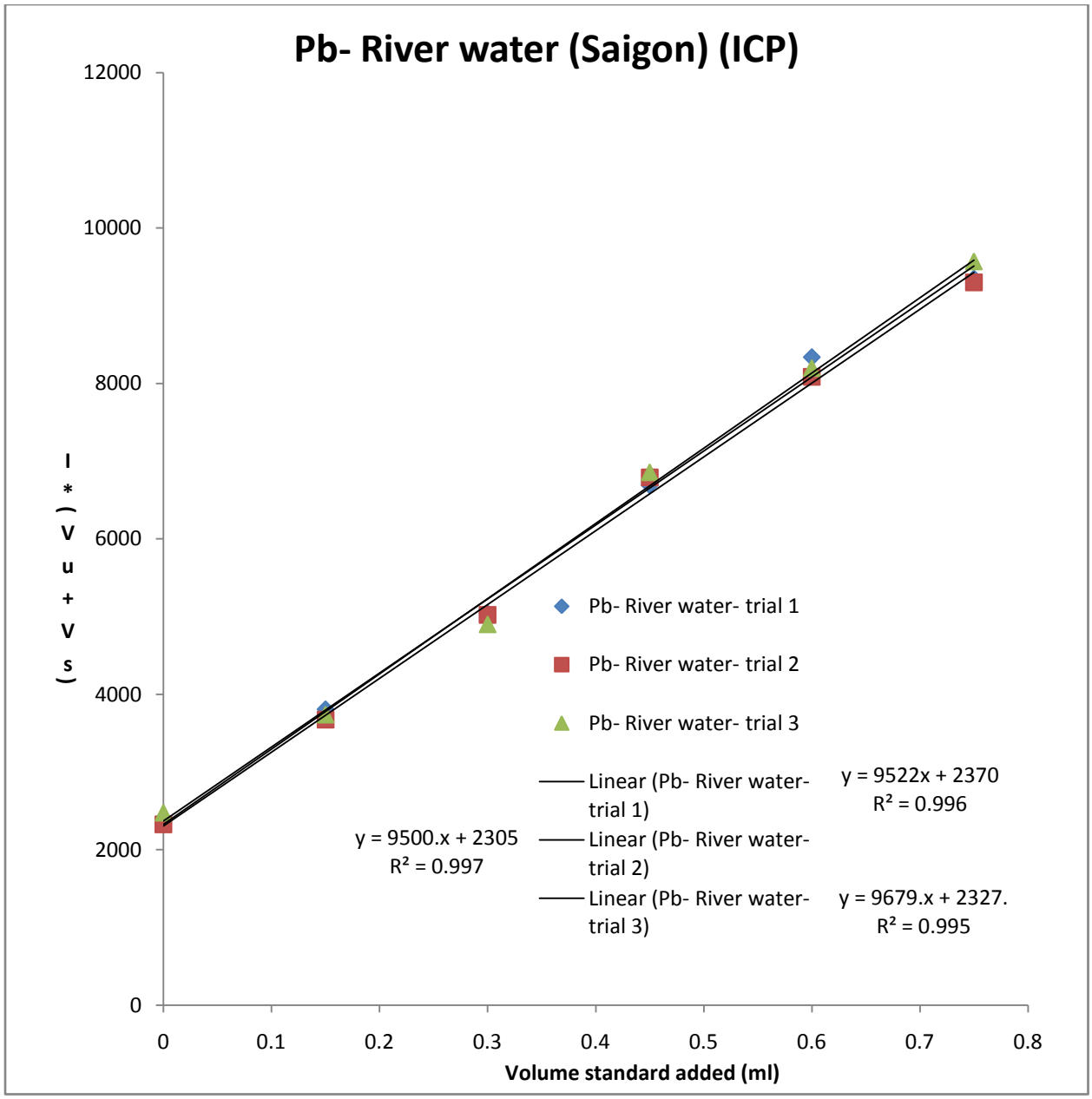

Figure 24A: Linear regression analysis for Pb ICP-OES results in river water sample from Saigon, Vietnam

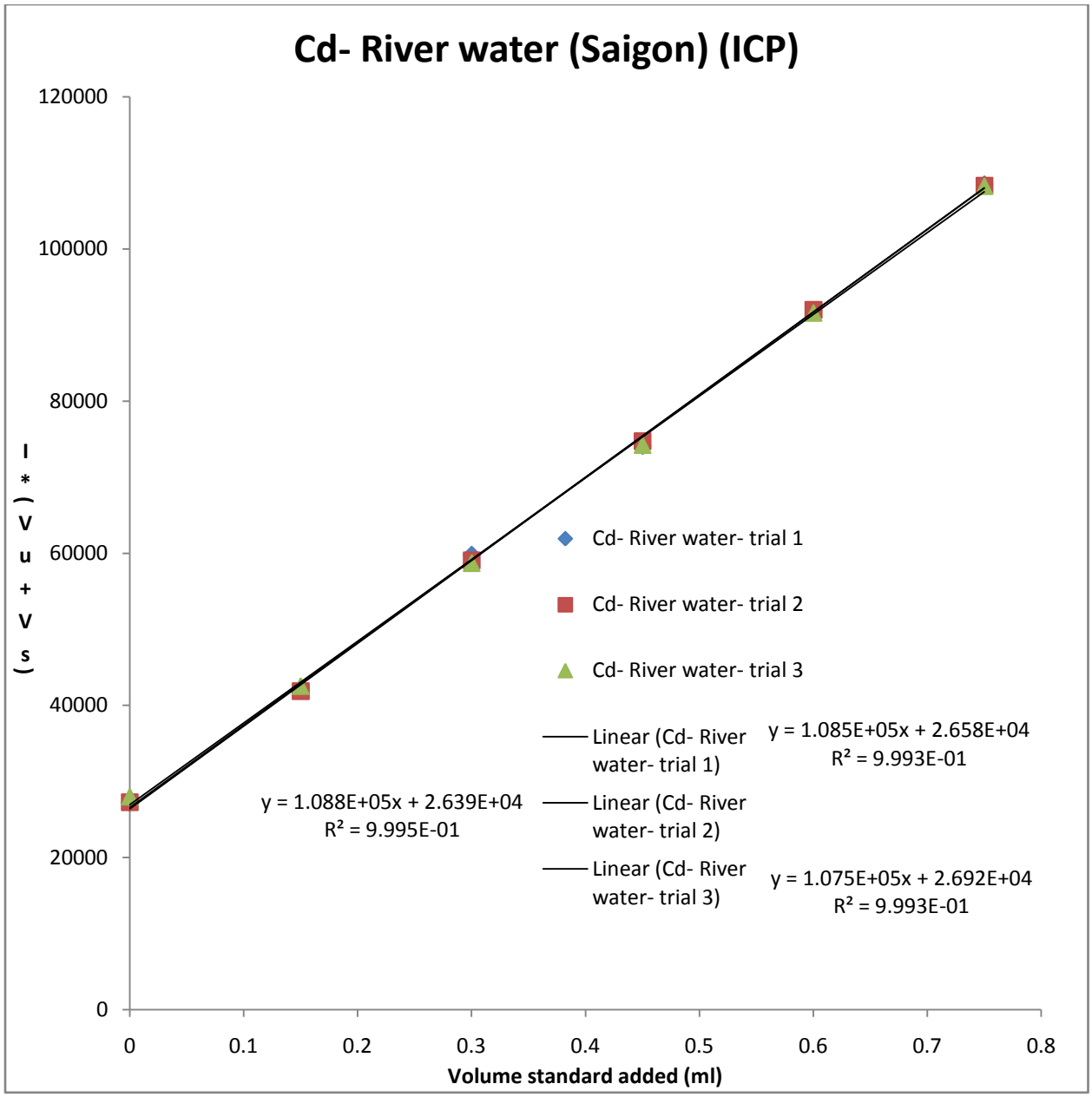

Figure 24B: Linear regression analysis for Cd ICP-OES results in river water sample from Saigon, Vietnam.

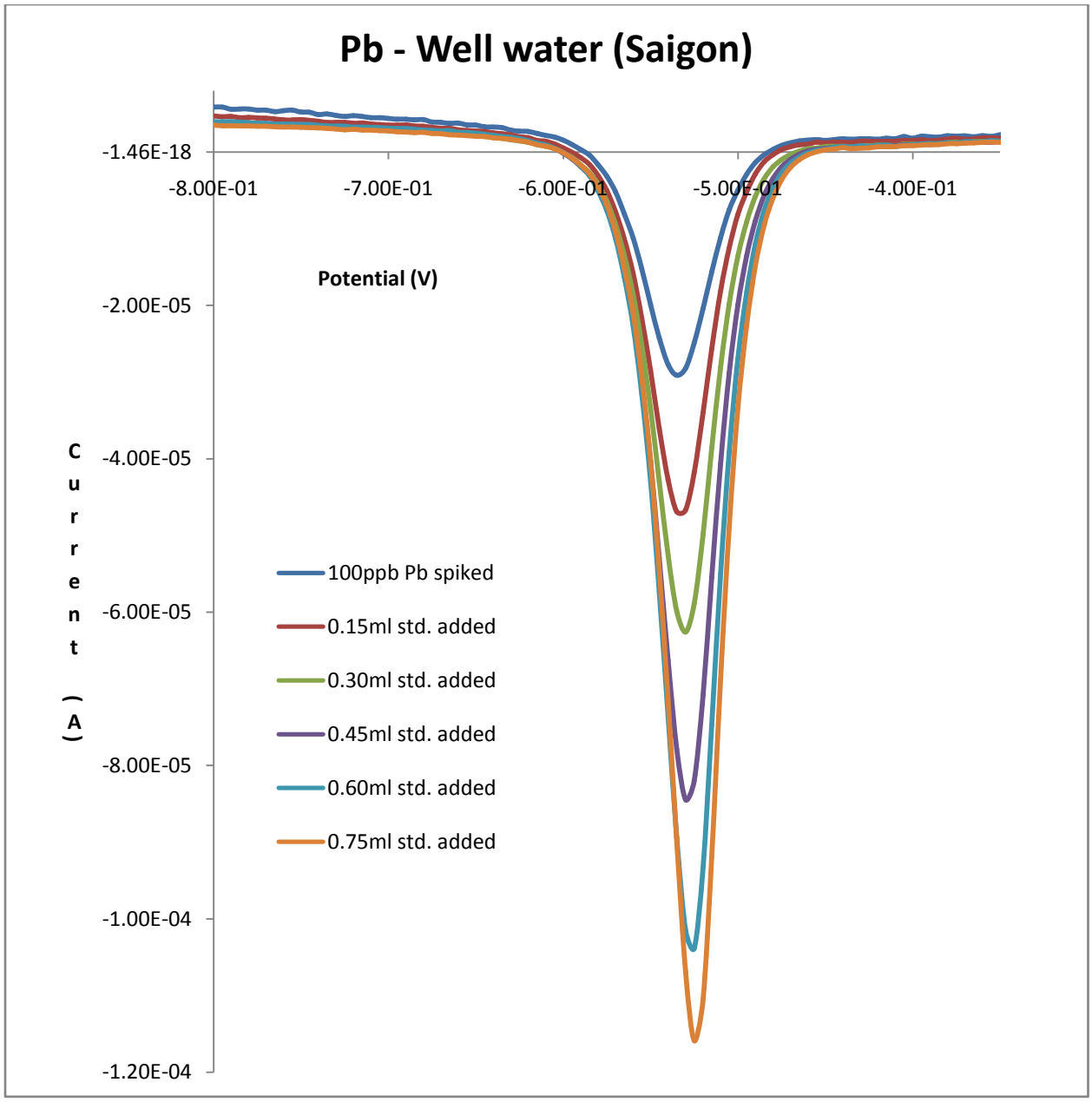

Figure 25A: SWASV analysis of Pb in well water sample from Saigon, Vietnam.

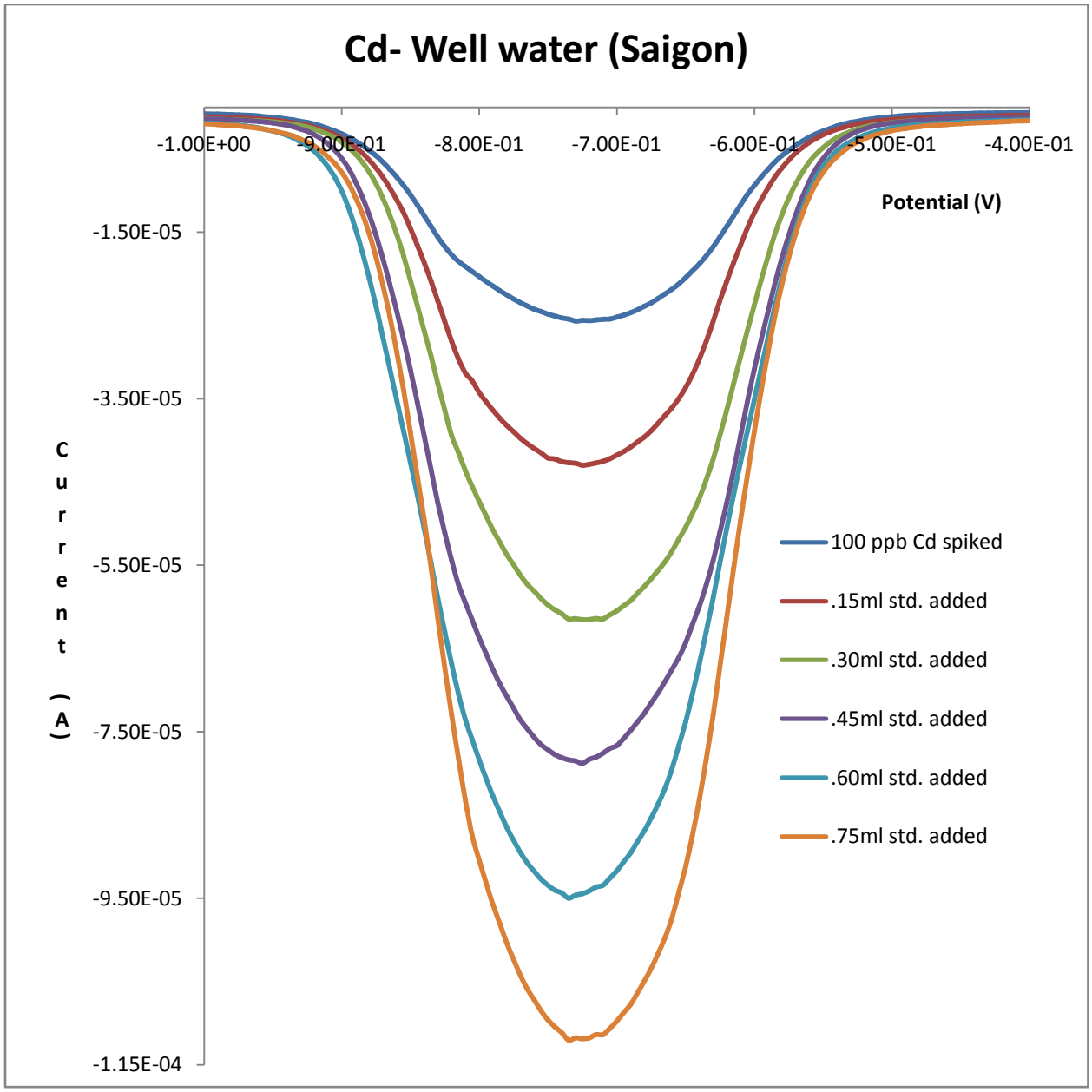

Figure 25B: SWASV analysis of Cd in well water sample from Saigon, Vietnam.

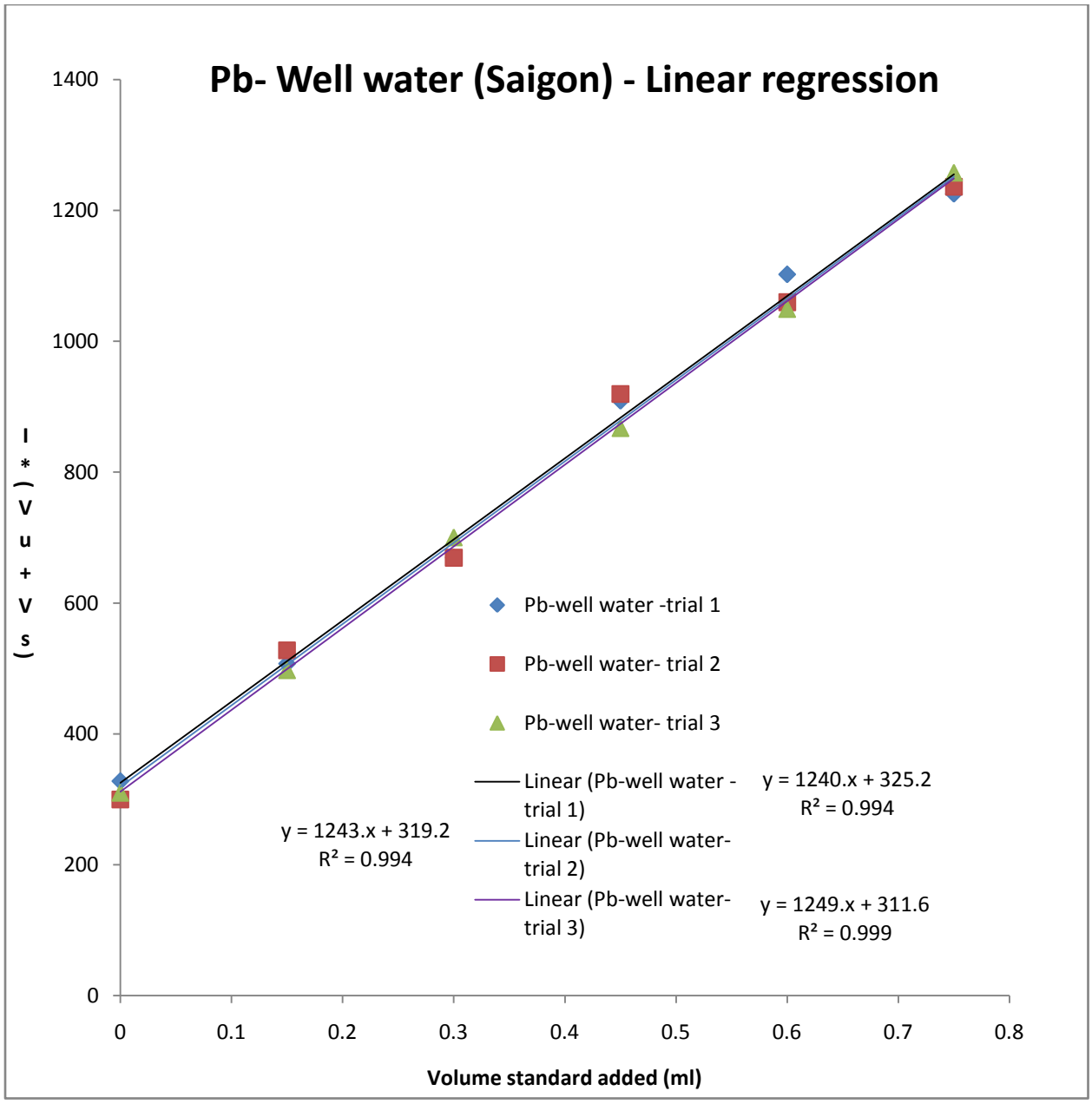

Figure 26A: Linear regression analysis for Pb SWASV results in well water sample from Saigon, Vietnam.

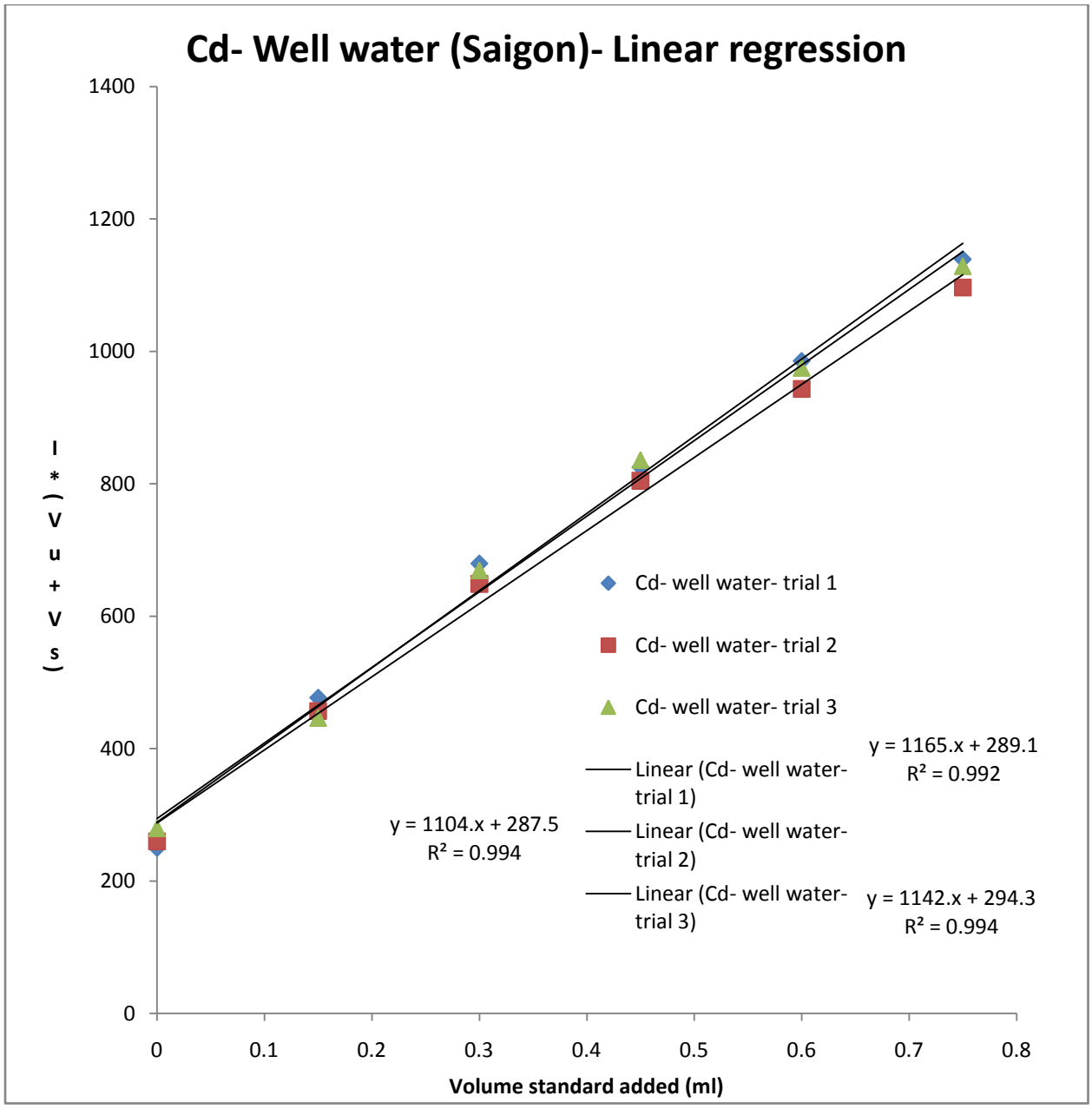

Figure 26B: Linear regression analysis for Cd SWASV results in well water sample from Saigon, Vietnam.

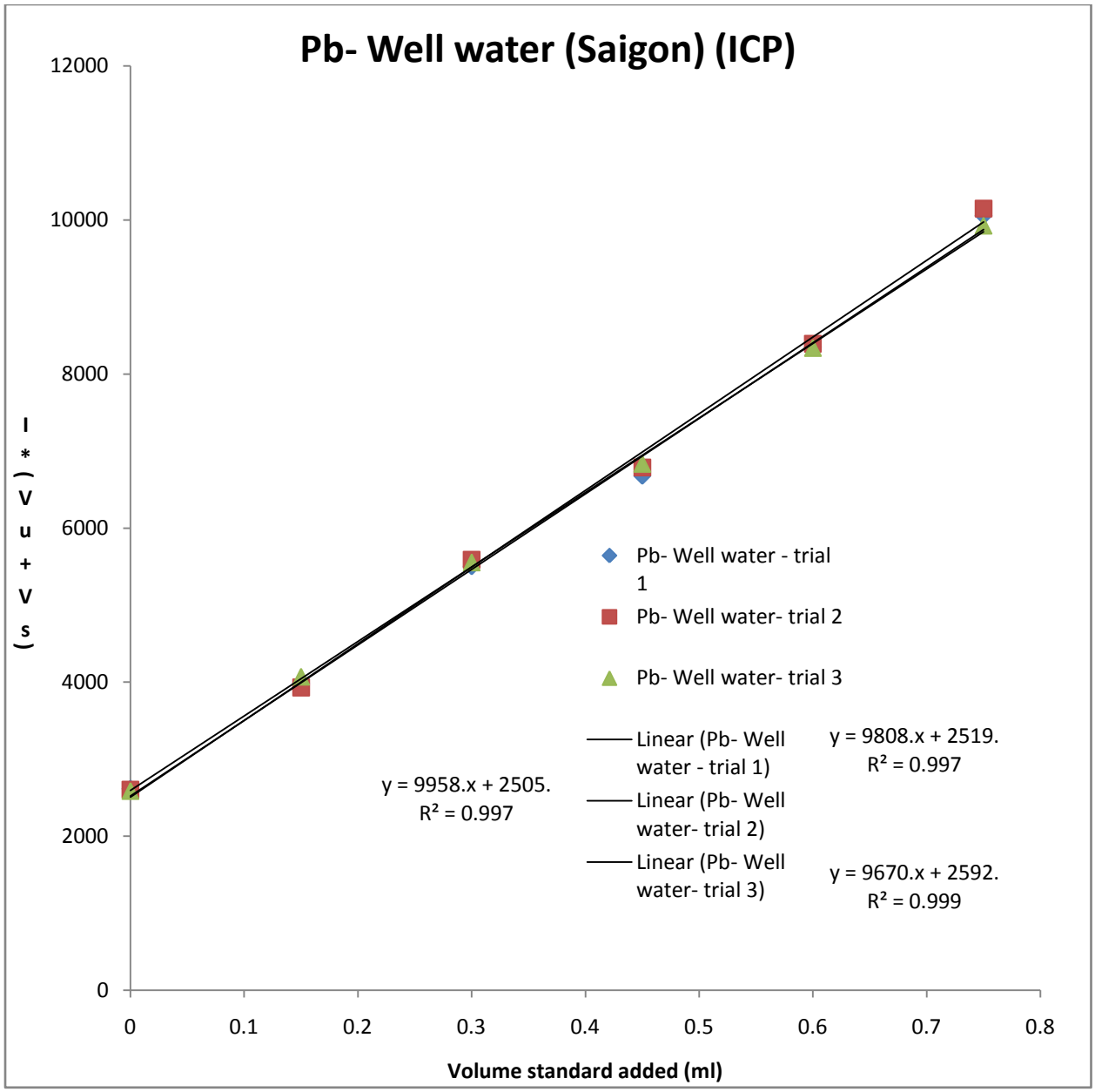

Figure 27A: Linear regression analysis for Pb ICP-OES results in well water sample from Saigon, Vietnam.

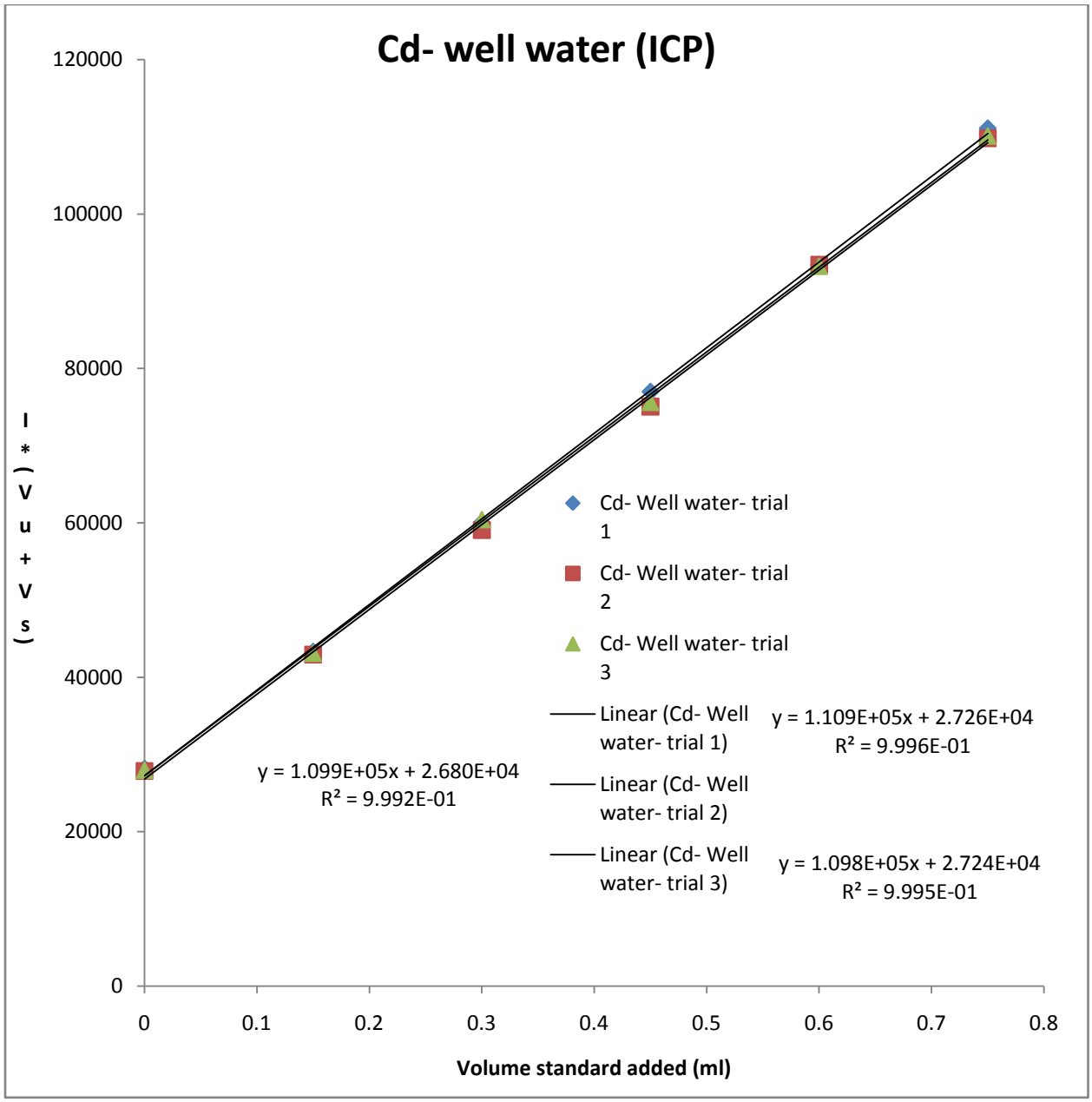

Figure 27B: Linear regression analysis for Cd ICP-OES results in well water sample from Saigon, Vietnam.

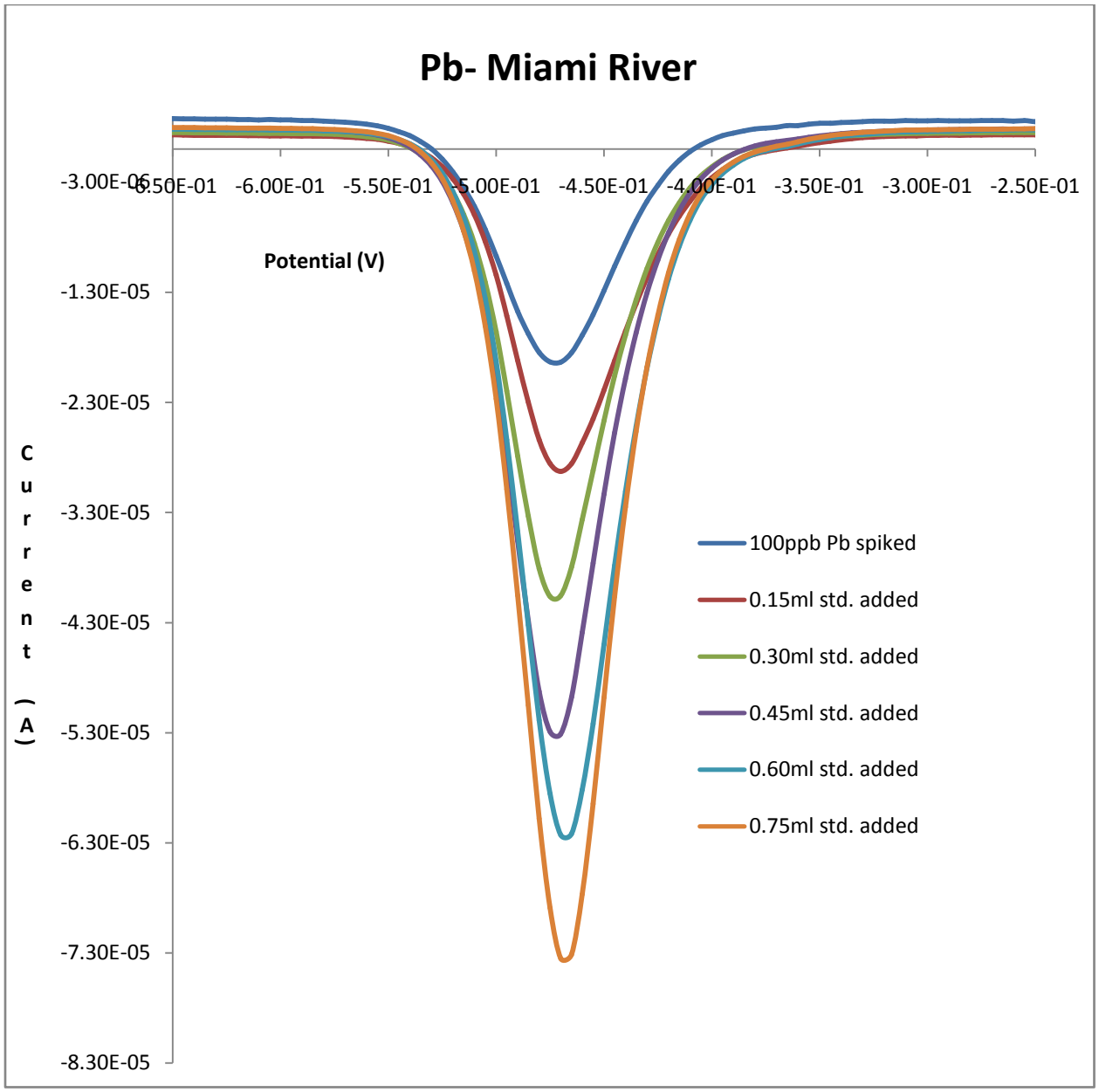

Figure 28A: SWASV analysis of Pb in Miami River water sample.

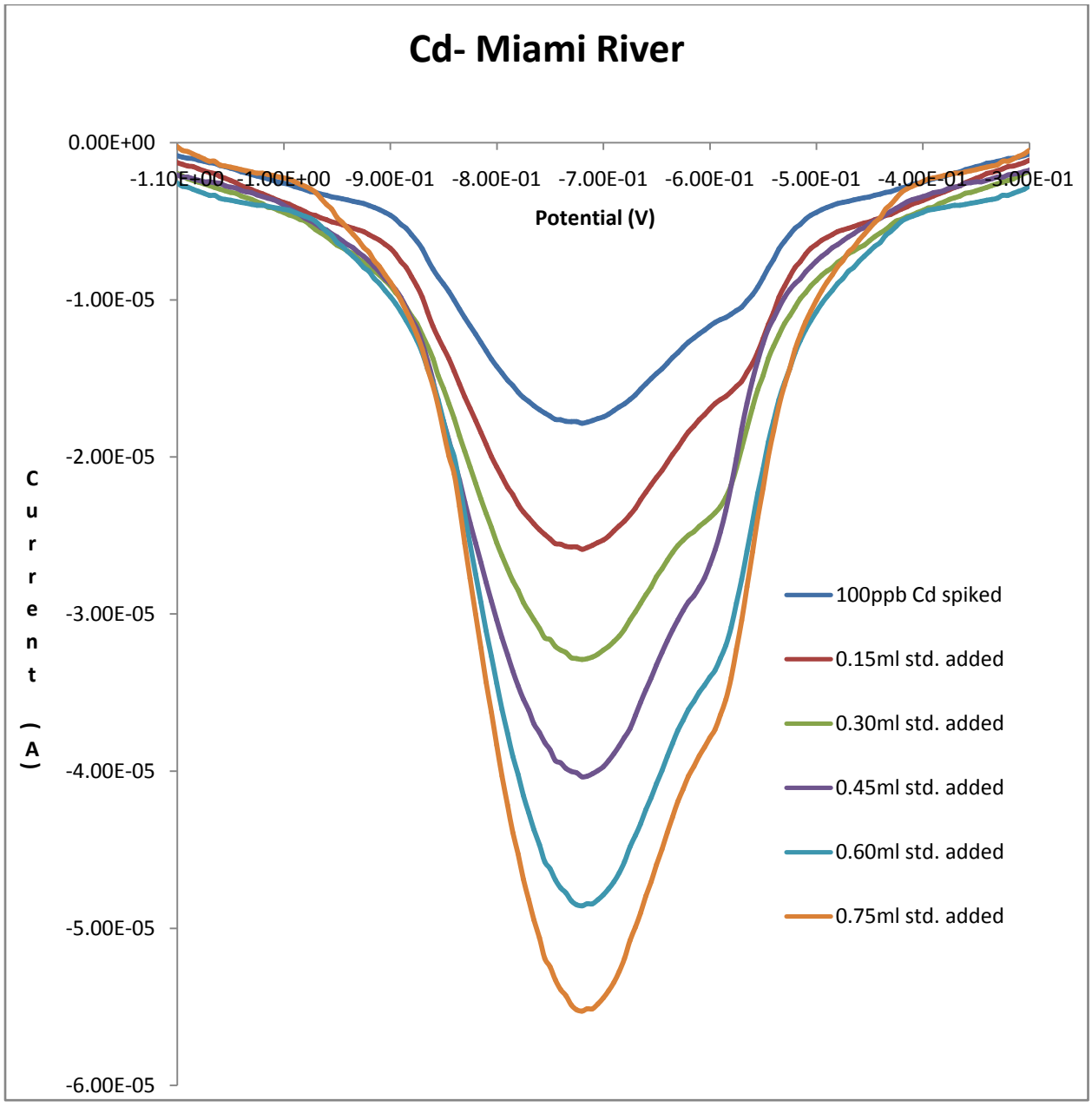

Figure 28B: SWASV analysis of Cd in Miami River water sample.

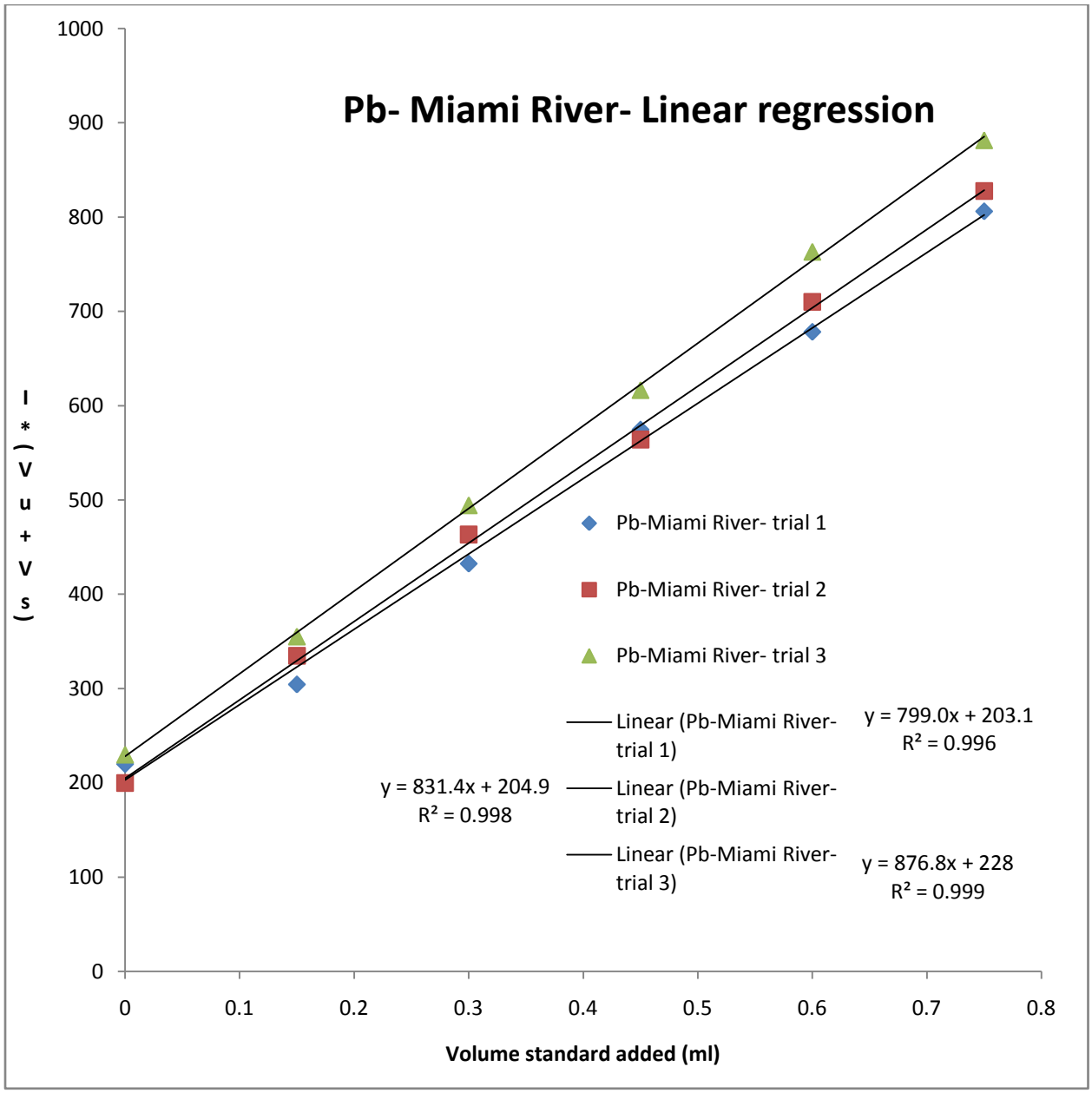

Figure 29A: Linear regression analysis for Pb SWASV results in Miami River water sample.

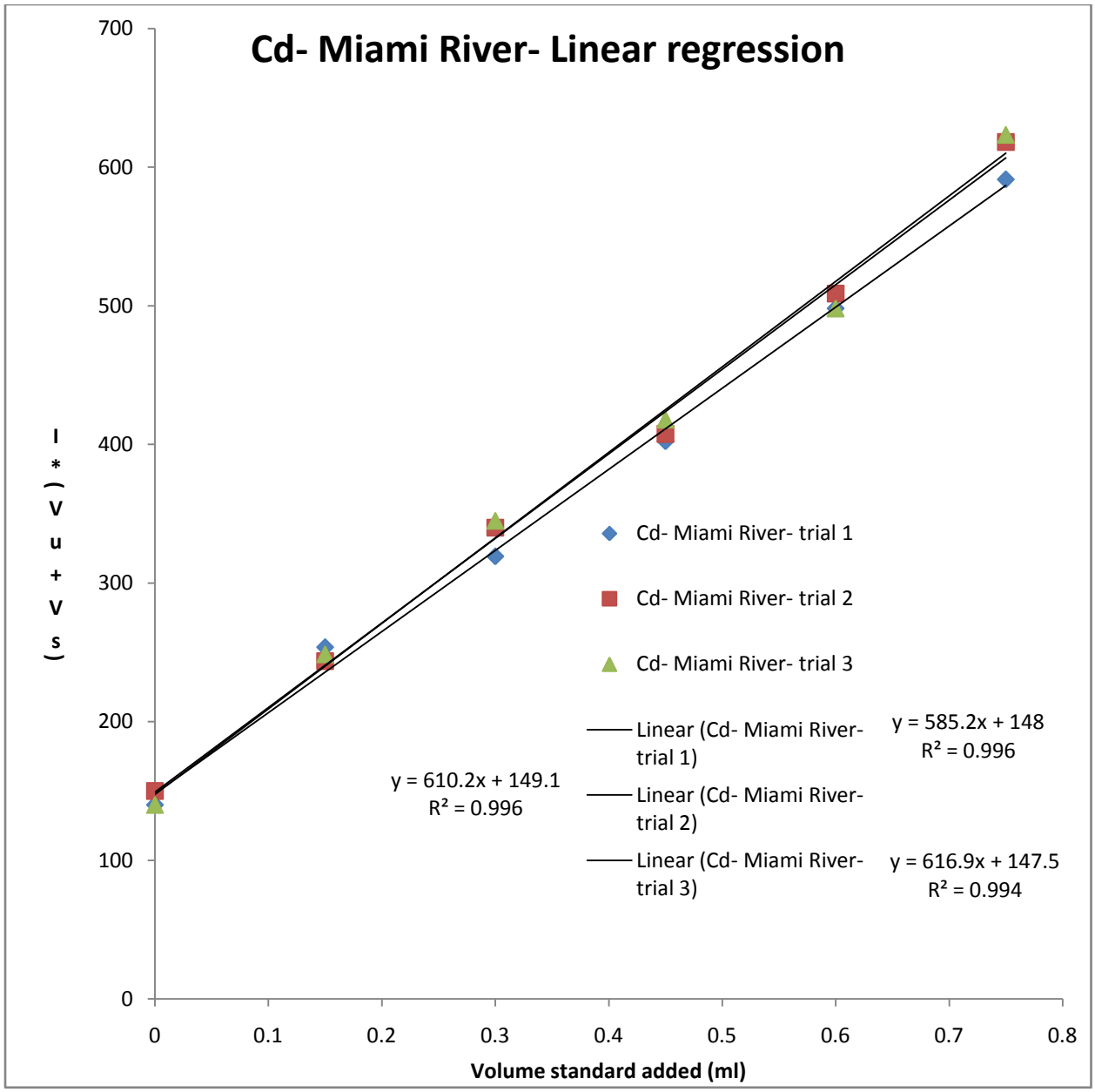

Figure 29B: Linear regression analysis for Cd SWASV results in Miami River water sample.

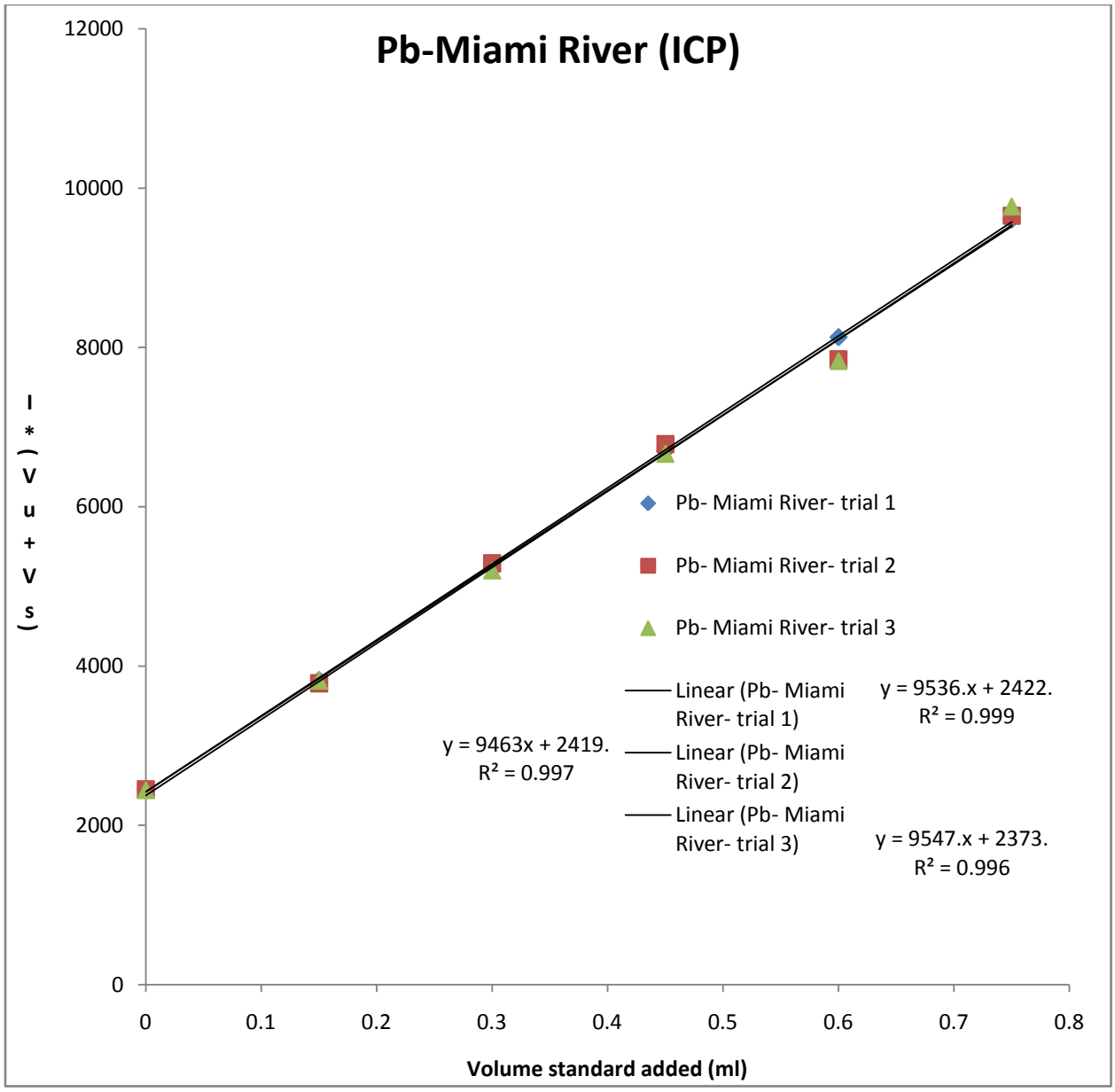

Figure 30A: Linear regression analysis for Pb ICP-OES results in Miami River water sample.

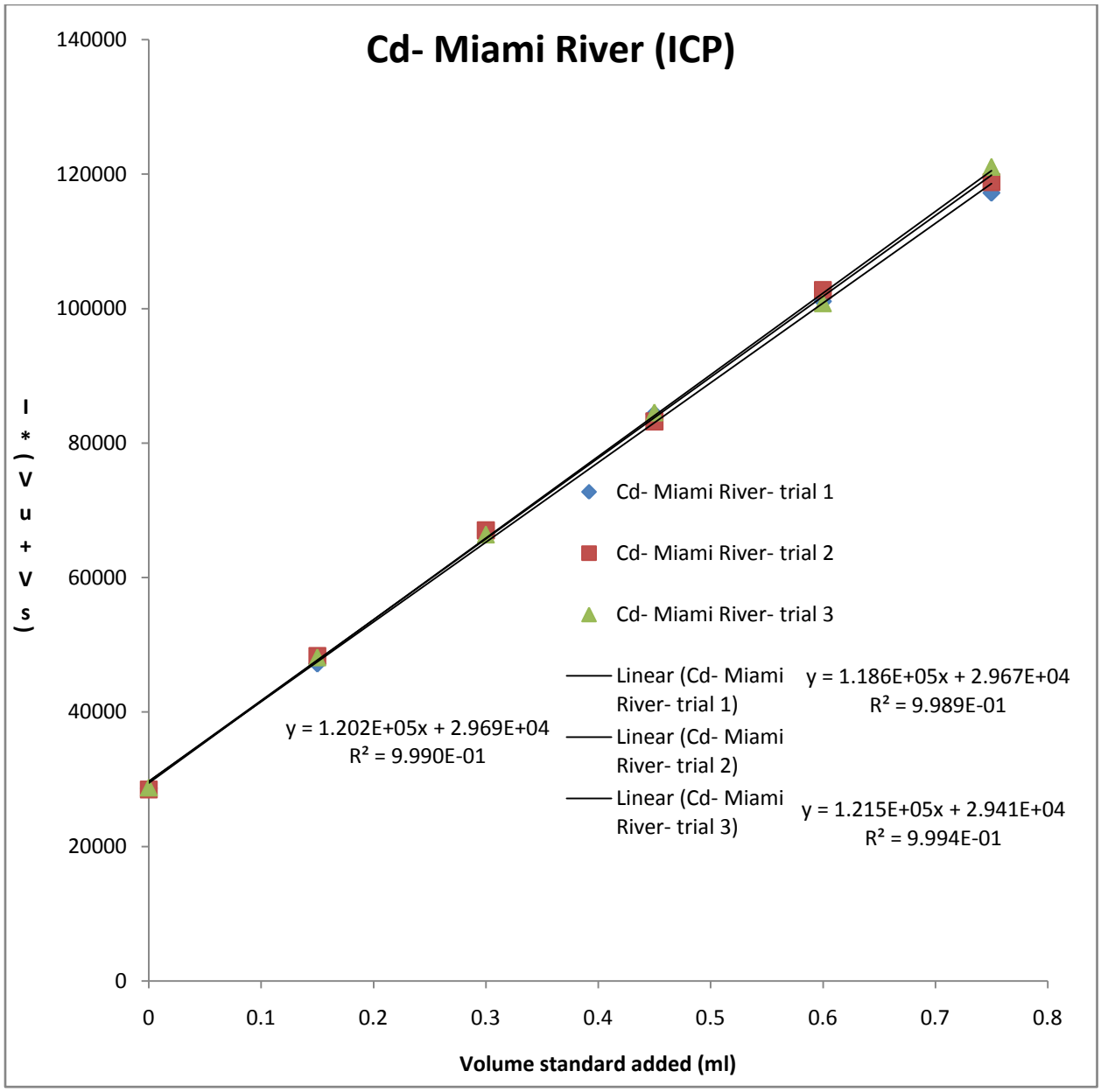

Figure 30B: Linear regression analysis for Cd ICP-OES results in Miami River water sample.

	SWASV determined concentration (ppb)	ICP-OES determined concentration (ppb)	% difference with respect to ICP
River water			
Pb	99 (± 2.8)	97 (± 1.8)	-2.1
Cd	102 (± 3.9)	98 (± 1.6)	-4.1
Well water			
Pb	102 (± 1.9)	104 (± 2.5)	1.9
Cd	101 (± 2.6)	98 (± 0.8)	-3.1
Miami River water			
Pb	102 (± 2.8)	100 (± 1.3)	-2.0
Cd	98 (± 2.7)	99 (± 1.5)	1.0

Table 1: SWASV and ICP analysis of 100 ppb spiked water samples.

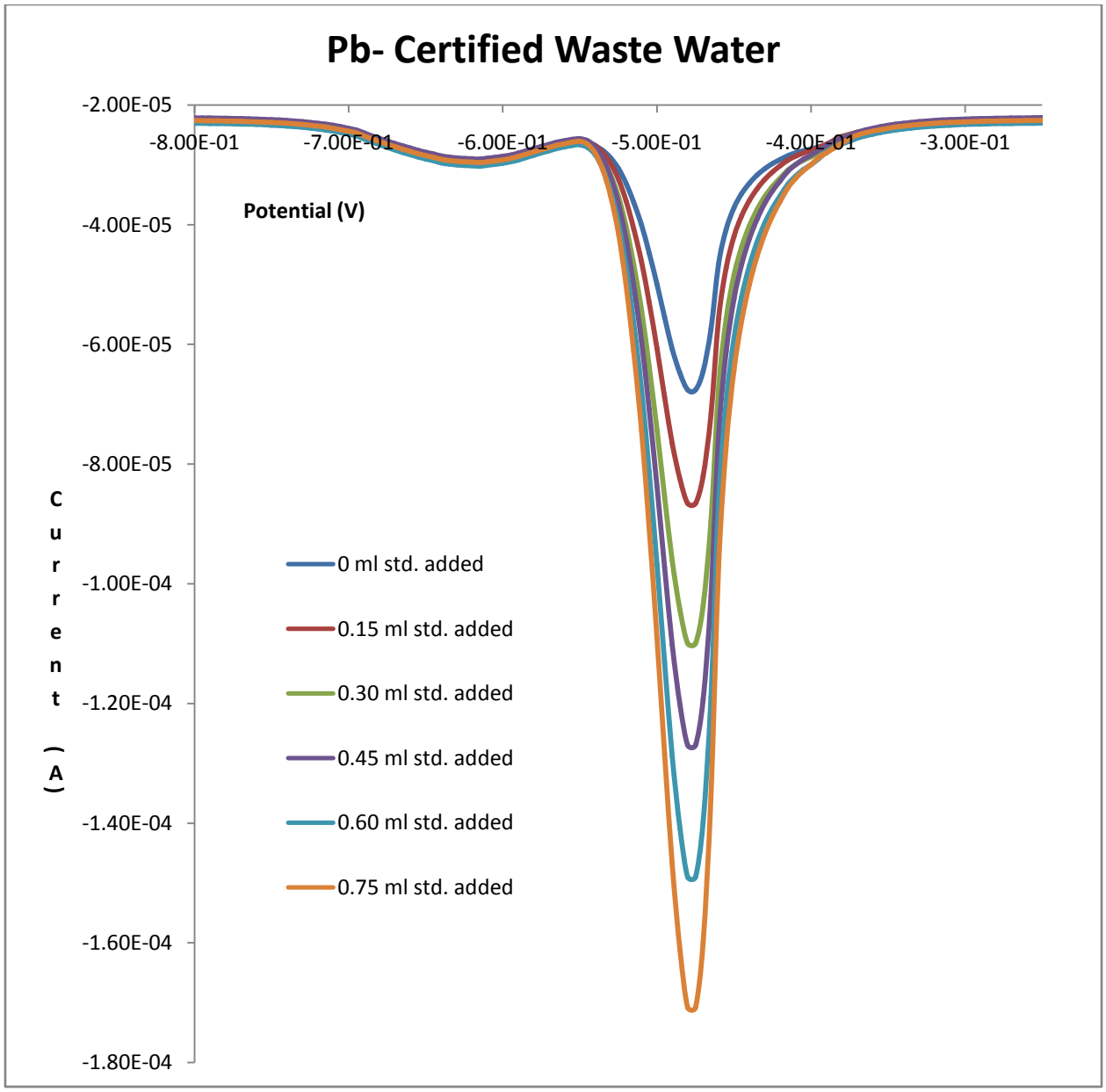

Figure 31A: SWASV analysis of Pb in certified standard reference waste water sample.

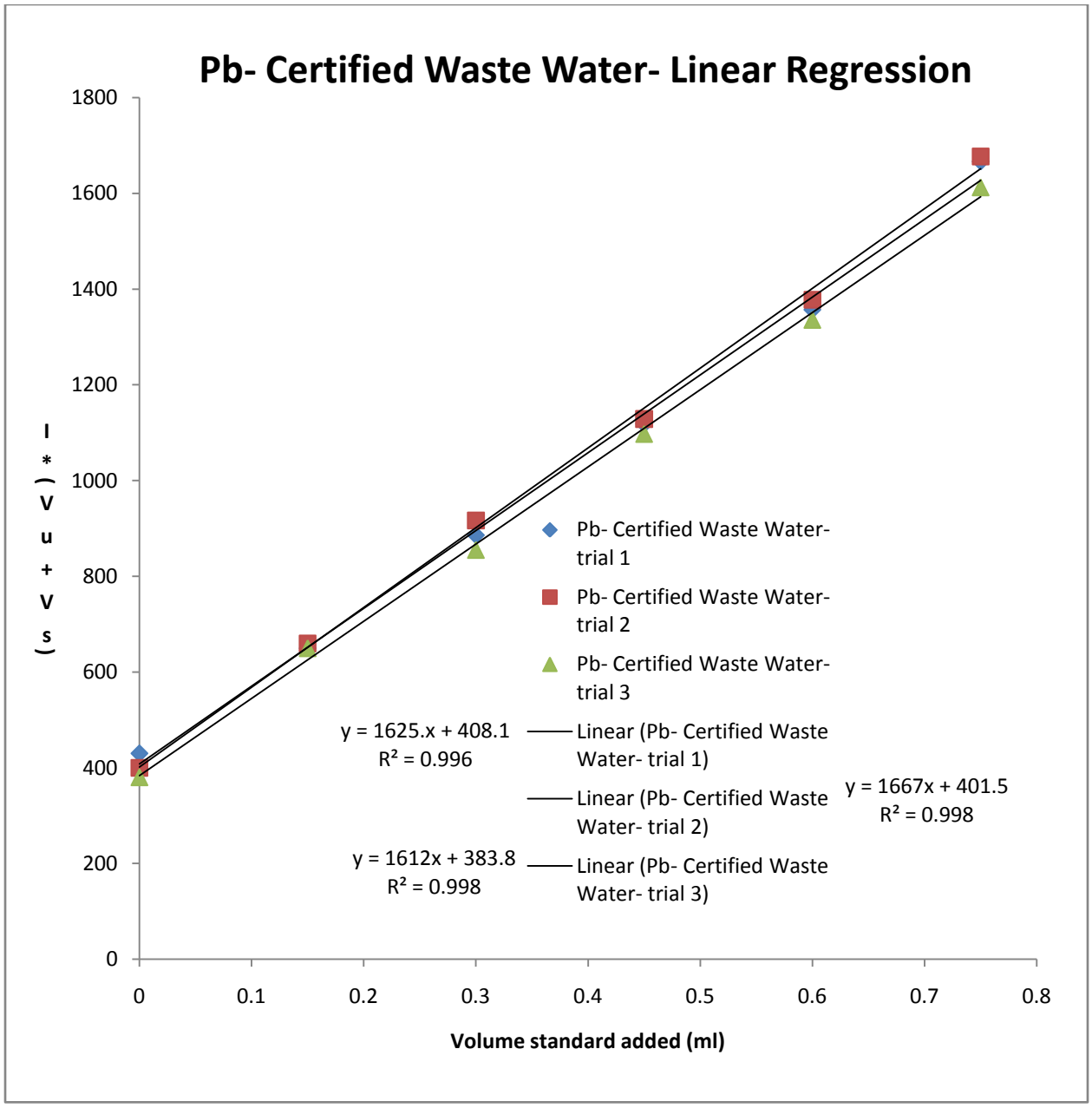

Figure 31B: Linear regression analysis for Pb SWASV results in waste water sample.

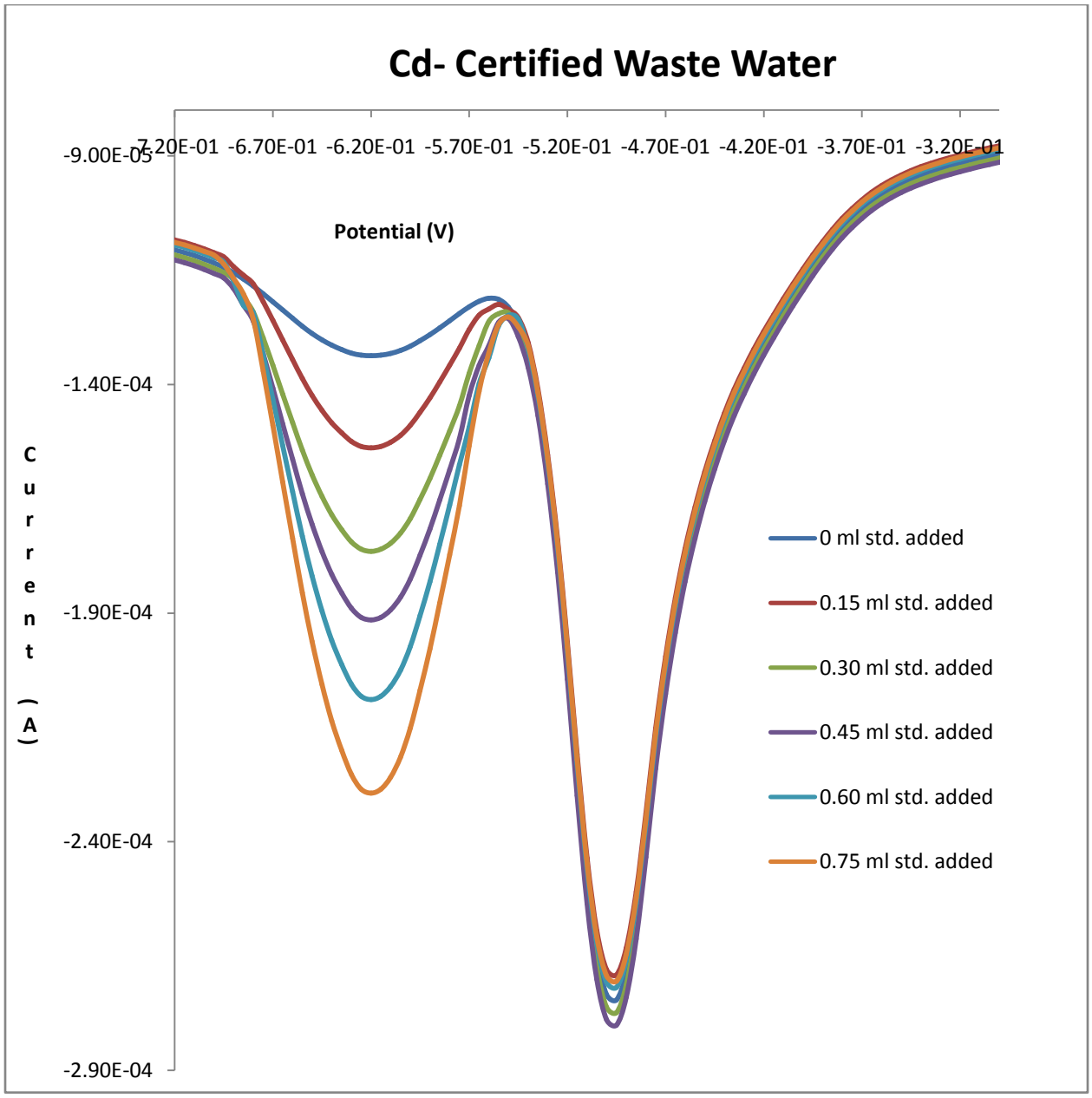

Figure 32A: SWASV analysis of Cd in certified standard reference waste water sample.

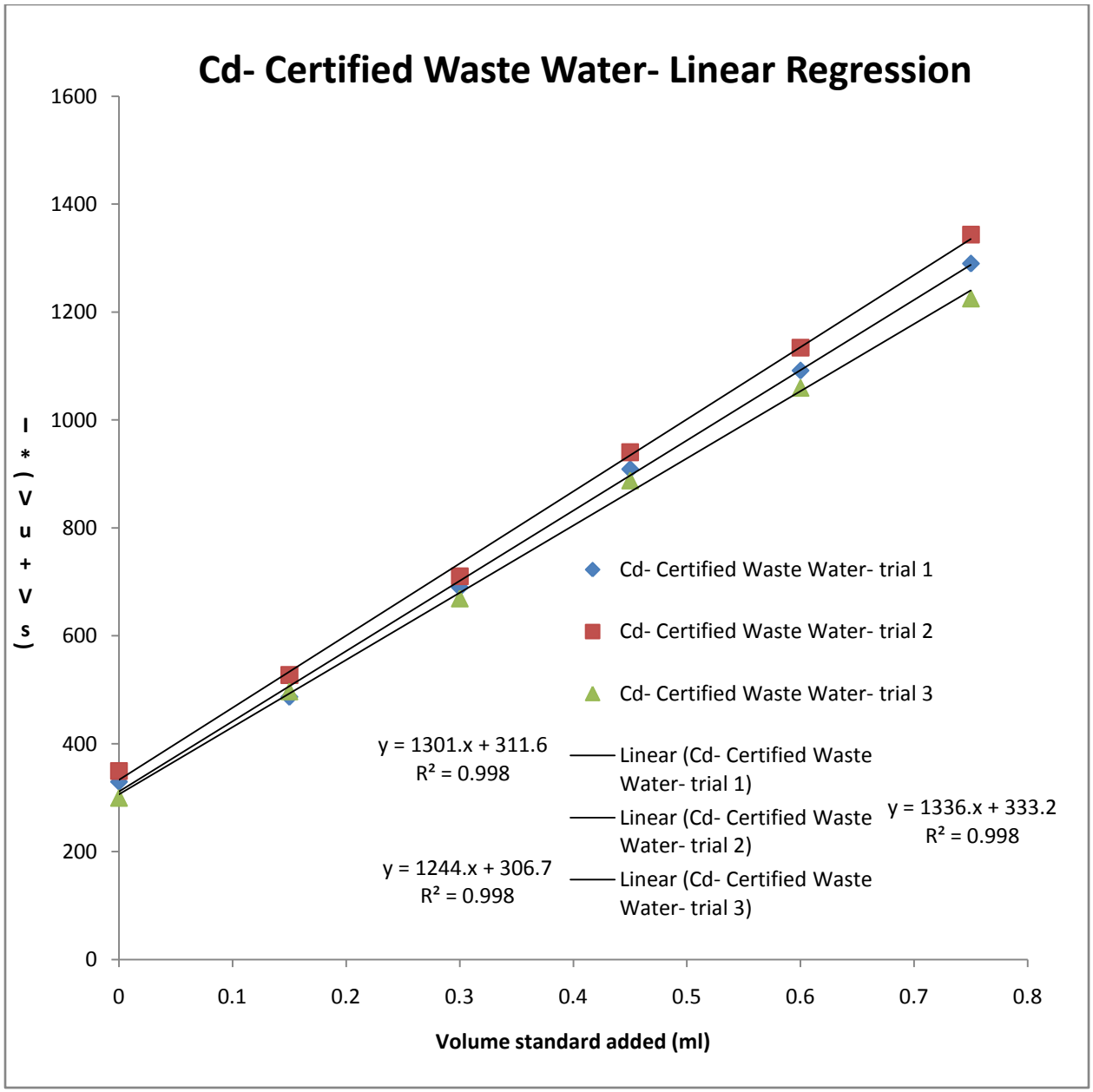

Figure 32B: Linear regression analysis for Cd SWASV results in waste water sample.

9) Interference analysis

The presence of interferences in real water sample can pose a serious problem for electrochemical analysis. Interferences can distort or obscure analytical signal by reacting with the analytes of interest or blocking the surface of working electrode. Therefore, it is useful to examine the effects of different interferences on the sensitivity of Pb and Cd using the optimal TiO_2/ZrO_2 /Tween 80 carbon paste composite electrode. This will provide some guidance as to what types of real water sample are suitable for analysis using the proposed sensor.

a) Surface active substances (SAS) interference

For this analysis, two compounds were selected as model compounds to study the interfering effect of surface active substances (substances that can block the surface of working electrode). These are: Triton X (non-ionic modeling compound) and Cetyl trimethylammonium bromide (CTAB) (ionic modeling compound). SWASV analysis of Pb and Cd (at 100ppb), individually, in presence of each SAS was carried out. The amount of SAS tested ranged from 1 to 1000 folds excess (weight to weight ratio) of the metals. Oxidative stripping current magnitudes were recorded at each different SAS concentration and normalized with the stripping current obtained when there is no SAS present (base value). Table 2 summarized the results of this analysis. Generally speaking for both metals, Triton-X appeared to interfere more severely than CTAB. For Cd, the effect of Triton X was insignificant up to 100 folds in excess. At Triton X concentration of 50 folds excess and below, the stripping current magnitude of Cd decreased less than 10%. However, as the amount of Triton X increased pass 100 fold excess of Cd, profound interfering affect was observed. For Pb, Triton X appeared to have a stronger interfering effect with this metal. The stripping current magnitude of Pb was above 80% of the base value when the concentration of Triton X was no more than 50 folds in excess, but declined

greatly with increasing concentration of Triton X. With respect to CTAB, the stripping current magnitude of Cd in the present of 200 folds excess of CTAB declined by 30%. At higher CTAB concentrations, the interfering effect became significant. Like Triton X, Pb appeared to be more susceptible to interference by CTAB compared to Cd as 100 folds excess of CTAB caused the stripping current of Pb to decline by 30%.

As mentioned, it was generally observed that of the two metals analyzed, Pb appeared to be more susceptible to SAS interference than Cd. In addition, Triton X (non-ionic modeling compound) appeared to be more problematic than CTAB (ionic modeling compound). From the results obtained, we concluded SWASV analysis of Pb and Cd using the TiO_2/ZrO_2 /Tween 80 electrode can be conducted in samples that contained marginal amount of SAS. If a sample is known to have a significant amount of SAS, then pretreatment (digestion or filtration) of the sample to reduce SAS concentration, would be necessary prior to SWASV analysis.

b) Di-valence metals interference

For this analysis, six di-valence metals were selected to investigate their interfering effect on Pb and Cd. These metals included Mg, Ca, Ni, Co, Cu, and Fe. SWASV analysis of Pb and Cd (at 100ppb), individually, in presence of each metal was carried out. The amount of SAS tested ranged from 20 to 2000 folds excess (weight to weight ratio). Oxidative stripping current magnitudes were recorded at each different interfering metal concentration and normalized with the stripping current obtained when there is no interfering metal present. The results of this study are summarized in Table 3A and 3B. Overall, for both Pb and Cd, Mg and Ca did not exhibit any significant interfering behavior even at high concentration. At 2000 folds excess, Mg and Ca only caused the stripping current of Pb to drop by 5% and 10%, respectively, (about 10% and 15% in the case of Cd). Although Fe appeared to have a stronger interfering effect toward

stripping analysis of Pb and Cd compared to Mg and Ca, the severity of Fe interference was still at tolerable level as 2000 folds excess of Fe only lead to about 15% and 20% decline in Pb and Cd stripping signals, respectively. Ni and Co, on the other hand, exhibited interfering behavior at a more significant level compared to the previously mentioned metals. However, their negative influence on SWASV analysis of Pb and Cd is still considered acceptable as 1000 folds excess of Ni and Co caused the stripping current of Pb to drop by 10% and 20%, respectively, (about 30% and 25% in the case of Cd). Of the six di-valence metals investigated, Cu appeared to exhibit the worst interfering behavior toward both Pb and Cd, especially at higher concentrations. However, at Cu concentration of 200 folds in excess or less, Cu interference on Pb and Cd analysis can be considered tolerable.

To sum up, it was observed that all six di-valence metals investigated exhibited a stronger negative influence on the analysis of Cd compared to Pb. In addition, the results of this study indicated that, using the TiO_2/ZrO_2 /Tween 80 electrode, SWASV can be carried out in samples that contain rather large excess of other metallic species compared to the amount of Pb and Cd.

	0 to 1	1 to 1	10 to 1	20 to1	50 to 1	100 to 1	200 to 1	500 to 1	1000 to 1
Pb									
Triton X	100.0	93.8	92.3	91.4	83.1	67.5	38.8	15.0	3.0
CTAB	100.0	100.9	95.6	89.2	90.0	70.7	51.1	36.8	14.7
Cd									
Triton X	100.0	97.3	93.2	95.3	90.6	79.5	51.2	30.5	6.3
CTAB	100.0	101.2	99.1	95.7	92.8	85.6	71.9	53.2	26.3

Table 2: Surface active substances interference analysis.

Pb	0 to 1	20 to 1	50 to 1	100 to1	200 to 1	500 to 1	1000 to 1	1500 to 1	2000 to 1
Mg	100.0	118.2	115.3	120.4	103.9	98.5	98.2	100.2	95.1
Ca	100.0	112.2	114.6	97.5	95.3	93.2	92.7	92.1	90.8
Ni	100.0	104.0	108.3	101.3	98.3	95.8	90.4	88.4	75.6
Co	100.0	95.9	94.3	92.7	90.7	87.3	80.9	72.7	65.0
Cu	100.0	99.3	93.8	88.2	82.9	76.3	65.2	51.9	39.4
Fe	100.0	102.0	100.1	93.2	90.4	89.6	88.6	87.4	85.3

Table 3A: Di-valence metals interference analysis for Pb.

Cd	0 to 1	20 to 1	50 to 1	100 to1	200 to 1	500 to 1	1000 to 1	1500 to 1	2000 to 1
Mg	100.0	105.0	100.7	103.8	98.1	95.1	93.1	90.6	88.2
Ca	100.0	121.9	115.5	107.8	96.7	99.2	91.0	88.2	85.3
Ni	100.0	98.2	95.3	93.8	90.9	79.3	71.7	65.3	49.3
Co	100.0	93.8	90.0	91.7	87.6	81.6	75.3	69.4	58.2
Cu	100.0	98.2	95.3	92.0	81.1	68.2	55.6	28.2	ND
Fe	100.0	101.7	98.8	94.3	91.0	87.7	86.6	83.2	80.9

Table 3B: Di-valence metals interference analysis for Cd.

10) Morphological characterization of electrode surfaces via scanning electron microscopy (SEM) and X-ray photoelectron spectroscopy (XPS)

Examining the morphological features of electrode surface would give a better understanding on how the sensor functions. For this study, SEM was employed to investigate the morphology of the proposed sensor surface. Figure 31 illustrated the surface of the unmodified electrode, and Figure 32A and 32B showed the surficial composition of the TiO_2/ZrO_2/ Tween 80 carbon paste composite electrode. From the SEM images, it can be observed that the surface of the unmodified electrode had a rather smooth, homogenous appearance compared to the TiO_2/ZrO_2/ Tween 80 carbon paste composite electrode surface, which exhibited a rougher, more heterogeneous appearance due to the presence of the crystalline micro-structures. It is hypothesized that these crystalline structures provided nucleation sites for oxidation-reduction of Pb and Cd at the sensor surface, thus enhancing the electro-analytical activity of the electrode [182]. Furthermore, from the XPS spectra (Figure 33A and B), it is observed that the Pb $4f_{7/2}$ line centers around 139 eV, which corresponds to PbO speciation; and the Cd $3d_{5/2}$ line centers around 406.5 eV, which corresponds to CdO speciation. This data indicated that Pb and Cd interacted with the TiO_2/ZrO_2/ Tween 80 carbon paste composite electrode surface via metal oxides formation. Such metal oxides formation is proposed to be the result of Pb and Cd ions bound to the oxygen groups on the TiO_2 and ZrO_2 crystallized micro-structures on the electrode surface during the redox process as illustrated in the schematic drawing (Figure 34).

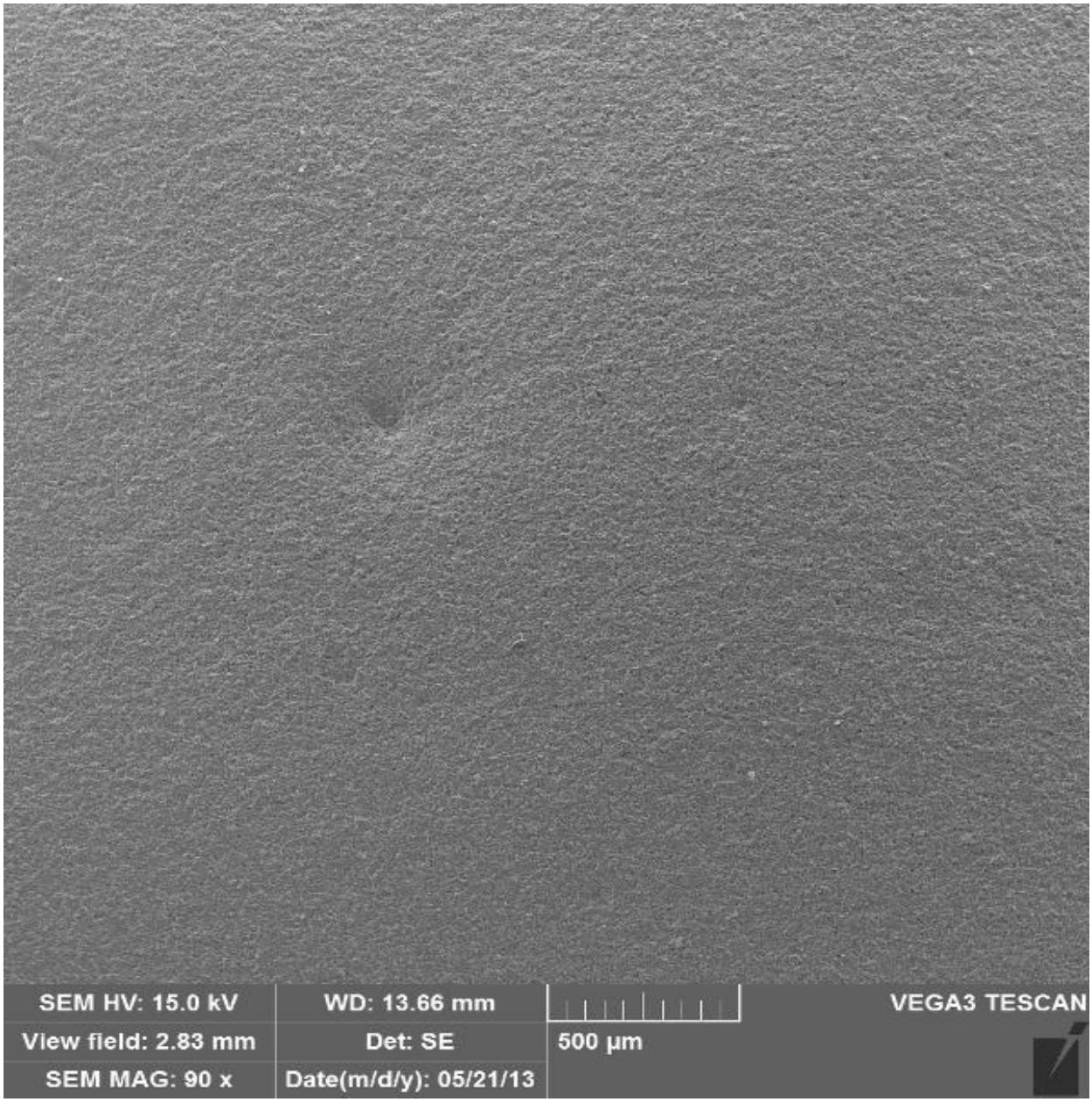

Figure 33: SEM image of unmodified electrode surface, 90X magnification.

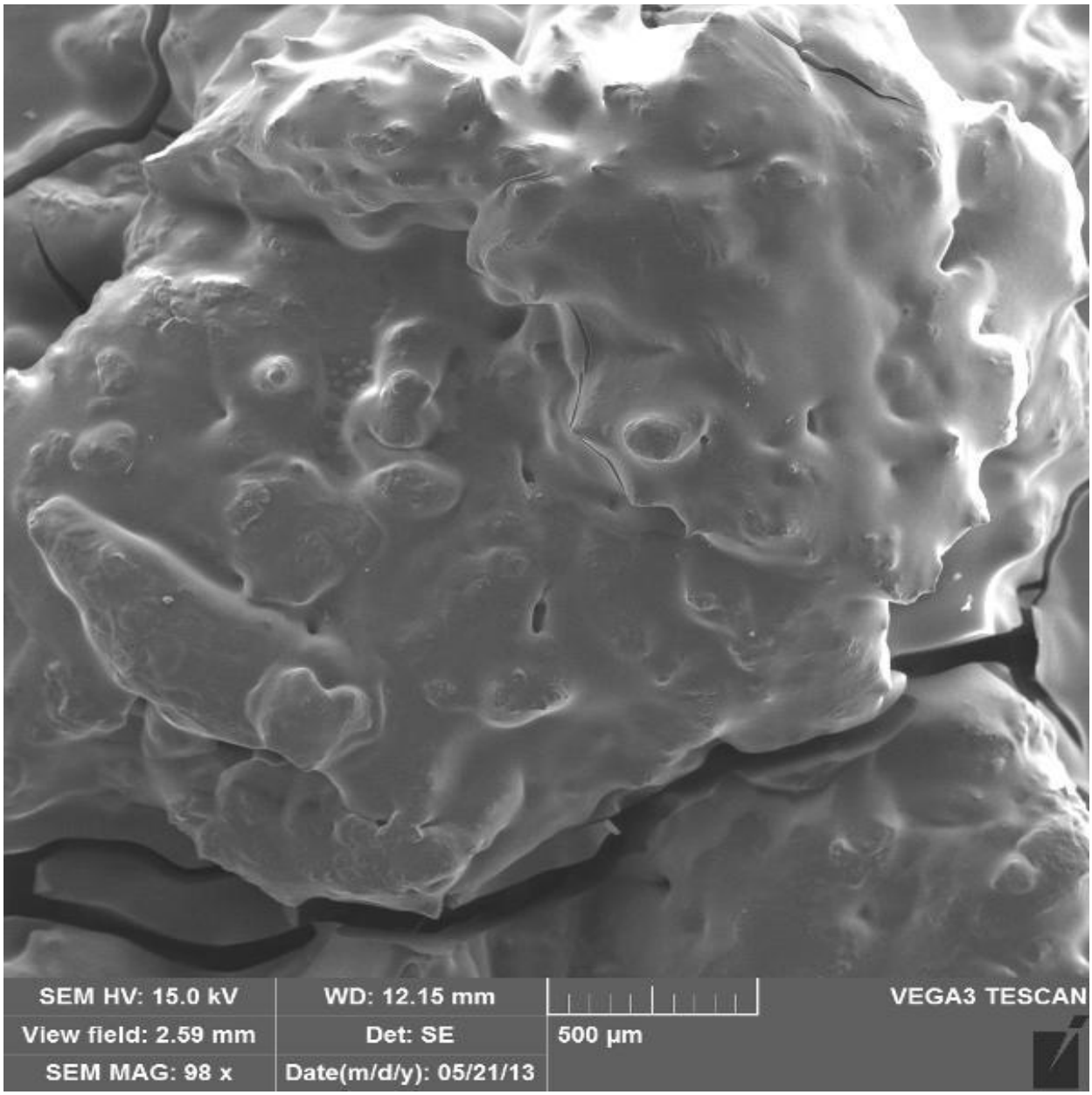

Figure 34A: SEM image of TiO_2/ZrO_2 carbon paste composite electrode surface at 98X magnification.

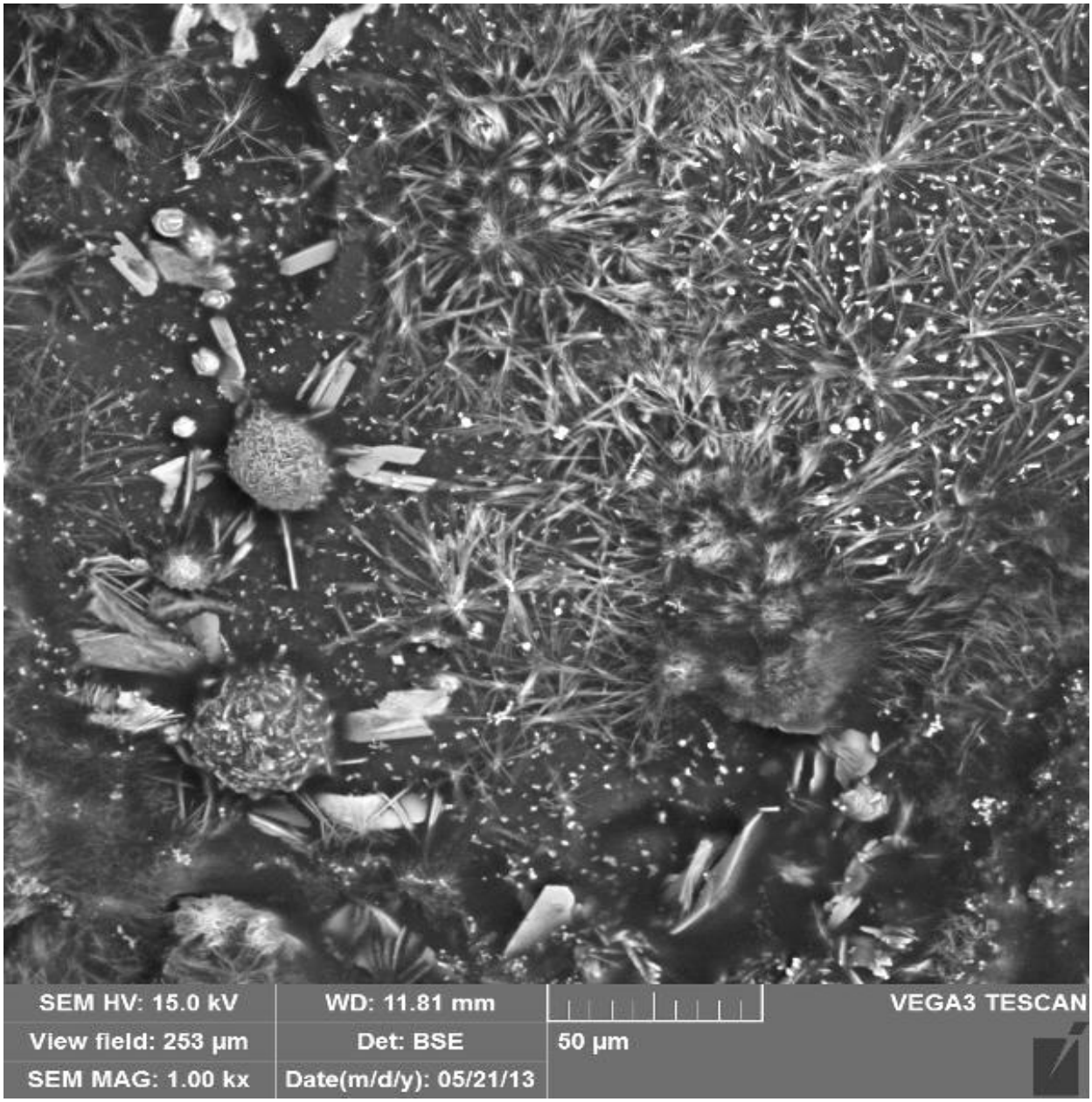

Figure 34B: SEM image of TiO_2/ZrO_2 carbon paste composite electrode surface at 1000X magnification.

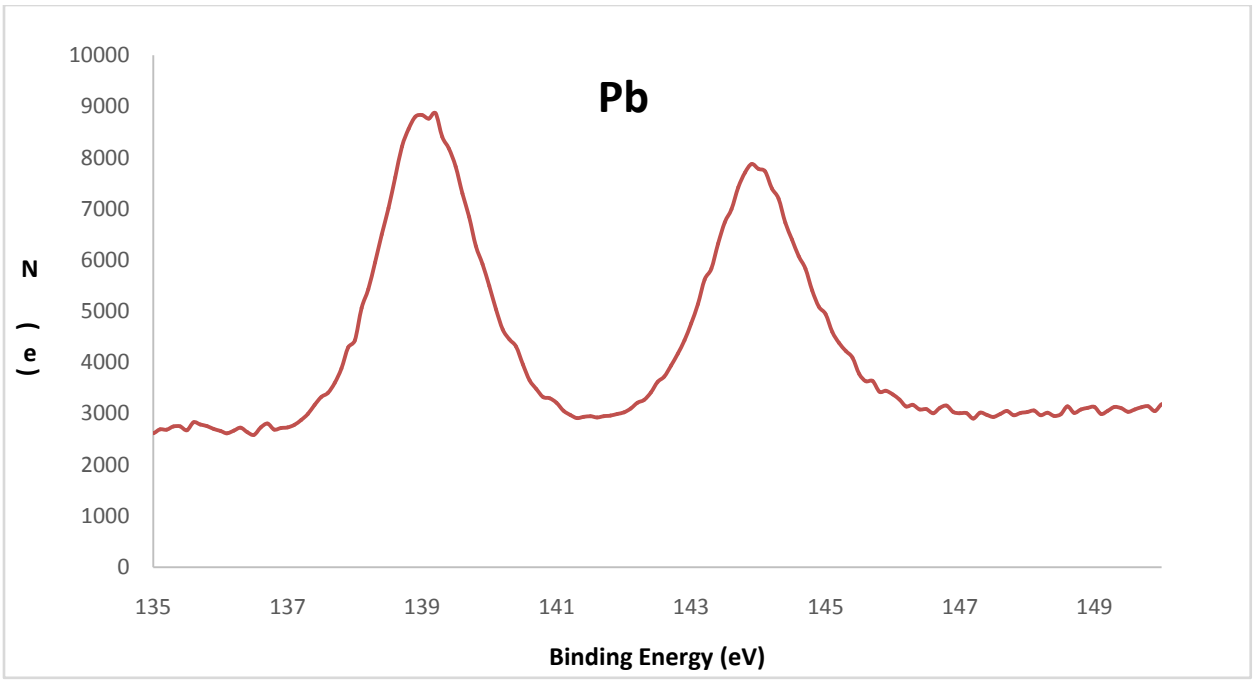

Figure 35A: High resolution XPS spectrum of Pb at the electrode surface.

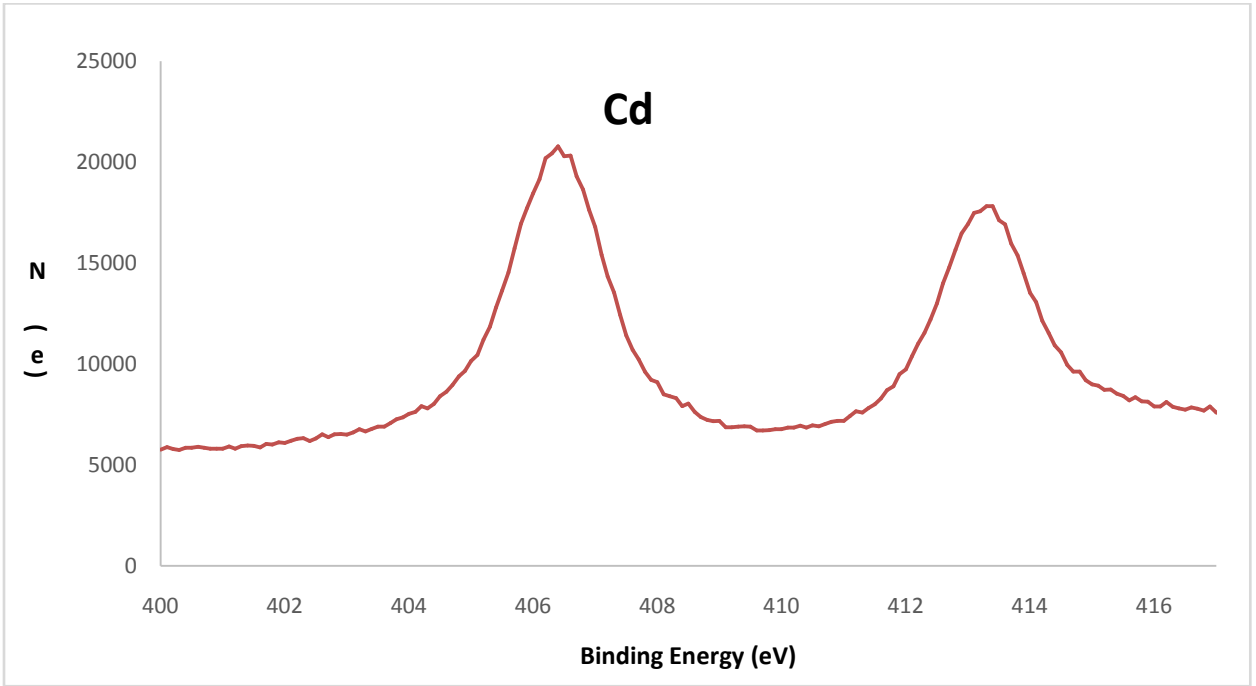

Figure 35B: High resolution XPS spectrum of Cd at the electrode surface.

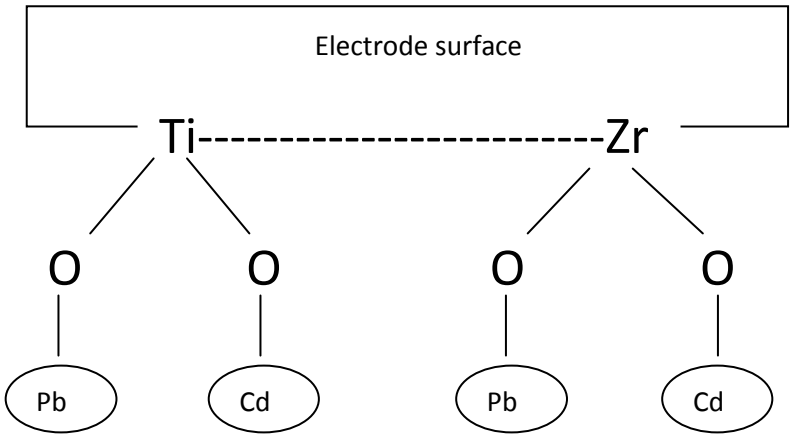

Figure 36: Proposed schematic interaction of Pb and Cd with the TiO_2 and ZrO_2 crystalline structures at the electrode surface.

IV. Summary and Conclusion

The study illustrated the successful development of a novel electro-chemical sensor for trace level quantification of Pb and Cd in aqueous media. The TiO_2/ ZrO_2/ Tween 80 carbon paste composite electrode was synthesized with Ti:Zr optimal ratio of 2:1 along with the addition of 0.5 ml Tween 80 directly into the carbon paste composite, and optimally heated at 375 ^{0}C for 10 minutes. Via CV analysis, the electrode surface area was estimated to be 0.028 (±0.003) cm^2. In addition, the electron transfer coefficients (α) were estimated to be 0.44 and 0.33, and the heterogeneous electron transfer rate constants (k_0) were calculated to be $5.64x10^{-3}$ and $2.42x10^{-3}$ (cm/s), for Pb and Cd respectively. Furthermore, at optimal pH of 3, the detection limits for Pb and Cd via CV analysis were estimated to be $7.6x10^{-6}$ M and $1.1x10^{-5}$ M, respectively. Asides from CV analysis, SWASV analysis of Pb and Cd, both individually and simultaneously, were carried out. The detection limit for Pb was estimated to be 0.48 ppb, and 0.77 ppb for Cd. Data from interference studies, using modeling compounds, suggested that the proposed electrode could tolerate a moderate amount of surface active substances and exhibited a relatively high tolerance level toward common di-valence metals. Moreover, analysis of Pb and Cd in real water sample illustrated the electrode potential for real world application, as the results obtained with SWASV agreed very well with that of ICP-OES. However, a drawback in the electrode synthesis process is the variability in term of micro-crystalline structural development at the electrode surface, thus sensitivity and residual current standardization of the electrode cannot be accomplished. Overall, the newly developed electrode exhibited favorable electro-chemical characteristics in detection of Pb and Cd in water solution. Certainly, possible applications for this novel electrode are not limited to just Pb and Cd as future studies could look into utilization

of the TiO_2/ ZrO_2/ Tween 80 carbon paste composite electrode to detect other heavy metals, for example Hg and As, as well as different classes of organic pollutants.

V. References

1. Wang J., Anal. Chim. Acta., 399 (1999) 21.
2. Lev O., Wu Z., Bharathi S., Glezer V., Modestov A., Gun J., Rabinovich L., Sampath S., Chem. Mater., 9 (1997) 2354.
3. Hench L. L.,West J. K., Chem. Rev., 90 (1990) 33.
4. Aurobind S. V., Amirthalingam K. P., GomathiH., Adv. Colloid. Interfac., 121 (2006) 1.
5. Rabinovich L., Lev O., Electranalysis, 13 (2001) 265.
6. Tsionsky M., Vanger A., Lev O., Sol-Gel Sci. Technol., 2 (1994) 595.
7. Guo Y., Guadalupe A. R., J. Pharmaceut. Biomed., 19 (1999) 175.
8. Chen Y., Lunsford S., Dionysiou D. D., Thin Solid Films, 516 (2008) 7930.
9. Chen Y., Lunsford S., Dionysiou D. D., Sensor Actuat. B-Chem., 137 (2009) 291.
10. Vytras K., Svancara I., Metelka R., J. Serb. Chem. Soc., 74 (2009) 1021.
11. Stozhko N. Y., Malakhova N. A., Fyodorov M. V., Brainina K. Z., J. Solid State Electrochem., 12 (2008) 1185.
12. Svancara I., Vytras K., Barek J., Zima J., Crit. Rev. Anal. Chem., 31 (2001) 311.
13. Svancara I., Walcarius A., Kalcher K., Vytras K., Cent. Eur. J. Chem., 7 (2009) 598.
14. Svancara I., Vytras K., Kalcher K., Walcarius A., Wang J., Electroanalysis, 21(2009) 7.
15. United States Department of Health and Human Services. Agency for Toxic Substances and Disease Registry. Toxicalogical Profile for Lead. August 2007.
16. King M., Ramachandran V., Kirk-Othmer Encyclopedia of Chemical Technology, 4th edition, John Wiley & Sons, New York, 1995.
17. Sutherland C. A., Milner E. F., Ullmann's Encyclopedia of Industrial Chemistry, 5th edition, VCH Publishers, New York, 1990.

18. Billick I. H., Gray V.E., United States Department of Housing and Urban Development. Lead Based Paint Poisoning Research: Review and Evaluation 1971-1977. 1978.
19. Giddings J. C., Chemistry, Man, and Environmental Change: An Integrated Approach. Harper & Row Publishers, Inc., New York, 1973.
20. United States Environmental Protection Agency. Drinking Water Contaminants. May 2011. <http://water.epa.gov/drink/contaminants/index.cfm#Inorganic>
21. GoldmanR. H., Baker E. L., Hannan M., Kamerow D. B., N. Engl. J. Med., 317 (1987) 214.
22. Feldman R. G., N. Engl. J. Med., 298 (1978) 1143.
23. Lanphear B. P., Eberly S., Howard C. R., Pediatrics, 106 (2000) 1.
24. Rosenman K. D., Sims A., Luo Z., Gardiner J., J. Occup. Environ. Med., 45 (2003) 546.
25. Den Hond E., Nawrot T., Staessen J. A., J. Hum. Hypertens., 16 (2002) 563.
26. Jin Y., Liao Y., Lu C., Li G., Yu F., Zhi X., Xu J., Liu S., Liu M., Yang J., Ecotoxicol. Environ. Saf., 63 (2006) 313.
27. Pagliuca A., Mufti G. J., Baldwin D., Lestas A. N., Wallis R. M., Bellingham A. J., J. Clin. Path., 43 (1990) 277.
28. Campbell J. R., Rosier R. N., Novotny L., Puzas J. E., Environ. Health Perspect., 112 (2004) 1200.
29. Dye B. A., Hirsch R., Brody D. J., Environ Health Perspect., 110 (2002) 997.
30. Gerlach R. F., Cury J. A., Krug F. J., Line S. R. P., Toxicology, 14 (2002) 27.
31. Skoczynska A., Smolik R., Jelen M., Arch. Toxicol., 67 (1993) 200.
32. Saenger P., Markowitz M. E., Rosen J. F., J. Clin. Endocrinol. Metab., 58 (1984) 363.
33. Diamond G. L., The Toxicology of the Kidney, CRC Press, London, 2005.
34. Loghman-Adham M., Environ. Health Perspect., 105 (1997) 928.
35. Lopez C. M., Pineiro A. E., Nunez N., Avagnina A. M., Villaamil E. C., Roses O. E., Pharmacol. Res. Commun., 42 (2000) 599.

36. ErfurthE. M., GerhardssonL., Nilsson A., Rylander L., Schutz A., Arch. Environ. Health, 56 (2001) 449.
37. Ng T. P., Goh H. H., Ng V. L., Ong H. Y., Ong C. N., Chia K. S., Chia S. E., Jeyaratnam J., Br. J. Ind. Med., 48 (1991) 485.
38. Rothenberg S. J., Poblano A., Schnaas L., Neurotoxicol. Teratol., 22 (2000) 503.
39. Fischbein A., Tsang P., Luo J. J., Roboz J. P., Jiang J. D., Bckesi J. G., Clin. Immunol. Immunopathol., 66 (1993) 163.
40. Lucchini R., Albini E., Cortesi I., Placidi D., Bergamaschi E., Traversa F., Neurotoxicology, 21 (2000) 805.
41. Bockelmann I., Pfister E. A., McGauran N., Robra B. P., J. Occup. Environ. Med., 44 (2002) 59.
42. Stollery B. T., Broadbent D. E., Banks H. A., Lee W. R., Br. J. Ind. Med., 48 (1991) 739.
43. Needleman H. L. ,Schell A., Bellinger D., Leviton A., Allred E. N., N. Engl. J. Med., 322 (1990) 83.
44. Robinson G. S., Baumann S., Kleinbaum D., Barton C., World Health Organization Regional Office for Europe, Environmental Health Document 3, Copenhagen, Denmark, 1985.
45. Needleman H. L., McFarland C., Ness R. B., Fienberg S. E., Tobin M. J., Neurotoxicol. Teratol., 24 (2002) 711.
46. ChiaS. E., ChiaK. S., ChiaH. P., Ong C. N., Jeyaratnam J., Scand. J. Work. Environ. Health, 22 (1996) 374.
47. Lanphear B. P., Dietrich K., Auinger P., Cox C., Public Health Rep., 115 (2000) 521.
48. Sallmen M., Lindbohm M. L., Nurminen M., Epidemiology, 11 (2000) 148.
49. Lerda D., Am. J. Ind. Med., 22 (1992) 567.
50. Selevan S. G., Rice D. C., Hogan K. A., Euling S. Y., Pfahles-Hutchens A., Bethel J., N. Engl. J. Med., 348 (2003) 1527.

51. Cocco P., Dosemeci M., Heineman E. F., J. Occup. Environ. Med., 40 (1998) 937.

52. Huang X. P., Feng Z. Y., Zhai W. L., Xu J. H., Biomed. Environ. Sci., 1 (1988) 382.

53. Fayerweather W. E., Karns M. E., Nuwayhid I. A., Nelson T. J., Am. J. Ind. Med., 31 (1997) 28.

54. Fracasso M. E., Perbellini L., Solda S., Talamini G., Franceschetti P., Mutat. Res., 515 (2002) 159.

55. United States Department of Health and Human Services. Agency for Toxic Substances and Disease Registry. Toxicalogical Profile for Cadmium. September 2008.

56. Morrow H., Kirk-Othmer Encyclopedia of Chemical Technology, John Wiley & Sons, New York, 2001

57. Herron N., Kirk-Othmer Encyclopedia of Chemical Technology, John Wiley & Sons, New York, 2003.

58. Lewis R. J., Hawley's Condensed Chemical Dictionary, 14th Edison, John Wiley & Sons, New York, 2001.

59. Shevchenko V., Lisitzin A., Vinogradova A., Stein R., Russian Arctic. Sci. Total Environ., 306 (2003) 11.

60. Alloway B. J., Steinnes E., Cadmium in Soils and Plants, Kluwer Academic Publishers, Netherlands, 1999.

61. Angelo R. T., Cringan M. S., Chamberlain D. L., Stahl A. J., Haslouer S. G., Goodrich, C. A., Sci. Total Environ., 384 (2007) 467.

62. Mason R. P., Laporte J. M., Andres S., Arch. Environ. Contam. Toxicol., 38 (2000) 283.

63. Townshend R. H., Br. J. Ind. Med., 39 (1982) 411.

64. Andersen O., Nielsen J. B., Svendsen P., Toxicology, 48 (1988) 225.

65. Chan O. Y., Poh S. C., Lee H. S., Tan K. T., Kwok S. F., Ann. Acad. Med. Singapore, 17 (1988) 283.

66. Blainey J. D., Adams R. G., Brewer D. B., Harvey T. C., Br. J. Ind. Med., 37 (1980) 278.

67. Davison A. G., Fayers P. M., Taylor A. J., Venables K. M., Darbyshire J., Pickering C. A., Lancet, 1 (1988) 663.

68. Hellstrom L., Elinder C. G., Dahlberg B., Lundberg M., Jarup L., Persson B., Axelson O., Am. J. Kidney Dis., 38 (2001) 1001.

69. Lemen R. A., Lee J. S., Wagoner J. K., Blejer H. P., Ann. N Y Acad. Sci., 271 (1976) 273.

70. Stayner L., Smith M. A., Thun M., Schnorr T., Lemen R., Ann. Epidemiol., 2 (1992) 177.

71. KagamimoriS., WatanabeM., NakagawaH., Okumura Y., Kawano S., Bull. Environ. Contam. Toxicol., 36 (1986) 484.

72. Staessen J., Bulpitt C. J., Roels H., Br. J. Ind. Med., 41 (1984) 241.

73. Jamall I. S., Naik M., Sprowls J. J., J. Appl. Toxicol., 9 (1989) 339.

74. Sakata S., Iwami K., Enoki Y., Kohzuki H., Shimizu S., Matsuda M., Exp. Hematol., 16 (1988) 581.

75. MasaokaT., AkahoriF., AraiS., Nomiyama K., Nomiyama H., Kobayashi K.,. Nomura Y., Suzuki T., Vet. Hum. Toxicol., 36 (1994) 189.

76. Jarup L., Berglund M., Elinder C. G., Nordberg G., Vahter M., Scand. J. Work. Environ. Health, 24 (1998) 1.

77. Nordberg G. F., Jin T., Kong Q., Ye T., Cai S., Wang Z., Sci. Total Environ., 199 (1997) 111.

78. Ezaki T., Tsukahara T., Moriguchi J., Furuki K., Fukui Y., Ukai H., Okamoto S., Sakurai H., Honda S., Ikeda M., Int. Arch. Occup. Environ. Health, 76 (2003) 186.

79. Uno T., Kobayashi E., Suwazono Y., Okubo Y., Miura K., Sakata K., Okayama A., Ueshima H., Nakagawa H., Nogawa K., Scand. J. Work Environ. Health, 31 (2005) 307.

80. Tang X. M., Chen X. Q., Zhang J. X., Quin W. Q., Mutat. Res., 241 (1990) 243.

81. Valverde M., Fortoul T. I., Diaz-Barriga F., Mejia J., Castillo E. R., Mutagenesis, 15 (2000) 109.

82. Wang J., Analytical Electrochemistry. VCH Publishers, Inc., New York, 1994.

83. Fisher A. C., Electrode Dynamics. Oxford University Press, Oxford, 1996.

84. Kissinger P. T., Heineman W. R., Laboratory Techniques in Electroanalytical Chemistry, 2nd ed., Marcel Dekker, Inc., New York, 1996.

85. Bard A. J., Faulkner L. R., Electrochemical Methods: Fundamentals and Applications. John Wiley & Sons, Inc., New York, 1980.

86. Settle F. A., Handbook of Instrumental Techniques for Analytical Chemistry, Volume 1, Prentice Hall PTR, New York, 1997, Chpt. 37.

87. Bott A. W., Current Separations, 12 (1993) 141.

88. Ingle J. D., Crouch S. R., Spectrochemical Analysis, Prentice Hall Inc., New Jersey, 1988.

89. Skoog D. A., Holler F. J., Crouch S. R., Principles of Instrumental Analysis, 6th ed., Thomson Brook/Cole, California, 2007.

90. Broekaert J. A. C., Analytical Atomic Spectrometry with Flames and Plasmas, Wiley-VCH, Weinheim, Germany, 2002.

91. United States Environmental Protection Agency. Center for Environmental Research Information Office of Research and Development. Determination of Metals in Ambient Particulate Matters Using Atomic Absorption (AA) Spectroscopy. June, 1999.

92. United States Environmental Protection Agency. National Technical Information Service. Inductively Coupled Plasmas-Atomic Emission Spectroscopy. February, 2007.

93. Zhou W., Wang Z. L., Scanning Microscopy for Nanotechnology: Techniques and Applications, Springer Science & Business Media Inc., New York, 2006.

94. Flegler S. L, Heckman J. W., Klomparens K. L., Scanning and Transmission Electron Microscopy: An Introduction, W. H. Freeman and Company, New York, 1993.

95. Goldstein J. I., Lyman C. E., Newbury D. E., Lifshin E., Echlin P., Sawyer L., Joy D. C., Michael J. R., Scanning Electron Microscopy and X-ray Microanalysis, 3rd edition, Kluwer Academic/ Plenum Publishers, New York, 2003.
96. Egerton R. F., Physical Principles of Electron Microscopy: An Introduction to TEM, SEM, and AEM, Springer Science & Business Media Inc., New York, 2005.
97. Echlin P., Handbook of Sample Preparation for Scanning Electron Microscopy and X-ray Microanalysis, Springer Science & Business Media Inc., New York, 2009.
98. Reimer L., Scanning Electron Microscopy: Physics of Image Formation and Microanalysis, 2nd edition, Springer, Munster, Germany, 1998.
99. Watt I. M., The Principles and Practice of Electron Microscopy, 2nd edition, Cambridge University Press, Great Britain, 1997.
100. Haine M. E., Cosslett V. E., The Electron Microscope, Interscience Publishers Inc., New York, 1961.
101. Lee H., Flynn N., Handbook of Applied Solid State Spectroscopy, Springer Science & Business Media Inc., New York, 2006.
102. Ebnesajjad S., Ebnesajjad C., Surface Treatment of Materials for Adhesion Bonding, William Andrew Publishing Inc., New York, 2006.
103. Powell C. J., Jablonski A., Tilinin I. S., Tanuma S., Penn D. R., J. Electron Spectrosc., 98-99 (1999) 1.
104. Brundle C. R., Conti G., Mack P., J. Electron Spectrosc., 178-179 (2010) 433.
105. Briggs D., Grant J. T., Surface Analysis by Auger and X-Ray Photoelectron Spectroscopy, IM Publication, New York, 2003.
106. Moulder J. F., Stickle W. F., SobolP. E., Bomben K. D., Handbook of X-Ray Photoelectron Spectroscopy, Physical Electronics, New York, 1995.
107. Ertas G., Demirok U., Suzer S., Appl. Surf. Sci., 249(2005) 12-15.

108. Oyama T., Nishizawa S., Yamamoto H., J. Surf. Anal., 3 (1997)558.
109. Vickerman C., Gilmore I., Surface Analysis: the Principle Techniques, John Wiley & Sons Inc., New York, 2009.
110. Fadley C. S., Nucl. Instrum. Meth. A, 601 (2009) 8.
111. Fadley C. S., J. Electron Spectrosc., 178-179 (2010) 2.
112. Blomfield C. J., J. Electron Spectrosc., 143(2005) 241.
113. Palchetti I., Marrazza G., Mascini M., Anal. Lett., 34 (2001) 813.
114. Matysik F., Matysik S., Brett A. M., Brett C. M. A., Anal. Chem., 69 (1997) 1651.
115. Brett C. M. A., Brett A. M., Matysik F., Matysik S., Kumbhat S., Talanta, 43 (1996) 2015.
116. Wang J., Taha Z.,Anal. Chem., 63 (1991) 1053.
117. Guo D., Li J., Yuan J., Zhou W., Wang E., Electroanalysis, 22 (2010) 69.
118. Brett C. M. A., D. A. Fungaro, Talanta, 50 (2000) 1223.
119. Tsai Y., Davis J., Compton R. G., Ito S., Ono N., Electroanalysis, 13 (2001) 7.
120. Fischer E., van den Berg C., Anal. Chim. Acta, 385 (1999) 273.
121. Zen J. M., Lee M. L., Huang S. Y., Hsu F. S., Chi N. Y., Chung M. J., J. Chin. Chem. Soc., 45 (1998) 39.
122. Limson J., Nyokong T., Anal. Chim. Acta, 344 (1997) 87.
123. Sherigara B.S., Shivaraj Y., Mascarenhas R. J., Satpati A.K., Electrochim. Acta, 52 (2007) 3137.
124. Song W., Zhang L., Shi L., Li W. D., Li Y., Long Y. T., Microchim. Acta, 169 (2010) 321.
125. Suren E.,Yilmaz S., Turkoglu M., Kaya S., Environ. Monit. Assess., 125 (2007) 91.
126. Ensafi A. A., Khayamian T., Benvidi A., Mirmomtaz E., Anal. Chim. Acta, 561 (2006) 225.
127. Dalangin R. R., Gunasingham H., Analyst, 119 (1994) 1603.
128. Cesarino I., Gouveia-Caridade C., Pauliukaite R., Cavalheiro E. T. G., Brett C. M. A., Electroanalysis, 22 (2010) 1437.

129. Kachoosangi R.T., Banks C. E., Ji X., Compton R. G., Anal. Sci., 23 (2007) 283.
130. Kirgoz U. A., Marin S., Pumera M., Merkoci A., Alegret S., Electroanalysis, 17 (2005) 881.
131. Wang J., Lu J., Hocevar S. B., Farias P. A. M., Anal. Chem., 72 (2000) 3218.
132. J. Li, S. Guo, Y. Zhai, E. Wang, Anal. Chim. Acta, 649 (2009) 196.
133. Wang Z. M., Guo H. W., Liu E., Yang G. C., Khun N. W., Electroanalysis, 22 (2010) 209.
134. Adraoui I., Rhazi M. E., Amine A., Anal. Lett., 40 (2007) 349.
135. Cao L., Jia J., Wang Z., Electrochim. Acta, 53 (2008) 2177.
136. Kokkinos C., Economou A., Talanta, 84 (2011) 696.
137. Bi Z., Chapman C. S., Salaun P., van den Berg C. M. G., Electroanalysis, 22 (2010) 2897.
138. Korolczuk M., Stepniowska A., Tyszczuk K., Intern. J. Environ. Anal. Chem., 89 (2009) 727.
139. Hull E., Piech R., Kubiak W. W., Electroanalysis, 20 (2008) 2070.
140. Guzsvany V., Nakajima H., Soh N., Nakano K., Imato T., Anal. Chim. Acta, 658 (2010) 12.
141. Toghill K. E., Xiao L., Wildgoose G. G., Compton R. G., Electroanalysis, 21 (2009) 1113.
142. Czop E., Economou A., Bobrowski A., Electrochim. Acta, 56 (2011) 2206.
143. Urbanova V., Vytras K., Kuhn A., Electrochem. Commun., 12 (2010) 114.
144. Mandil A., Idrissi L., Amine A., Microchim. Acta, 170 (2010) 299.
145. Gong J., Zhou T., Song D., Zhang L., Hu X., Anal. Chem., 82 (2010) 567.
146. Khaled E., Hassan H. N. A., I. H. I. Habib, Metelka R., Int. J. Electrochem. Sci., 5 (2010)158.
147. Vedhi C., Selvanathan G., Arumugam P., Manisankar P., Ionics, 15 (2009) 377.
148. Roa G., Ramirez-Silva M. T., Romero-Romo M. A., Galicia L., Anal. Bioanal. Chem., 377 (2003) 763.
149. Zheng H., Yan Z., Dong H., YeB., Sensor Actuat. B-Chem., 120 (2007) 603.
150. G. Yang, X. Qu, M. Shen, C. Wang, Q. Qu, X. Hu, Microchim. Acta, 160 (2008) 175.
151. Cabello-Carramolino G., Petit-Dominguez M. D., Anal. Chim. Acta, 614 (2008) 103.
152. Mojica E., Santos J., Micor J., World Appl. Sci. J., 2 (2007) 512.

153. Hu C., Wu K., Dai X., Hu S., Talanta, 60 (2003) 17.
154. Yantasee W., Deibler L. A., Fryxell G. E., Timchalk C., Lin Y., Electrochem. Commun., 7 (2005) 1170.
155. Yantasee W., Fryxell G. E., Lin Y., Analyst, 131 (2006) 1342.
156. Javanbakht M., Khoshsafar M., Ganjali M. R., Badiei A., Norouzi P., Hasheminasab A., Curr. Anal. Chem., 5 (2009) 35.
157. Yantasee W., Lin Y., Fryxell G. E., Busche B. J., Anal. Chim. Acta, 502 (2004) 207.
158. Shams E., Alibeygi F., Torabi R., Electroanalysis, 18 (2006) 773.
159. Sanchez A., Morante-Zarcero S., Perez-Quintanilla D., Sierra I., del Hierro I., Electrochim. Acta, 55 (2010) 6983.
160. Navratil T., Sebkova S., Kopanica M., Anal. Bioanal. Chem., 379 (2004) 294.
161. Banks C. E., Hyde M. E., Tomcik P., Jacobs R., Compton R. G., Talanta, 62 (2004) 279.
162. Foord J. S., Hao W., Eaton K., Phys. Stat. Sol. A, 202 (2005) 2116.
163. Krasnodebska-Ostrega B., Piekarska J., Electroanalysis, 17 (2005) 815.
164. Bonfil Y., Brand M., Kirowa-Eisner E., Electroanalysis, 15 (2003) 1369.
165. Yi H., Mei P., J. Appl. Electrochem., 38 (2008) 1623.
166. Lu M., Toghill K. E., Compton R. G., Electroanalysis, 23 (2011) 1089.
167. Banks C. E., Compton R. G., Anal. Sci., 21 (2005) 1263.
168. Khun N.W., Liu E., Electrochim. Acta, 54 (2009) 2890.
169. Sheela T., Basavanna S., Viswanatha R., Kalachar H. C. B., Naik Y. A., Electroanalysis, 23 (2011) 1150.
170. Carregalo S., Merkoci A., Alegret S., Microchim. Acta, 147 (2004) 245.
171. Bas B., Piech R., Niewiara E., Ziemnicka M., Stobierski L., Kubiak W. W., Electroanalysis, 20 (2008) 1655.
172. Wu K., Hu S., Fei J., Bai W., Anal. Chim. Acta, 489 (2003) 215.

173. Cueto L. F., Sanchez E., Torres-Martinez L. M., Mater. Charact. 55 (2005) 263-271.

174. Setoyama N., Kaneko K., Rodríguez-Reinoso F., J. Phys. Chem. 100 (1996) 10331-10336.

175. Chang S. M., Dong R. A., Chem. Mater. 19 (2007) 4804-4810.

176. Sawyer D.T., Heineman W.R., Beebe J. M., Chemistry Experiments for Instrumental Analysis, John Wiley & Sons, Inc., New York, 1984.

177. Nicholson R. S., Anal. Chem. 37 (1965) 1351-1355.

178. Heinze J., Ber. Bunsenges. Phys. Chem. 85 (1981) 1096-1103

179. Valente A., Ribeiro A., Lobo V., Jimenez A., J. Mol. Liq. 111 (2004) 33-38.

180. Macero D., Rulfs D., J. Electroanal. Chem. 7 (1964) 328-331.

181. Nguyen P. K., Lunsford S., Talanta 101 (2012) 110-121.

182. Nguyen P. K. Q., Lunsford S. K., J. Electroanal. Chem. (2013), http://dx.doi.org/10.1016/j.jelechem.2013.10.021